MICROMETEOROLOGICAL FLUXES AND CONTROLS ON EVAPOTRANSPIRATION FOR A JACK PINE STAND GROWING ON RECLAMATION SOIL COVER, FORT MCMURRAY, ALBERTA

by

Paul Adrian Moore

B.A. (Environmental Studies), Carleton University, Ottawa Ontario, Canada, 2006

A thesis submitted to

The Faculty of Graduate Studies and Research

In partial fulfillment of the requirements of the degree of

Master of Science

Department of Geography and Environmental Studies

Carleton University

Ottawa, Ontario

August 2008

Your file Votre référence
ISBN: 978-0-494-44133-6
Our file Notre référence
ISBN: 978-0-494-44133-6

Abstract

Fluxes of energy and water vapour over natural boreal forest stands are expected to vary during the growing season due to temporal variations in radiant input, soil and biophysical properties, and moisture conditions. It is uncertain whether or not biophysical processes occurring at oilsand reclamation sites mirror those of natural boreal ecosystems. Therefore, to asses this, turbulent fluxes of energy and mass were measured using the eddy covariance technique over a 15-year-old planted jack pine (*Pinus banksiana*) stand on reclamation soil cover in northern Alberta during the 2007 growing season.

In response to a number of issues raised in the literature regarding the eddy covariance method and subsequent data analysis, a number of diagnostic tools were used to assess data quality. Results show that: a 30 minute averaging period was adequate for this study site; high frequency spiking and otherwise statistically unusual behaviour resulted in on average <5 % of data being rejected, with poorer performance by the infrared gas analyser compared to the 3-D sonic anemometer particularly during rainy conditions; no less than 80 % of all half hours were considered stationary; and the results of the integral turbulence characteristic parameter were inconclusive.

The first half of the field season (May-Jul.) was predominantly dry, with relatively constant levels of daily evapotranspiration being supplied by soil moisture stored from spring snowmelt. Drought-like conditions developed for a short period when soil moisture was limiting on evapotranspiration (max daily near surface soil suction of -1595 kPa). Higher than average rainfall in August resulted in soil moisture being recharged, near zero daily soil suction, and latent heat flux as a proportion of equilibrium

levels increasing from 0.4 to 0.8 while the canopy was dry. During the relatively dry, warm period that prevailed during the first half of the study period, midday energy portioning was predominantly to sensible heat with a common Bowen ratio equal to or greater than 2. Computed as a daily average, however, energy partitioning between sensible and latent heat was more equal as a result of small yet consistently positive latent heat flux values at night. The release of energy stored in the soil significantly contributed to the positive latent heat fluxes at night. In the second half of the study period, with increased precipitation and available soil moisture, midday energy partitioning to turbulent fluxes was fairly equal, while daily latent heat fluxes exceeding sensible heat fluxes. Daily evapotranspiration ranged from 0.2 – 3.6 mm d^{-1} (0.5 – 8.7 MJ $m^{-2}d^{-1}$), with mean values over the study period of 1.75 ± 0.75 mm d^{-1} (4.3 ± 1.8 MJ m^{-2} d^{-1}). The soil heat flux was the smallest measured component of the energy balance, with maximum daily values reaching 1.4 MJ m^{-2} d^{-1}.

In addition to examining the magnitude and temporal variability of the mass and energy fluxes at the study site, the biotic and abiotic factors which control evapotranspiration were assessed due to their roles in water balances, nutrient cycling, and productivity. Soil moisture availability had a significant effect on the seasonal variability of ET. Bulk surface resistance was found to exert a strong biological control on the latent heat flux with mean decoupling coefficient values of 0.15 – 0.30, where the effects of the atmospheric vapour pressure deficit, photosynthetic photon flux, and available water was examined using a non-linear multiplication model.

Acknowledgments

I would like to start by thanking my supervisor, Dr. Sean Carey, for his invaluable comments and suggestions. His generous and friendly nature helped in making this a thoroughly enjoyable experience.

I would also like to acknowledge the generous contribution of a number of data processing algorithms developed by Elyn Humphreys and her former colleagues at UBC, and her assistance in all things MATLAB.

A number of people were involved in instrument setup and calibration, data collection, and support services. Technical support, including instrument setup and calibration, was provided by Mike Treberg. Soil data instrumentation and data management was provided by Sophie Kesler and O'Kane Consultants Inc. Precipitation instrumentation and data management was provided by Syncrude Canada Ltd. Field support from Peggy Elsen, Joel Defoe, and Carl Mendoza of the University of Alberta was also indispensible.

Acknowledgments are also in order for the staff of Syncrude's Environmental Affairs for their hard work and dedication to restoring lands disturbed by oil sands mining operations to functioning ecosystems through multidisciplinary research, and for encouraging student lead research.

Finally, I would like to thank my wife, Erin, for her support and patience throughout this process.

Table of Contents

List of Symbols

Symbols	Units	Description
Greek		
Δ	g m^{-3} $°C^{-1}$	slope of saturation vapour density versus temperature curve
Ψ_s	Pa	soil suction
Ω		decoupling coefficient
α		Priestly-Taylor coefficient, $\alpha = LE/LE_{eq}$
β		Bowen's ratio, $\beta = H/LE$
γ	g m^{-3} $°C^{-1}$	psychrometric constant
ε	W m^{-2}	residual flux density
ζ		stability, $\zeta = (z-d)/L$
θ_s	m^3 m^{-3}	volumetric water content
θ_v	°C	virtual potential temperature
λ	J kg^{-1}	latent heat of vaporization
ρ	g m^{-3}	density
σ_x	units of x	standard deviation of variable x
σ^2_x	units of x^2	variance of variable x
τ	N m^{-2}	momentum flux density
χ_c	µmol CO_2	CO_2 mole fraction

	mol^{-1} moist air	
χ_v	mmol $H_2O_{(g)}$	water vapour mole fraction
	mol^{-1} moist air	

Roman

C	J m^{-3} K^{-1}	volumetric heat capacity of soil
D	mm	vertical drainage
E	mm	evaporation
F_c	μmol m^{-2} s^{-1}	CO_2 flux density
G	W m^{-2}	ground heat flux density
H	W m^{-2}	sensible heat flux density
K↓	W m^{-2}	incoming solar radiation flux density
K↑	W m^{-2}	outgoing solar radiation flux density
L	m	Obukhov scaling length
L↓	W m^{-2}	incoming long-wave radiation flux density
L↑	W m^{-2}	outgoing long-wave radiation flux density
LE	W m^{-2}	latent heat flux density
LE_{eq}	W m^{-2}	equilibrium latent heat flux density
LE_{PM}	W m^{-2}	Penman-Monteith model estimate of LE
M	W m^{-2}	rate of change in soil heat storage in top 5 cm
P	mm	precipitation
R	μmol m^{-2} s^{-1}	respiration
R_a	W m^{-2}	available radiation flux density (R_n – G)
R_n	W m^{-2}	net radiation flux density (K↓ – K↑ + L↓ – L↑)

S	mm	soil moisture storage
T_a	°C	air temperature
T_{soil}	°C	soil temperature
T_v	°C	virtual temperature
T_k		net sky transmissivity
U_k		Canopy gap fraction
W	mm	Maximum canopy storage
d	m	zero-plane displacement
f	Hz	frequency
g	$m^2\ s^{-1}$	acceleration due to gravity
h	m	canopy height
k		von Karman constant
r_a	$m\ s^{-1}$	aerodynamic resistance
r_c	$m\ s^{-1}$	canopy resistance
r_s	$m\ s^{-1}$	surface resistance
t	s, min, hr, day	time
u	$m\ s^{-1}$	average wind speed; or streamwise wind speed
u_*	$m\ s^{-1}$	friction velocity
v	$m\ s^{-1}$	cross-stream wind speed
w	$m\ s^{-1}$	vertical wind speed
x	m	distance
z	m	eddy covariance measurement height

Abbreviations

BREB		Bowen ratio energy balance
EPEA		Environmental protection and enhancement act
GEP	$\mu mol\ m^{-2}\ s^{-1}$	gross ecosystem productivity
GPP	$\mu mol\ m^{-2}\ s^{-1}$	gross primary productivity
IRGA		infrared gas analyzer
LAI	$m^2\ m^{-2}$	leaf area index (projected)
NEE	$\mu mol\ m^{-2}\ s^{-1}$	net ecosystem exchange of CO_2
NEP	$\mu mol\ m^{-2}\ s^{-1}$	net ecosystem productivity
PAR	$\mu mol\ m^{-2}\ s^{-1}$	photosynthetically active radiation
PPFD	$\mu mol\ m^{-2}\ s^{-1}$	photosynthetic photon flux density
RH	%	relative humidity
S.D.		standard deviation
S.E.		standard error
VPD	kPa	vapour pressure deficit

Subscripts (unless otherwise stated)

a	air / aerodynamic
c	carbon dioxide / canopy
eq	equilibrium
h	heat
m	mineral / momentum
o	organic
s	surface / soil

w	water
v	water vapour / virtual

List of Tables

List of Figures

1 Introduction

The boreal region, or taiga as it is known in Eurasia, is one of the world's largest biomes, occupying an approximate area of $1.6x10^7$ km^2 (~60% forest) between 50° and 70° latitude in the Northern hemisphere (Baldocchi et al., 1997a; NRCan – CFS, 2005). Because of the large extent of the boreal forest, its influence on regional climate, and its role in global carbon cycling (Blanken et al., 2001), numerous studies have been conducted to quantify energy, water (Amiro and Wuschke, 1987; Black et al., 1996; Blanken et al., 1997; McCaughey et al., 1997; Baldocchi et al., 1997a; Barr et al., 2000), and carbon exchanges (Baldocchi et al., 1997b; Black et al., 2000; Barr et al., 2006) between the surface and atmosphere in order to gain a better understanding of these exchange processes and their controls.

More recent micrometeorological investigations in the boreal region focus on sites that have been disturbed by fire or harvesting (Amiro et al., 2006a; Amiro et al., 2006b; Barr et al., 2006; Kljun et al., 2006). Disturbance to Canadian forests, with significant portions occurring in the boreal region, is largely the result of logging ($0.9x10^6$ ha in 2005), forest fires ($2.5x10^6$ ha yr^{-1} on average and ranging from $0.7 – 7.6x10^6$ ha yr^{-1}), and insect infestation/defoliation ($16.0x10^6$ ha in 2005) (NRCan – CFS, 2007).

Regeneration of these disturbed areas occurs both naturally and through forest management practices. However, more recent oil and gas exploration, particularly oil sands operations concentrated in northern Alberta, cause significant disturbance to the landscape where natural regeneration would be impossible on a meaningful timescale without some degree of reclamation engineering. In fact, all oil sands projects are

required to submit detailed plans for mine closure and landscape reclamation in order to be licensed by the provincial government.

The oil sands industry is an important part of the Canadian economy, with production approaching 50% of national crude supply. Oil sands operations currently employ over 100,000 people (upstream), and would generate over $40 billion in annual revenues based on current production levels and price of $100+ per barrel. Expanding mining in Alberta's Athabasca region has already disturbed over 750 km^2, and projections indicate that over 2000 km^2 will be affected by 2015 (Qualizza et al., 2004). Furthermore, as of late 2007, nearly 65,000 km^2 of mineral rights had been obtained for potential future oil sands development (Alberta Energy).

According to the Alberta Environmental Protection and Enhancement Act (EPEA) oil sands operators are required to return mined areas to a pre-disturbance land capability. Only once a reclamation certificate has been issued by the province is the operator absolved of liability.

Typical boreal forest stands, which are composed largely of mixed or uniform spruce (*Picea*) and pine (*Pinus*) species with aspen (*Populus tremuloides*) common in more southerly boreal regions, take on the order of 50-100 years to reach maturity. This length of time for potential liability is undesirable for oil sands operators. Therefore, an assessment of productivity or other environmental indicators is desired which can assess whether a particular reclamation stand is on an optimal or suboptimal development trajectory along with an associated risk of future stand mortality. Since many trees species will have overcome direct competition due to shading from other understory plant species and have been exposed to the natural range of regional climatic variability within

a 15-20 year period, such a timeframe would be considered appropriate for assessment of reclamation success for a particular site.

Following mining operations and initial reclamation work, landforms are constructed which have an uplands topography in what was once a relatively flat boreal landscape. Soil covers of different thickness and composition are used to cap overburden or process material, and different tree species planted to promote growth of target ecosystems. These factors combine to create reclamation sites where the soil-vegetation-atmosphere continuum and surface hydrology is highly modified (Carey, 2006; Elshorbagy et al., 2005).

Consequently, there is uncertainty regarding whether or not biophysical processes occurring at these sites mirror those of natural boreal ecosystems. This is in part due to the disturbed nature of the soil profile which limits water availability and promotes salinization from oxidation of saline-sodic shale overburden exposed during mining.

One key requirement of successful constructed soil covers is that they have a water holding capacity sufficient to meet evaporative demands (Qualizza et al., 2004; Elshorbagy et al., 2005) over the dry growing season typical in Northern Alberta. In Northern Alberta, following spring snowmelt, evapotranspiration (ET) is the dominant hydrological process responsible for water loss. Evapotranspiration, which is influenced by both environmental conditions and biophysical properties (Blanken et al., 1997; Wilson and Baldocchi, 2000), in turn affects ecosystem properties and processes such as soil moisture content, productivity, nutrient cycling, and water balances (Wever et al., 2002).

Because of the significance of ET in the water balance (Amiro and Wuschke, 1987), and its influence on nutrient cycling, and ecosystem productivity, the assessment of success of a particular reclamation strategy requires an understanding of the biophysical processes controlling ET in addition to examining how they differ in response to modified edaphic and microclimatic conditions.

It is only by instrumenting the ecosystem, quantifying its essential elements, and gaining understanding of ecosystem function through modeling that improvements can be made to the reclamation process, both reducing cost for the operators and, more importantly, reducing liability.

The focus of most research programs in oil sands reclamation revolves around quantifying and understanding several key issues which are i) water and energy balances; ii) salt balances, including organic and inorganic species; iii) plant and ecological responses to i and ii; and iv) how to manage these balances optimally (Barbour et al., 2004). The research conducted as part of this study focused on issues i and iii, where some of the key findings are to be used in addressing issue iv.

This study reports on the 2007 growing season energy and mass exchange between the surface and atmosphere for a 15 year old jack pine (*Pinus banksiana*) stand growing on 50 cm of till overlying tailings sand. In order to assess evapotranspiration for this constructed ecosystem a number of objectives are outlined:

1. Assess the reliability of turbulent flux data collected using the eddy covariance technique based on the concerns raised in the literature, including but not limited to the choice of coordinate rotation, averaging length, and tests of stationarity and adequately developed turbulence.

2. Report on the magnitude and temporal variation of diurnal and growing season energy and water vapour fluxes at the study site.
3. Examine environmental and biophysical factors that limit ET on daily and seasonal time scales.
4. Compare simple relations resulting from the interaction of micro and mesoclimate, biophysical properties of the jack pine, and engineered soil covers to corresponding relations for jack pine stands regenerated following harvesting growing in a natural setting.

2 Theory

This chapter discusses the essential micrometeorological theory necessary for conceptualizing, measuring, and interpreting the pertinent energy and mass fluxes for the environmental system being studied. Outlined herein are: (i) the general system view used to conceptualize the environmental system, including the essential governing equations of the surface boundary layer; (ii) the equations for the mass/energy budget framework; (iii) the eddy covariance technique; and (iv) equations used to examine the controls on evapotranspiration.

2.1 A Systems View

In using the experimental method when investigating an environmental system, much of the current research conducted in the environmental sciences is based on general systems theory as outlined by Chorley (1971). At its most basic level, the systems approach conceptualizes the environment within a mass and/or energy budget framework where stores of mass or energy are linked by flows between them. However, in order to make scientific investigations tractable, the system in question must be bounded so that all necessary elements of the system are defined in both space and time.

There are a number of variables that describe the form of a system from a microclimatological perspective. These variables include wind speed, atmospheric pressure, temperature, humidity, and concentration of trace gases like CO_2. Owing to the flows of mass, energy and momentum to and from a control volume, the system can be said to be in dynamic equilibrium since the state of the system, described by the above environmental variables, fluctuates around a given mean and is bounded.

$$I - O - \Delta S = 0 \tag{2.1}$$

Equation (2.1) can be used to describe the non-steady state conservation of mass, energy or momentum in the system; where I is the input, O is the output, and ΔS is the change in storage. The processes that describe the flows of energy, mass, and momentum are radiative, convective, conductive, and diffusive exchange mechanisms.

2.2 Energy Balance

The surface net-radiation balance, which varies both temporally and spatially, can be described in the general form:

$$R_n = K\downarrow - K\uparrow + L\downarrow - L\uparrow \tag{2.2}$$

where R_n is the net radiant energy flux density (hereafter flux) at the surface (W m^{-2}), K is shortwave (or solar) radiation flux (W m^{-2}), L is longwave (or terrestrial/infrared) radiation flux (W m^{-2}), and ↓ and ↑ denote downwelling and upwelling respectively. Furthermore, longwave radiation can be described using the Stephan-Boltzman equation where $L = \varepsilon\sigma T^4$, where ε is the surface emissivity (equal to 1.0 for a black-body radiator), σ is the Stephan-Boltzman constant (5.67×10^{-8} W m^{-2} K^{-4}), and T is the surface and sky temperature for upwelling and downwelling longwave radiation, respectively.

According to Oke (1987), net all-wave radiation is considered one of the most important energy exchange mechanisms because, for the majority of earth systems, it represents the driving force for weather and climate, as well as a limiting factor for biophysical processes. Any net imbalance between the terms of Equation (2.2) results in an energy convergence (divergence) at the surface which is dissipated (supported) by conductive or convective means. In this way the net radiation and energy balance equations are linked through R_n. The energy budget can be described as:

$$R_n = H + LE + G(+S) + \varepsilon \quad (2.3)$$

where H and LE are the turbulent sensible and latent heat fluxes respectively (W m^{-2}), G is the soil heat flux at the surface (W m^{-2}), S is an additional term added when heat storage is considered within the vegetation and air column below the measurement height and it includes the rate of change of storage in the sensible and latent heat within the air and vegetation between the surface and the measurement height (W m^{-2}), and ε is the residual flux term associated with both systematic and random errors. The degree to which the surface energy balance can be closed is one measure of data quality (Baldocchi et al., 1997), and it is used as an independent test of the applicability of the eddy covariance method (Baldocchi, 2003). It is assumed that the difference between available energy (R_n-G) and the turbulent fluxes (H+LE) should be zero. The degree to which the surface energy balance can be closed is of particular importance when studying sites that do not conform to the ideal situations characterized below.

2.3 Mass Balance

The primary components of the water balance (Eq. 2.4) are precipitation (P), evapotranspiration (ET), runoff (R), changes in soil storage (ΔS), and deep drainage (D), all typically expressed as a depth of water (e.g. mm).

$$P = ET + R + \Delta S + D \quad (2.4)$$

It is common for forest ecosystems to omit the runoff component of the water balance with certain caveats. This simplification is based on forest ecosystems in temperate regions with moderate to low levels of precipitation, growing on flat terrain over an extensive area.

In ecosystems like the boreal forest, where annual precipitation is low, ET may constitute the largest water flux during the mid and late growing season (Amiro and Wuschke, 1987). ET is an important process, especially where horizontal movement of water in the system is negligible, and is controlled by the interaction of a number of environmental and biological factors (Baldocchi et al., 1997a; and Wever et al., 2002).

According to Oke (1987), it is important to critically evaluate the choice of time integral over which Equation (2.4) is evaluated. This is because the different processes that are part of the water mass balance operate at different time scales where, for example, ET is a relatively continuous process and P is intermittent. Consequently, depending on the time scale chosen, Equation (2.4) will not necessarily balance. Cumulative sums or changes are thus best evaluated over longer time scales such as seasonally or annually.

2.4 Eddy Covariance Technique

2.4.1 Principles of Eddy Covariance

Above the laminar boundary layer of a given surface, atmospheric flow is turbulent, such that the bulk transport of mass, energy and momentum between the surface and atmosphere is the result of convection, or eddies. Though the turbulent motion of the air causes instantaneous variations in the properties it caries when measured at a point, principles of mass continuity stipulate that over a reasonable period of time the adiabatic mass balance of dry air at constant pressure is zero with respect to the vertical near the surface (Oke, 1987; Lee et al., 2004). The principle behind eddy covariance, then, is that eddies are non-discriminatory to the properties being transported and that the vertical wind speed along with the entities carried in an air parcel co-vary at

the same frequency and at proportional magnitudes. The eddy covariance technique, therefore, attempts to measure the instantaneous deviation of vertical wind speed, along with any of its scalar properties (temperature, water vapor and CO_2 mixing ratios), from their mean value.

For example, Amiro and Wuschke (1987) measured sensible heat flux density using the eddy correlation technique, in which

$$H = \rho C_p \overline{w'T'} \tag{2.5}$$

$$LE = \lambda \overline{w'\rho_v'} \tag{2.6}$$

$$F_C = \overline{w'\rho_C'} \tag{2.7}$$

$$\tau = -\rho \overline{u'w'} \tag{2.8}$$

where ρ is density (g m^{-3}) and C_p is the specific heat of moist air, w is vertical wind velocity (m s^{-1}), T is temperature (°C), λ is latent heat of vaporization (J g^{-1}), ρ_v is vapor density (g m^{-3}), and ρ_c is the mass density of CO_2 (g m^{-3}). The prime in the covariance terms denotes the instantaneous deviation of the various species from their local mean values, and the overbar signifies a time average that is typically binned into 30-60 minutes intervals.

2.4.2 Assumptions

According to Stull (1988) two main equations form the basis of boundary layer meteorology: they are the ideal gas law and the scalar conservation equation for both mass and energy. The general form of the scalar conservation equation (Eq. 2.9) for a theoretical control volume in an incompressible fluid with turbulent flow is:

$$\frac{d\bar{c}}{dt} = \underbrace{\frac{\partial \bar{c}}{\partial t}}_{I} + \underbrace{\bar{u}\frac{\partial \bar{c}}{\partial x} + \bar{v}\frac{\partial \bar{c}}{\partial y} + \bar{w}\frac{\partial \bar{c}}{\partial z}}_{II} = \underbrace{\nu_c\left(\frac{\partial^2 \bar{c}}{\partial x^2} + \frac{\partial^2 \bar{c}}{\partial y^2} + \frac{\partial^2 \bar{c}}{\partial z^2}\right)}_{III} + \underbrace{S_c}_{IV} - \underbrace{\left(\frac{\partial \overline{u'c'}}{\partial x} + \frac{\partial \overline{v'c'}}{\partial y} + \frac{\partial \overline{w'c'}}{\partial z}\right)}_{V}$$

(2.9)

where c is a general scalar, u, v, and w are the three orthogonal components of the wind vector, x, y, and z are the components of the position vector, ν is molecular viscocity, and S is the source/sink term. Equation (2.9) is conceptually divided into five terms, where I represents the storage term, II accounts for the flux in all orthogonal directions, III represents molecular diffusion or viscosity, IV is the source/sink strength, and V represents turbulent divergence.

There are three primary assumptions that underlie the use of the eddy covariance technique that are made regarding the physical behaviour of the surface boundary layer which permit the simplification of the governing equations into the form commonly used (Baldocchi, 2003; Finnigan et al., 2003) . These assumptions are used to greatly simplify the analysis of the surface flux derived from the point measurement of mean and fluctuating components of vertical wind velocity and its scalar properties.

To simplify modeling of the environmental system, generally situations are considered where: (i) atmospheric conditions are stationary; (ii) the terrain is flat with extensive homogeneous ground cover (Baldocchi, 2003); (iii) conductive or diffusive flow is largely restricted to ground heat profiles or near surface interactions; and (iv) air density fluctuations in the lower atmosphere are negligible (Stull, 1988).

The first assumption is that wind velocity and scalar properties of the atmosphere are steady with time, meaning that the statistical properties of the time series are not time dependent. With respect to Eq. (2.9), steady-state conditions imply that $\partial c/\partial t = 0$.

Analysis of eddy covariance data is complicated with the passing of quick moving frontal systems over flux measurement sites since there is a rapid change in the scalar properties between the two air masses.

Second, it is assumed that the surface being studied has relatively homogenous vegetation cover over an extensive area and is on flat terrain (Oke, 1987). At fine enough scales, all natural surfaces are heterogeneous which could present difficulties for the eddy covariance technique since measurements are typically made at a single point. Therefore, the conservation equation (2.9) is integrated over a representative surface patch, or rather, control volume (Finnigan et al., 2003). Again, with respect to Eq. (2.9), the assumption of flat homogeneous terrain implies that the partial derivatives with respect to x and y go to zero. Under the second assumption, measurements can be made at a point, since it is assumed that the measurements are equivalent to the area average for the study site (ergotic principle) because of the symmetry imposed on the flow field by homogeneity, and no advection.

Third, Equation (2.9) above includes a molecular diffusion/viscosity term that is commonly ignored. This simplification is appropriate when turbulent effects are much greater than molecular diffusion. Examination of Reynolds numbers for typical boundary layer velocity and length scales indicates that turbulent transport is several orders of magnitude greater than molecular diffusion except very close to surfaces (Stull, 1988).

Finally, it is assumed that air density in the lower atmosphere is constant, so that measurements of the instantaneous deviation of air density from its mean value do not need to be considered (Oke, 1987). However, density fluctuations do occur, resulting in

only negligible effects on H, but with more significant effects on LE and Fc. Air density can be linked to pressure through the Ideal gas law

$$\frac{n}{V} = \frac{p}{RT} \tag{2.10}$$

where n is the number of moles of gas, V is the volume of gas (m^{-3}), p is pressure (Pa or J m^{-3}), R is the universal gas constant (J mol^{-1} K^{-1}), and T is temperature (K). Through the molar weight of the gas, molar density and mass density are interchangeable. Air density, expressed as pressure using Dalton's law can be considered as the sum of the partial pressures of its constituent components

$$p = p_a + p_v + p_c \tag{2.11}$$

where the subscripts a, v, and c denote dry air, water vapour, and trace gas constituents, where trace gas constituents are generally considered negligible. Fluctuations in total air density are calculated from measurements of pressure and temperature. The effect of temperature and water vapour pressure fluctuations on air density and subsequently on turbulent fluxes is corrected for using the method described by Webb et al. (1980) using the following equations:

$$\overline{w'T'} = \overline{w'[T_s/(1+0.32\chi_v)]'} \tag{2.12}$$

$$E = (1+\mu\sigma)\left[E_{raw} + (\overline{\rho}_v/\overline{T})\overline{w'T'}\right] \tag{2.13}$$

$$F = F_{raw} + (\overline{\rho}_c/\overline{\rho}_a)[\mu/(1+\mu\sigma)]E + (\overline{\rho}_c/\overline{T})\overline{w'T'} \tag{2.14}$$

where $\mu = M_a / M_w$ is the ratio of molar weight of water to air, and $\sigma = \rho_v / \rho_a$ is the ratio of mass density of water vapour to dry air. This formulation shows the relation between measured and real fluxes using values obtained with an eddy covariance system using an open-path IRGA. An alternate method of obtaining fluxes which have been corrected for

the effects of variable heat and moisture content would be to calculate the covariances of molar mixing ratios instead of mass density.

Though these conditions are rarely ever met over the course of an investigation, they offer a good first approximation to the surface source/sink strength. Though storage terms are relatively straight forward to account for in forest ecosystems by measuring temperature, moisture, and CO_2 concentrations within the canopy profile, an accurate assessment of advective fluxes is beyond the technical feasibility of most research projects.

In summary these assumptions/simplifications, following integration over the height of the control volume (again, horizontal integration ignored due to assumed homogeneity) yields the following flux form of the conservation equation (Finnigan, 2002; Baldocchi, 2003):

$$\overline{w'c'} = \int_0^h S_c(z)dz \tag{2.15}$$

where $\overline{w'c'}$ is the vertical flux measured as the average covariance of turbulent components, and S_c is the source/sink strength integrated over the height of the control volume to account for the combined effects of the canopy and forest floor.

2.5 Controls on Evapotranspiration

In order to further interpret the controls on ET, the Penman-Monteith equation (2.16) is commonly used, which is a combination model approach to estimating ET using aerodynamic and energy balance principles (Oke, 1987). The rationale for using the Penman-Monteith equation is that it provides a framework that incorporates the abiotic

and biotic factors controlling canopy ET (Baldocchi et al., 2000a; Restrepo and Arain, 2005). This equation describes latent heat flux as follows:

$$LE = \frac{\Delta(R_n - G - S) + \rho_a C_a VPD g_a}{\Delta + \gamma(1 + g_a/g_c)} \tag{2.16}$$

where Δ is the relation between saturation vapor pressure and temperature, VPD is the atmospheric vapor pressure deficit, g_a and g_c are the aerodynamic and canopy conductance respectively, and γ is the psychrometric constant (Oke, 1987). Using the measurements of latent heat flux obtained from the eddy covariance technique, the Penman-Monteith equation can then be used to describe the change in canopy conductance throughout the season (Humphreys et al., 2003).

Furthermore, a derivation of the Penman-Monteith equation can be used to provide a measure of the availability of water to meet atmospheric demands (Carey, 2006). Priestley and Taylor (1972) described the equilibrium evaporation (2.17) from a freely evaporating surface which, conceptually, is when canopy conductance goes to infinity as a result of a fully saturated atmosphere (or rather when VPD goes to zero). This simplifies the Penman-Monteith equation and is termed equilibrium ET

$$LE_{eq} = \frac{\Delta}{\Delta + \gamma}(R_n - G - S) \tag{2.17}$$

and where the Priestly-Taylor α value is the ratio of LE to LE_{eq}. The resulting values are supposed to characterize the degree of coupling between available energy and LE, where low values are common for dry, low productivity systems, such as for jack pine stands (Baldocchi et al., 2000a). α under saturated atmospheric conditions has typically been found to exceed 1.0, with common values of 1.26 reported for non water stressed crops (Jarvis and McNaughton, 1986). This is said to be the result of entrainment of warmer

and drier air from above a capping inversion as the atmospheric boundary layer grows during convective conditions present during the daytime.

Finally, to evaluate the relative importance of canopy conductance and available energy to changes in the rate of evaporation, the decoupling coefficient (2.18), Ω, is used:

$$\Omega = \left[1 + \frac{\gamma}{s + \gamma} \frac{g_a}{g_c} \right]^{-1} \tag{2.18}$$

where the control of evaporation by canopy conductance increases as the decoupling coefficient approaches zero (McNaughton and Jarvis, 1983). Low values of Ω typically measured in boreal forest ecosystems point to the conservative nature of surface evaporation and the strong control by canopy conductance.

3 Background

The primary goals of micrometeorological investigations are to i) quantify the physical and biological processes that affect the microclimate and ii) understand how these processes vary with time and space. According to a number of studies, our recent understanding of processes involved in surface-atmosphere exchanges is inadequate (Baldocci et al., 1997; McCaughey et al., 1997; Blanken et al., 2001; Restrepo and Arain, 2005). Therefore, studies of ET over the last 10 – 20 years have taken place in a variety of ecosystems to better understand the nature of the controlling interactions and the links between ET and other system processes (Wever et al., 2002). Furthermore, long-term studies indicate that there is considerable seasonal and inter-annual variability of ET and energy fluxes (Baldocchi et al., 1997a; McCaughey et al., 1997; Wever et al., 2002; Humphreys et al., 2003). Many of these current studies are part of land-surface research networks such as FLUXNET and the Boreal Ecosystem-Atmosphere Study (BOREAS), where the eddy covariance technique is used to determine energy, water, and carbon fluxes (Olson et al., 2004).

It is argued that these pursuits have merit, first, because better empirical data will allow for improvement on the current mechanistic models of surface-vegetation-atmosphere (SVAT) exchanges (Law et al., 2000), which will lead to better predictive capabilities of future system responses to climate forcings (Wever et al., 2002). Second, analysis of data from long-term studies of a particular site could lead to the development of general relations between ecosystem parameters and fluxes which could be applied to other sites with similar vegetation and climate (Wever et al., 2002).

This chapter will review micrometeorological investigations of mass and energy transfer along the soil-vegetation-atmosphere continuum with particular emphasis on ET, jack pine and boreal forest research.

3.1 Recent Advances Using EC

Since the 1990s, studies reporting on the exchanges of water vapour and sensible heat flux for jack pine and other tree species growing in the Canadian boreal region have primarily cited the use of the eddy covariance method (Amiro and Wuschke, 1987; Baldocchi and Vogel, 1996; Baldocchi et al., 1997a; McCaughey et al., 1997; Amiro et al., 2006a) while other methods such as the aerodynamic or Bowen ratio energy balance method (BREB) have become less commonly used. For example, a review of boreal forest energy exchange studies in North America, Europe, and Russia by Eugster et al. (2000) presents 17 sites using EC exclusively, 10 sites using EC to measure at least the sensible heat flux with other components of the energy balance determined by a variety of methods, and 8 sites using BREB, where all BREB studies took place no later than 1991.

The shift towards using EC for continuous flux measurements began following improvements in sonic anemometry technology (Grelle and Lindroth, 1996) and technical feasibility studies where general measurement reliability was assessed (Amiro and Wuschke, 1987). Furthermore, the time-scale over which EC systems were deployed increased from a few weeks in the mid 80s to seasonal and annual time-scales in the early to mid 90s (Aubinet et al., 2000) following robust system design requiring a minimum of maintenance such as that presented in Grelle and Lindroth (1996).

As a result of the body of research produced using EC and a closer examination of its theoretical underpinnings, there has been a recognition of several potential key errors in the application of EC to progressively more topographically complex terrain or areas with greater spatial variability in surface cover (Baldocchi, 2003; Finnigan et al., 2003; Lee et al., 2004). Some of these errors include: the use of traditional 3-D coordinate rotation (Tanner and Thurtell, 1969) in complex terrain resulting in unrealistic rotation angles; the choice of an averaging period that is too short to capture total covariance, particularly over tall vegetation; and recognition of averaging, detrending, or filtering methods acting as a high pass filter.

Furthermore, consistent lack of energy balance closure using the eddy covariance method has lead to a more robust accounting of mass and energy storage terms, particularly over tall vegetation which has a relatively large control volume over which to integrate storage terms (Wilson et al., 2002). Better accounting of storage terms has consistently revealed that although daily fluxes are negligible, half hourly values could be significant.

Although there are a variety of potential causes for the lack of energy balance closure which are summarized by Twine et al., (2000), Massman and Lee, (2002), and Wilson et al. (2002), it is now generally accepted that a significant factor for poor EC performance is the result of stable atmospheric conditions which are common at night. As a result of suppressed turbulent mixing under stable conditions, there is a higher likelihood of energy/mass convergence within the canopy space and understory, where flux loss from drainage flows can occur in sloped terrain. Nighttime measurement of

storage terms was found to be particularly important for assessing EC performance and for applying temporal corrections to half hourly fluxes (Jarvis et al., 1997).

3.2 Research Networks

A significant amount of the current and recent monitoring of surface-atmosphere exchanges has taken place as part of one of a number of research networks, such as FLUXNET or BOREAS-BERMS. These research networks consist of micrometeorological tower sites that use eddy covariance methods to measure the long-term exchange of carbon, water vapour, and energy between various terrestrial ecosystems and the atmosphere. These long term annual studies were needed to answer simple, yet important questions such as whether particular land surfaces were a net source/sink of CO_2 (Grelle and Lindroth, 1996).

FLUXNET is a collection of regional networks including AmeriFlux, CARBOEUROFLUX, Fluxnet-Canada, and other smaller networks with the goal of improving the understanding of processes involved in CO_2, water vapour, and energy exchange, across a range of land surfaces and time-scales at the ecosystem level. FLUXNET is partially funded by NASA for validation of Earth Observing System measurements and SVAT models in general (Baldocchi et al., 2001; Olson et al., 2004). Similarly BOREAS, which was established in 1994 and continued under the Boreal Ecosystem Research and Monitoring Sites (BERMS) since 1997, is a semi-continuous multi-investigator experiment with similar goals as FLUXNET, but with focus on boreal forest sites in central Canada (Baldocchi et al., 2001; Barr et al., 2006).

Both BOREAS and FLUXNET support calibration and flux measurement intercomparisons so that data from different regions is compatible for model

parameterization. Based on the principal objectives of BOREAS, an explicit experimental design was employed so that there could be reconciliation between observations made at different spatial scales (Sellers et al., 1995).

3.3 Focus of Past Research

Based on the literature generated from these research networks and other sources, the ecosystems studied consist primarily of temperate and boreal forests, in addition to peatland and cropland (Greco and Baldocchi, 1996; Grelle et al., 1997; Ehman et al., 2002; Olson et al., 2004). According to Shuttleworth et al. (1989), past micrometeorological research has been concentrated in temperate latitudes as a result of both financing and practicality. Somewhat lacking, is the study of the surface-atmosphere exchanges of mass and energy for tropical forests outside of the Amazon region, as well as highly disturbed or degraded systems and their early successional communities in relation to surface-atmosphere exchanges of mass and energy.

Significant research has been conducted on describing the form of these successional communities and the processes by which their recovery trajectories are affected by mining practices (particularly coal mining) from an ecological and biochemical perspective (Johnson et al., 1982; Bradshaw, 1997; Holl, 2002). However, little research has gone into describing surface-atmosphere exchanges of these disturbed or degraded sites from a microclimatological or meteorological perspective though a number of such studies on sites affected by fire, logging, and mining disturbance are in progress or recently published (Humphreys et al., 2006; Amiro et al., 2006b; Carey, 2008).

Some early micrometeorological research has been conducted in Alberta on an oilsand overburden pile, covered by short vegetation (Carey, 2008). Over the course of this study it was found that there was a significant change in ET between years in response to changes in vegetation species. Under such conditions, the controlling factors of ET, atmospheric, vegetation, and soil conductance varied among the years presenting a complex picture of landform biometeorology. It was suggested that as succession continues, evaporation rates would increase and latent heat fluxes would account for a greater portion of the surface energy balance.

Especially in areas where soil characteristics have been drastically altered from those which existed previously, it cannot be assumed that the controls affecting biophysical processes occurring on degraded sites, consisting of successional communities, mirror those of their analogous natural ecosystems.

3.4 Boreal Research and Jack Pine

A number of studies summarize the magnitude and seasonal variability of energy and water vapour exchange rates above boreal forest canopies using eddy covariance for common Canadian species such as jack pine (Baldocchi et al., 1997a; McCaughey et al., 1997; Amiro et al., 2006a), black spruce (Jarvis et al., 1996), and aspen (Black et al., 1996; Blanken et al., 2001) and Eurasian species such as Siberian/Scots pine and Norway spruce (Grelle et al., 1997; Kelliher et al., 1998). These papers, particularly those for jack pine, identified information gaps that existed at the time on several issues regarding fluxes of energy and water vapour over boreal forest stands. These included (1) when mass and energy fluxes of a boreal forest are significant; (2) how much energy fluxes will change during the growing season; (3) how much energy fluxes vary across the boreal

landscape; and (4) how darker and rougher boreal forests will use available solar energy and an enhanced turbulent capacity to evaporate water, to heat the air and soil, and to drive primary productivity.

Results of these and other similar studies, partially summarized in Table 3.1, show that during the growing season, the most significant energy partitioning for jack pine stands is to sensible heat (see Eugster et al., 2000, for a compilation of characteristic surface energy exchange parameters for arctic and boreal forest ecosystems). Furthermore, daily sums of ET over the growing season were conservative, with typical daily values ≤ 2 mm d^{-1}, despite daily R_n being similar to more southerly locales as a result of greater daylight time. Notable exceptions tended to occur in periods directly following rainfall events when the canopy was wet or when soil moisture conditions were not limiting.

The boreal region where jack pine stands grow is typically characterized by cool temperatures (mean annual air temperature ~ 0°C) and relatively low annual precipitation (<500 mm yr^{-1}) where evaporation rates are only weakly coupled to net radiation (Baldocchi et al., 1997a, 2000a). As such, as the soil moisture content decreases with time after spring snowmelt or precipitation events, and stomatal closure reduces ET below that expected from a freely evaporating surface.

Long-term control on ET by canopy conductance is the result of the low leaf area index (LAI) of boreal forests as a response to low moisture availability and potential nutrient deficiencies (Baldocchi et al., 1997a; Baldocchi et al., 2001). Ewers et al. (2005) illustrates that in comparison to other boreal tree species, transpiration as a function of leaf area for jack pine is greater than black spruce or aspen for both a 20 and 37 year old

cohort, where the difference is greater for the younger cohort. This further emphasizes the importance of the relatively low LAI of jack pine imposing a long-term control on potential ET.

Since the results of Ewers and others were for a mixed forest, it could be argued that the effect of typical edaphic conditions that prevail where spruce, aspen, and jack pine grow would not be an issue. Black spruce tend to grow under mesic conditions, where they are the dominant boreal tree in lowland areas such as peat bogs, but are found to range throughout both upland and lowland sites; whereas jack pine are typically found to grow under xeric conditions, in upland areas with sandy, well-drained soil and rocky outcrops (Amiro and Wuschke, 1987).

However, despite potential differences in soil moisture characteristics, including available water holding capacity, and unsaturated hydraulic conductance across a range of moisture contents, Addington et al. (2006) demonstrate that stomatal conductance was not significantly affected for longleaf pine (*Pinus palustris*) growing in xeric and mesic habitats. Adaptations that were suggested to cause this were lower sapwood to leaf area ratio and higher root to leaf area ratio for the xeric site compared to the mesic site. Although there are physiological differences between longleaf and jack pine, they both tend to have a long tap root and grow in upland areas with well drained sandy soil.

With respect to rooting habit, jack pine tend to be more deeply rooted compared to other boreal conifer species (e.g. tamarack (*Larix*), black and white spruce (*Picea mariana* & *Picea glauca*), and balsam fir (*Abies balsamea*)) of a similar age when growing under similar climatic conditions in sandy soil (Bannan, 1940). Although jack pine had deep tap roots, sometimes exceeding 1.2 m depth for specimen 3 m or taller,

allowing them to access soil moisture deeper within the soil profile, Bannan (1940) indicates that the root system of jack pine tended to cover a significantly smaller horizontal area compared to other boreal conifer species at the same site.

Specific understory vegetation at sites where jack pine grow varies according to location, specific edaphic conditions, openness of the canopy, and homogeneity of the tree species in the area under investigation. However, common to most jack pine sites are various types of berries and lichen such as blueberry (*Vaccinium angustifolium*), fruticose lichens (Amiro and Wuschke, 1987), bearberry (*Arctostaphylos uva-ursi*), ligonberry (*Vaccinium vitis-idaea*), reindeer lichen (*Cladina mitis*) (Strong and La Roi, 1985), alder (*Alnus crispa*), bearberry, bog cranberry (*Vaccinium vitisideae*), and lichens (*Cladina* spp.) (Baldocchi et al., 1997a).

Table 3.1: Summary of various boreal forest stand characteristics, mean daily ET and energy partitioning from May – Sept.

Species	Site	Age (Year)	Height (m)	d.b.h. (cm)	LAI (m^2 m^{-2})	Density (stem ha^{-1})	Soil Texture	ET (mm d^{-1})	β	Source
Jack pine *Pinus banksiana*	53.9°N 104.7°W	60-75 (1994)	13	11.7	1.9-2.2	1600-2400[2]	Sand	0.6 – 1.8	1.35	Baldocchi et al., 997a,b
Jack pine *Pinus banksiana*	55.9°N 98.3°W	25 (1994)	2.3	---	0.7-1.1	5700-42000[2]	Sand	0.5 – 2.0	2.0	McCaughey et al., 1997
Jack pine *Pinus banksiana*	53.9°N 104.7°W	<10 (2001)	2	1	0.6-1.0	8625	Sand	0.5 – 2.0	1.85	Amiro et al., 2006a
Black spruce *Picea mariana*	54.0°N 105.1°W	115 (1994)	10-11	8	4.5	5900	Peat over till	0.2 – 3.5	1.0-2.5	Jarvis et al., 1997
Aspen *Populus tremuloides*	53.7°N 106.2°W	70 (1994)	21	17	1.8[†]	830	Silty-clay	5.0 – 6.0 (max)	0.3-0.6[1]	Black et al., 1996
Siberian pine *Pinus sylvestris*	61°N 89°E	215 (1996)	16	28.0	1.5[*]	290	Sand	0.8 – 2.3	---	Kelliher et al., 1998
Norway spruce & Scots pine	60.3°N 17.3°E	50 (1995)	23-28	---	4-5	---	Sandy till	< 5.0	0.6-1.7	Grelle et al., 1997

[*] - LAI determined by biomass measurement.
[†] - Value is for aspen canopy only, and excludes the hazel understory.
[1] - Based on ensemble daytime monthly averages during full leaf (Blanken et al., 2001)
[2] – Based on values from Chen, 1996.

4 Methodology

4.1 Site Description

The study site (57° 03.8' N, 111° 39.8' W, elev. ~310m) is located on Syncrude Ltd's Mildred Lake mine site, about 40 km NNW of Fort McMurray, Alberta. The stand is a planted 15 year old jack pine forest growing on flat terrain, with sloping terrain (~10°) to the east and west due to its location on a tailing dyke that has a slope and bench profile. Uniform fetch extends several hundred meters to the north and south, with limited fetch (<100 m) to the east and west (Fig.4.1).

The region surrounding the study site is dominated by land disturbed by construction and mining activities, peat bogs, and mixed vegetation cover including white spruce, aspen, and jack pine. Some of the major landscape features directly surrounding the study site are a buffalo pasture several hundred meters to the west, a 9 km^2 tailings pond less than a kilometer to the east, and the mine processing plant approximately 2 km to the south (Fig. 4.2). There are however forests of various ages and species immediately surrounding the study area; the area to the east is dominated by relatively sparse young white spruce $\leq$ 2 m in height, and to the west the area is covered by relatively denser more mature trees.

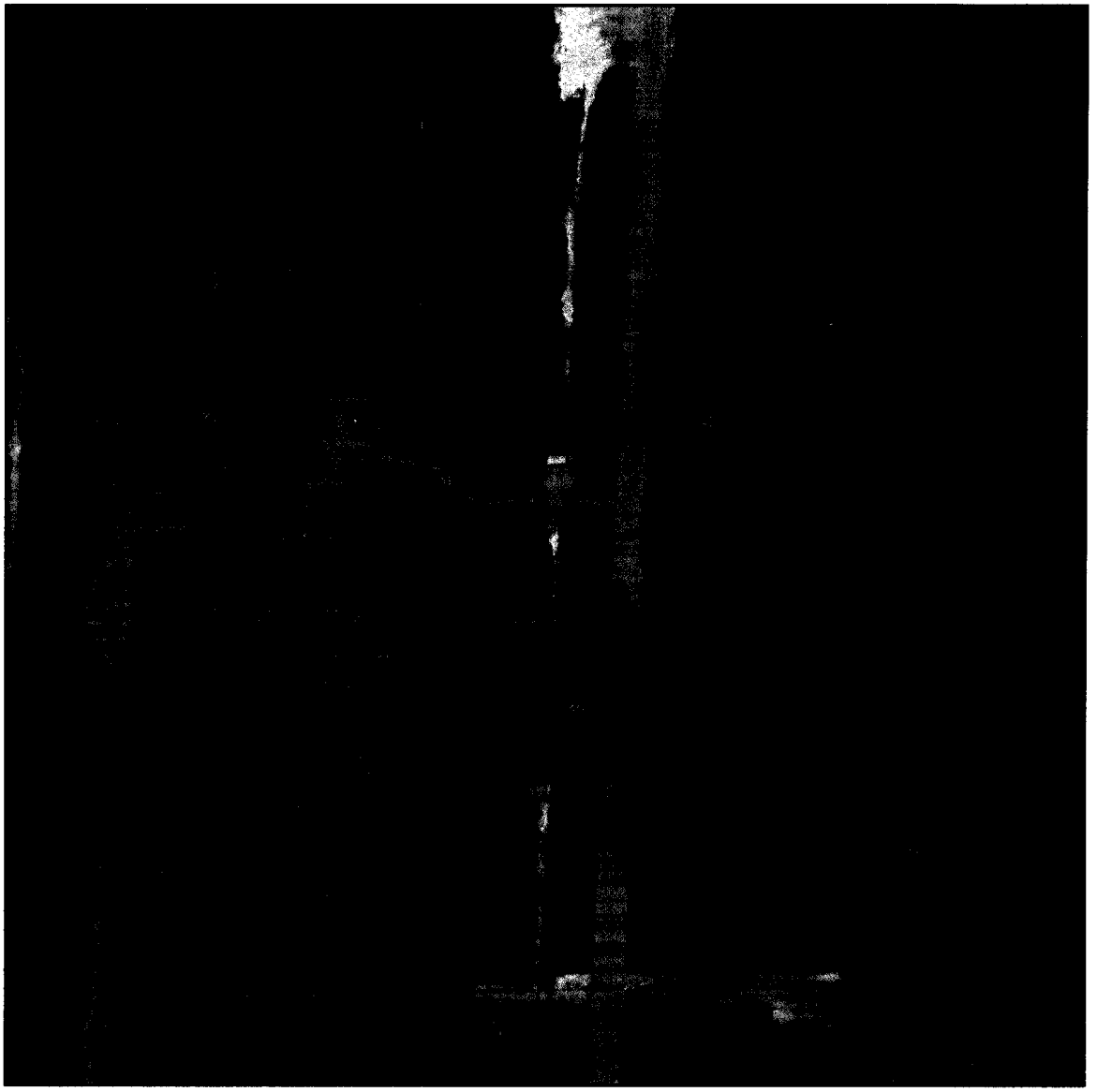

Figure 4.1: Satellite photo (Google Earth) of jack pine study site on cell 6 of Mildred Lake Settling Basin and surrounding area. Area of uninterrupted fetch containing only 15 year old jack pine on flat terrain is enclosed by the black polygon.

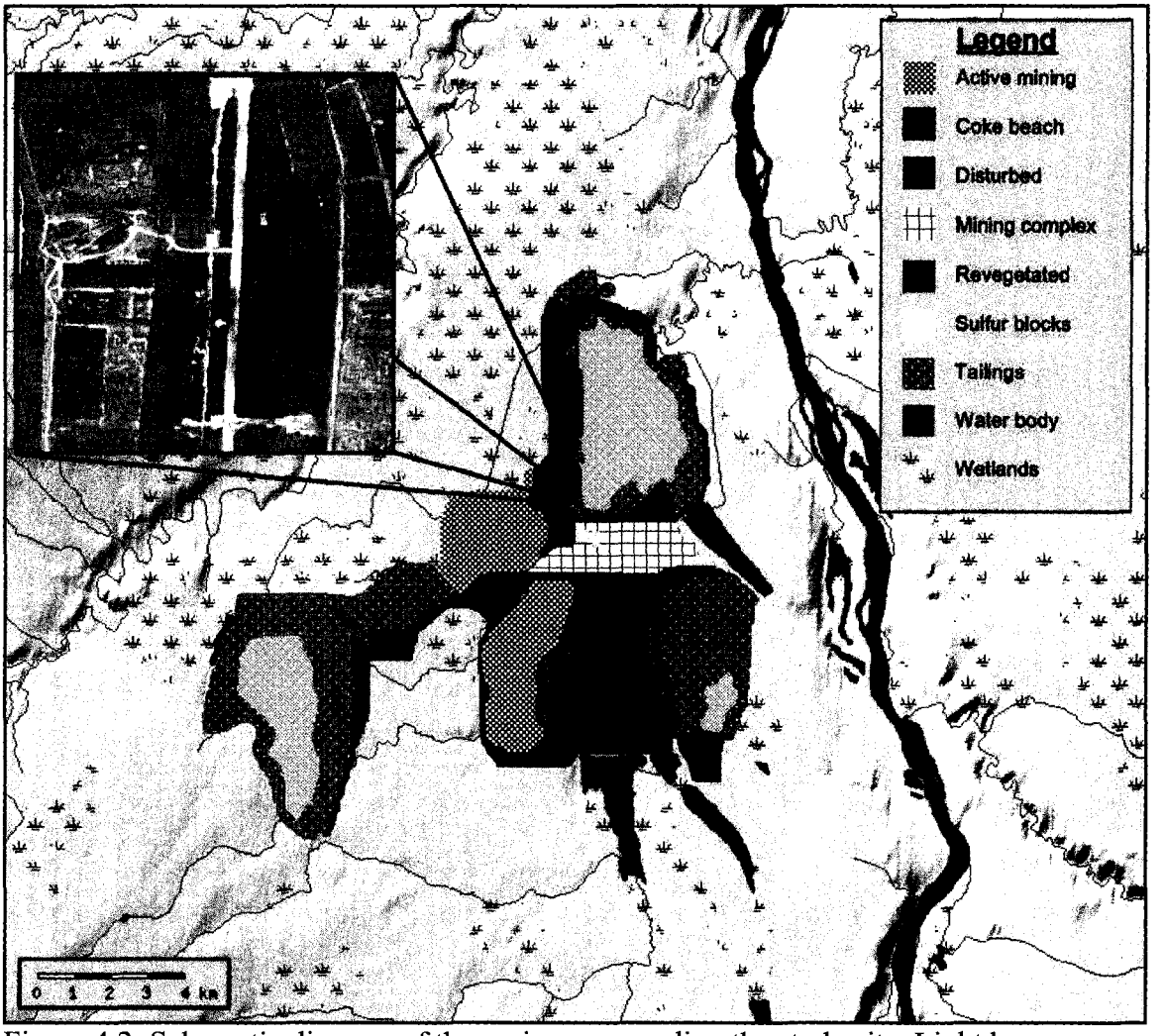

Figure 4.2: Schematic diagram of the region surrounding the study site. Light brown mottled texture within areas designated as tailings can be a combination of open water or unconsolidated tailings. The location highlighted corresponds to the area displayed in Figure 4.3.

The study site is located in a continental boreal climate regime, where, according to climate normals (1971-2000) from the Fort McMurray airport (56° 39' N, 111° 13' W, elev. ~370 m), mean daily temperature ranges from -18.8°C to 16.8°C (Jan. - Jul.), with average annual precipitation of 456 mm, of which 313 mm typically falls during the study period (Environment Canada) which ran from doy 139-282 (mid-May to early Oct.). The growing season for the Fort McMurray region is relatively short with between 60 - 70 frost-free days (Crown and Twardy, 1975).

General stand characteristics were determined by sampling 50 random trees in a ~1 ha sample area surrounding the tower on doy 222 (10 August). The results indicate that the jack pine stand had a mean height of 4.5 ± 0.7 m, a diameter at breast height of 6.5 ± 1.3 cm, and a stand density of *ca.* 2500 stems ha^{-1}. Virtually 100% of the tree species in the stand are jack pine, with a combination of young white spruce and jack pine surrounding the site. The understory vegetation consisted mainly of herbaceous species such as white and red clover (*Trifolium repens* and *T. pratense*), sweet clover (*Melilotus spp.*) raspberry (*Rubus ideaus*), buffaloberry (*Shepherdia canadensis*), bird's-foot trefoil (*Lotus corniculatus*), common yarrow (*Achillea millefolium*), and grasses. The soil is till down to an average depth of 40 cm, under which is a sandy soil derivative from the oil sands extraction process.

Micrometeorological measurements began on doy 139 (19 May 2007), and ended doy 282 (9 October 2007), with soil monitoring sensors running continuously since installation in November, 2006.

4.2 Flux Measurements

To measure the turbulent fluxes of energy, momentum, and scalars at the site, an open-path eddy covariance system was used, mounted approximately 4 m above the canopy at height of 8.8 m. The EC instrumentation consisted of a CSAT3-3D sonic anemometer-thermometer (Campbell Scientific Inc. (CS), Logan, UT) and an open-path LI-7500 infrared gas analyzer (IRGA) (LI-COR Inc., Lincoln, NE). The three orthogonal components of wind speed, as well as virtual temperature derived from the speed of sound, were obtained from the sonic anemometer. Water vapour and carbon dioxide (CO_2) mass density were measured using the open-path IRGA. A HMP45C temperature-humidity probe (Vaisala, Helsinki, Finland) and a 05103 wind monitor (R.M. Young Co., Traverse City, MI) were used to check half-hourly averaged values obtained from EC instrumentation.

Radiant fluxes of various wavelengths were measured with instrumentation mounted at a height of 6.3 m. Net all-wave radiation was measured using a CNR1 net-radiometer (Kipp and Zonen, Delft, Holland). Incoming and reflected shortwave radiation was obtained from the pyranometer sensors, which are part of the aforementioned net-radiometer. Incoming and reflected photosynthetic photon flux density (PPFD) was measured using two QSO-S quantum sensors (Apogee Instruments, Logan, UT).

For the remaining component of the energy balance (Eq. 2.3) measured at the study site, ground heat flux (G) was obtained using a soil heat flux plate at 5 cm and the average measurement from three thermocouples inserted 3cm below the surface located directly north of the tower, 3 m from the base. In order to account for soil heat storage in the top 5 cm of soil, Equation (4.1) was used to obtain G at the surface.

$$G_0 = G_{5cm} + M \tag{4.1}$$

where M is the rate of change of heat stored in the top 5 cm of soil and defined as:

$$M = zC\frac{\Delta T}{\Delta t} \tag{4.2}$$

where z is the thickness of soil above the heat flux plate (m), C is the volumetric heat capacity of the soil (J m^{-3} K^{-1}), and ΔT is the change in temperature (K) over the time interval Δt (s).

All EC data was recorded at 10Hz using a CR1000 measurement and control system (CS), storing both high-frequency data and online fluxes calculated every half hour. Climate data, including R_n, G, and PPFD, were measured every 10 s with 30 min averages stored using a CR23X data-logger (CS).

4.3 Supplementary Measurements

Precipitation data was measured using a tipping-bucket rain gauge (TE52M, Texas Electronics, Dallas, TX), located less than 1 km west of the tower. Daily precipitation totals were also cross referenced against measurements made at the Fort McMurray airport (Environment Canada). Although there is some agreement between the two data sets, there are significant differences in both magnitude and timing. A significant portion of summer rainfall in the region is the result of high intensity, short duration convective storms with high spatial variability. Furthermore, over the period measured, nearly 25% of rainfall occurred in the first or last two hours of the day, potentially affecting which day it was recorded on. The correlation of precipitation to values measured at other weather stations at Syncrude was much better, ranging between 80 – 90%, compared to 26% for the Fort McMurray airport data.

Soil moisture, soil suction (both calibrated to the specific soil layers), and soil temperature were measured in a profile at depths of 5, 15, 30, 50, and 80 cm. Volumetric water content (VWC) was measured using CS616 water content reflectometers (CS), soil suction using 229 water matric potential sensors (CS), and soil temperature using thermistors (107B, CS). Soil data was recorded every minute and averaged over 4 hours using a CR10X data-logger (CS). To interpolate soil data to coincide with EC and climate data recorded every 30 minutes, a piecewise cubic hermite interpolating polynomial was used (The MathWorks, 2007).

Periodic or one time measurements were made for stand height, diameter at breast height, density, and leaf (or rather plant) area index. Stand density for the jack pine was estimated using the variable-area transect method presented by Krebs (1999). This involved measuring the distance from a random point to the n^{th} individual parallel to a fixed width transect and was calculated as:

$$\hat{D} = \frac{n^{th} N - 1}{w_t \sum (l_i)} \tag{4.3}$$

where n^{th} is the rank of the individual (2^{nd}), N is the sample size (50), w_t is the transect width (m) (2 m) and l_i (m) is the distance between the random point and the n^{th} individual.

This method yielded a stand density of approximately 0.22 stems m^{-2} or 2176 stems ha^{-1}. This corresponds reasonably well with an initial estimate of ~2850 stems ha^{-1}, which was obtained from the estimated tree count in the sample area (2500 stems) and the area of the sample plot (~0.88 ha – using GPS coordinates). The variable-area transect method assumes a random spatial distribution of trees, which is not the case for the ordered planted rows of the jack pine stand. However, using the Kolmogorov-Smirnov

test statistic for goodness of fit to a random normal distribution, the null hypothesis that the spatial distribution of the jack pine stand is not different from a random distribution is not rejected at the critical value $\alpha = 0.10$, but is rejected at $\alpha = 0.05$.

LAI was assessed at three locations every other week from doy 140 (20 May) to doy 207 (26 July), using a LAI-2000 plant canopy analyzer (LI-COR) with a 180° view restriction. Measurements were made under both cloudy and clear sky conditions, typically during early or mid afternoon due to logistical constraints. In addition to the use of the 180° view restriction, an attempt was made to reduce direct beam radiation by casting a shadow on the sensor by placing the operator between the sun and the sensor, as suggested in the LAI-2000 instruction manual. In situations where the LAI-2000 could view needles lit by direct sunlight, the possibility of LAI being underestimated increased.

A further source of error in the LAI measurement comes from underestimations resulting from the clumped arrangement of needles on shoots of coniferous stands (Stenberg, 1996). A correction factor for clumping was not assessed because it is partly offset by woody material being in the sensor view field. According to Chen (1996) optical measurements of LAI for conifers by instruments such as an LAI-2000 can be in error up to 15 – 40% as a result of instrument error, needle clumping, and woody area.

4.4 Methods of Analysis

4.4.1 Flux Covariance Computations

The eddy covariance method was used to measure turbulent fluxes of sensible heat (H), latent heat (LE), and carbon dioxide (F_c) on a continuous basis, where mean covariances between vertical wind speed (w') and the respective scalars (T, ρ_v, ρ_c) were calculated according to Equations (2.5 - 2.7) in Section (2.3.1).

Sonic anemometer wind vectors were mathematically rotated following the tilt correction algorithms presented by Wilczak et al. (2001), also known as the planar fit method. Rotation into the planar fit coordinate system was used as opposed to the natural wind coordinate system presented by Tanner and Thurtell (1969) because of shortcomings outlined by Law et al. (2004). The traditional coordinate rotation involves mathematically rotating the component wind vectors such that mean vertical wind ($\overline{w}$), lateral wind ($\overline{v}$), and cross-wind momentum ($\overline{v'w'}$) are forced to zero for every averaging period (Restrepo and Arain, 2005). This results in the x-axis being parallel and the z-axis normal to the mean wind streamline (Humphreys, 1999). This can cause problems in sloping or complex terrain, resulting in flux bias errors as a result of over-rotation (Law et al., 2004). Furthermore, rotation into natural wind coordinates every averaging period effectively acts as a high-pass filter, excluding the contributions of eddies with a period greater than the averaging period. The planar fit method differs because it involves a post-field procedure which aligns the z-axis normal to the mean streamline plane, which is determined from observations made over a period much longer than a single averaging period. In this way, the z-axis is fixed over all averaging periods for a given site so long as the sonic anemometer is not moved or repositioned.

The relative difference between turbulent fluxes measured using the planar fit of Wilczak et al. (2001) and the traditional coordinate rotation of Tanner and Thurtell (1969) was assessed from doy 140 – 180. Results were not consistent between H and LE, where planar fit values differed by 2.1 ± 27 % and -3.7 ± 32 % from 3-axis coordinate rotation, respectively. The relative difference for the CO_2 flux over the same sample period was -6.2 ± 25 %.

Detrending or mean removal was used to separate the turbulent flux from deterministic atmospheric motions. It is analogous to Reynold's averaging (e.g. $s = \bar{s} + s'$), where the time-series s is composed of its mean component (overbar) and the instantaneous deviation (prime). According to Stull (1988), the separation of mean and turbulent components has a physical basis, known as the spectral gap, where a separation of scales exists where little atmospheric motion occurs at time scales with period between approx. 0.5-1hr. Without a separation of scales, the turbulent component would contain deterministic low frequency motions.

Law et al. (2004) identify that the 15-30 minute averaging period commonly employed in eddy covariance is based on studies of fluxes from short vegetation (corn stubble) over flat, homogenous terrain. Recent papers have suggested that the optimum averaging length need not fall within this traditional boundary and depends on site characteristics and instrument setup, particularly measurement height (Finnigan et al., 2003), because the separation of scales may not be as pronounced or the spectral gap may be located at a different frequency.

Examining the spectra and cospectral plots would allow for the spectral gap to be identified. However, this involves comparison to some chosen standard. An alternate method suggested by Law et al. (2004) that provides an unbiased method for choosing the averaging period involves using ogive curves (Eq. 4.4) which are integrals of the (co)spectral curves that show the cumulative contribution of eddies of increasing period to the total transport:

$$Og_{w,c}(f_o) = \int_{f_o}^{f_{max}} Co_{w,c}(f)df \tag{4.4}$$

where $Co_{w,c}$ is the cospectral density of vertical velocity and a scalar *c*, f is frequency, and $Og_{w,c}(f_0)$ is the cumulative probability for frequency f_0. The frequency at which the ogive reaches an asymptote during stable conditions corresponds to the appropriate averaging period (Foken and Wichura, 1996).

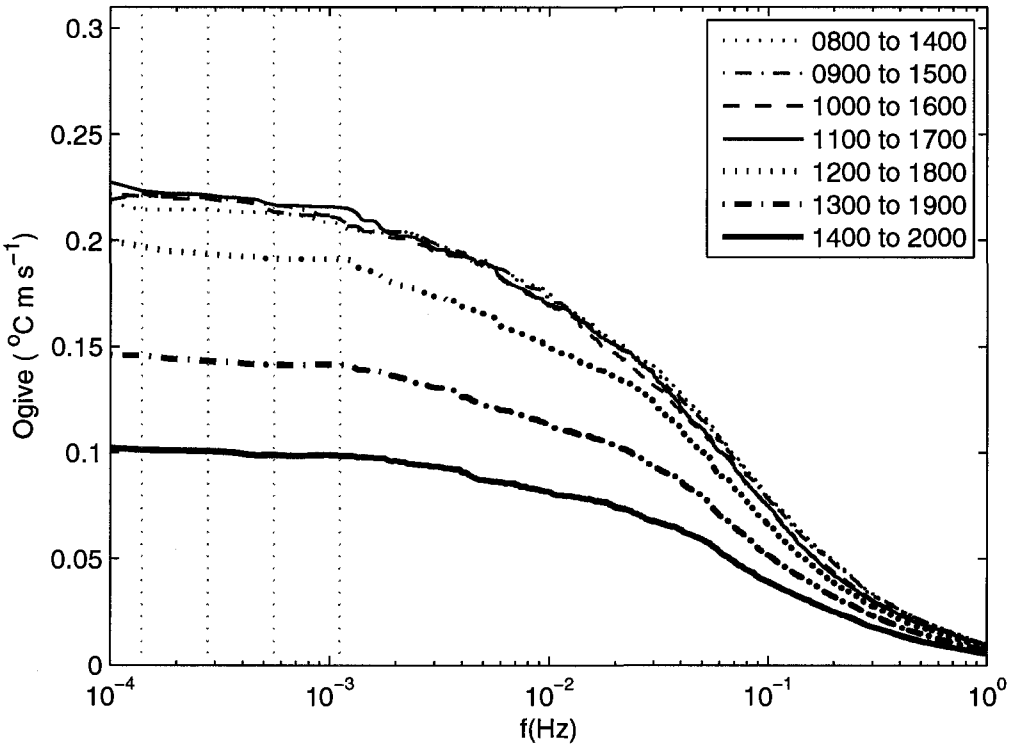

Figure 4.3: Ogive plots for the wT cospectra at the Mildred Lake jack pine tower on 30 May, 2007. Ogives are based on 6-hr high frequency data centered on each hour running from 1100 to 1700, thus covering the period 0800 to 2000. Vertical dashed lines correspond to a period of 120, 60, 30, and 15 minutes, from left to right.

One of the main problems with progressively longer averaging periods is that they are assumed to contain undesirable non-stationary periods. To try and minimize the effects of non-stationarity on the assessment of longer averaging periods, all half hourly data for the day chosen was subject to the steady state test (see section 4.5.4) used by Foken and Wichura (1996) which compares the covariance of the whole interval to the average covariance of smaller intervals. Intervals with less than a 30% relative difference between bulk and ensemble covariances are considered to be reasonably stationary; where all half hours used in the ogive test meet this criterion.

The results of the ogive test (Fig. 4.3) for 30 May 2007 show that an initial asymptote is reached at approximately 15 minutes. For all but the last 3 time periods there is a slight increase immediately after the 30 minute period, remaining constant until a period of 120 minutes. For the last three averaging periods, the ogive continues to increase, though only very gradually, for averaging periods greater than 30 minutes. Frequencies equivalent to averaging periods greater than 120 minutes are excluded since the number of eddies sampled with large periods of evolution would be very small, thus potentially generating large uncertainty from random error. The Ogive test indicates that the 30 minute averaging period used to calculate fluxes is adequate for measurements made over the jack pine forest canopy.

4.4.2 Calculation of zero-plane displacement

The zero-plane displacement (d) is the theoretical height above the surface where momentum is absorbed by the canopy as a result of skin and form drag (Monteith and Unsworth, 1990), which relates to the height at which wind speed extrapolates to zero ($d' = d + z_0$) (Campbell and Norman, 1998). This height can be determined by directly

measuring the wind speed profile at several heights, but d and z_0 are commonly approximated as a function of canopy height, with typical values of d = 0.67h, and z_0 = 0.1h (Oke, 1987). It should be noted that d and z_0 are a function of wind speed and direction, where increasing wind speed deforms the plant canopy and regular features, such as rows, alter the apparent surface roughness (Campbell and Norman, 1998).

Zero-plane displacement is used in calculating the log wind profile, which is expressed as:

$$U = \frac{u_*}{k}\left[\ln\left(\frac{z-d}{z_0}\right) - \Psi_m(\zeta)\right] \tag{4.5}$$

where U is equivalent to the cup wind speed at height z, u_* is the friction velocity ($u_* = \left(\overline{u'v'}^2 + \overline{v'w'}^2\right)^{0.5}$, z_0 is the surface roughness length, and $\Psi_m(\zeta)$ is a stability correction factor for stable and unstable conditions (Brutsaert, 1982). In practice *d* is commonly used as part of a thermal stability parameter (ζ) (Garratt, 1992) so that comparisons can be made for flux relations stratified by stability. For example, when comparing turbulent spectra/cospectra of different periods, frequency (f) can be normalized by ζ, which serves to phase shift spectra so that peak frequencies are coincident. The thermal stability parameter is expressed as:

$$\zeta = \frac{z-d}{L} \tag{4.6}$$

where *z* is the measurement height, *d* is the zero-plane displacement, and *L* is the Monin-Obukhov scaling length. The scaling length *L* is the height where turbulent production by shear and form drag and suppression by negative buoyant forces are in balance (Garratt, 1992), and is expressed as:

$$L = -\frac{u_*^3 \theta_v}{kg\overline{w'\theta_v'}} \tag{4.7}$$

where θ_v is the virtual potential temperature, k is the Von Karman constant (0.4), and g is the acceleration due to gravity. In some formulations of *L*, the virtual potential temperature in the numerator is substituted for virtual temperature (T_v).

Zero-plane displacement was determined using an iterative method presented in Humphreys (1999), where *d* was initially set to the typical value of 0.67h and then used to evaluate ζ and isolate half hours with neutral or near-neutral stability ($|\zeta|<0.02$). The ratio of U/u_* for these half hours was substituted into a modified log wind profile equation based on Equation (4.5) to obtain a new estimate for *d*. The mean value of *d* was used to subsequently recalculate ζ and identify new neutral half hours. This process was repeated until the change in *d* between iterations became negligible. During the iteration process, z_o was evaluated as a fixed proportion of d ($a = z_o / d$).

Work by Shaw and Pereira (1982) presented in Campbell and Norman (1998) demonstrates that there is a relation between canopy density and foliage distribution, measured as plant area index (PAI), and the ratio of either z_0 or *d* to canopy height (h). Based on their results, with a PAI of approximately 1.5 for the jack pine stand, d = 0.60h and z_0 = 0.12h. This is in general agreement with the results of the iterative method described above where d was estimated as 3.72 ± 0.26 m, 2.90 ± 0.22 m, and 2.36 ± 0.21 m for z_0/d equal to 0.1, 0.15, and 0.2 respectively. The values of *d* correspond to 0.83h, 0.64h, and 0.52h. Using the intermediate values generated by the iterative method, *d* was taken to be 2.90 m (0.64h) resulting in z_0 equal to 0.10h based on a z_0/d ratio of 0.15.

4.4.3 Calculation of aerodynamic resistance

In describing the convective exchanges of energy and mass in the surface boundary layer, it is useful to use Ohm's Law where the magnitude of fluxes is dependent on resistance (Oke, 1987). Aerodynamic resistance represents the impediment of transfer for heat ($r_{a,h}$), water vapour ($r_{a,v}$), and momentum ($r_{a,m}$). Assuming the same flux source/sink location, $r_{a,h} = r_{a,v}$, and can be expressed as a function of $r_{a,m}$ (Liu et al., 2006):

$$r_{a,h} = \frac{\phi_h}{\phi_m} r_{a,m} + r_b \tag{4.8}$$

where ϕ_m and ϕ_h are the stability correction factors for momentum and heat, $r_{a,m}$ is equal to u/u_*^2, and r_b is excess resistance with several parameterizations, such as:

$$r_b = \frac{\ln\left(\frac{z_{o,m}}{z_{o,h}}\right)}{k u_*} \tag{4.9}$$

where $z_{o,m}$ and $z_{o,h}$ are surface roughness parameters for momentum and heat. For simplicity, when r_b takes the form of Equation (4.9) it is assumed that $\ln(z_{o,m}/z_{o,h}) = 1.6$ based on $z_{o,h} = 0.2 z_{o,m}$ (Campbell and Norman, 1998).

Aerodynamic resistance (or conductance) is used primarily in the Penman-Monteith equation (Eq. 2.16) which is used to assess the controls on ET. Two separate formulations of ϕ and r_b were compared (Table 4.1) when calculating $r_{a,h}$, where parameterization for ϕ was taken from Campbell and Norman (1998) and Arya (1988), and for r_b from Campbell and Norman (1998) and Liu et al. (2006) . Results indicate that

the different parameterizations of r_b and ϕ produce similar $r_{a,h}$ estimates. For consistency, the Campbell and Norman (1988) parameterizations were used for both ϕ and r_b.

Table 4.1: Results of $r_{a,h}$ calculations using different parameterizations of r_b and ϕ, where CN refers to Campbell and Norman (1998). Values are expressed as the fractional difference ± 1SD from $r_{a,h}$ calculated using CN parameterization, and separated by stability.

	Stable (ζ>=0)		Unstable (ζ<0)	
	ϕ_{CN}	ϕ_{Arya88}	ϕ_{CN}	ϕ_{Arya88}
$r_{b\text{-}CN}$	--	- 0.03 ± 0.04	--	- 0.02 ± 0.02
$r_{b\text{-}Liu\ et\ al.\ 06}$	0.01 ± 0.08	- 0.02 ± 0.05	0.07 ± 0.12	0.05 ± 0.11

4.4.4 Modelling of canopy wetness

A simple model was developed to determine when the canopy was wet or dry. This information was used to determine when to use equations for free evaporation or ET when assessing evaporative controls.

The canopy wetness model (Fig. 4.4), in essence, calculates the mass budget of the canopy based on three main elements: (i) water intercepted by the canopy, (ii) drainage/stem flow, and (iii) evaporative loss from a wet canopy. Evaporative loss from the canopy is estimated using Equation (4.10) obtained from the coupled hydrological model of Kuchment and Demidov (2006):

$$E_C = \rho_a \frac{q^*(T_f) - q}{r_a} \eta(1 - U_k) \tag{4.10}$$

where E_C is the wet canopy evaporative loss, ρ_a is the density of air, q^* and q are saturated and measured specific humidity respectively, r_a is aerodynamic resistance, and U_k is the canopy gap fraction. Also, it has been assumed that not all of the canopy contributes equally to evaporative loss due to exponential distribution of water within the canopy, and thus is estimated as $\eta = 1 - \exp(- C_{i-1}/W)$; where C is canopy storage, and W is maximum potential canopy storage. Some constraints are placed on estimated values, such as E_C, which cannot exceed canopy storage (C_{i-1}). Furthermore, direct measurements of LE are not used in place of E_C because direct measurements include evaporative loss from the understory and the soil surface.

An estimate of the free throughfall coefficient was obtained using a simplified methodology from Llorens and Gallart (2000), where the canopy gap fraction was analyzed based on pixel counts of 36 greyscale digital photographs. U_k was determined to be 0.87 ± 0.03, where areas identified as sky were considered an open path for rainfall. This method is assumed to overestimate U_k during clear sky conditions as a result of reflectance of direct beam radiation depending on needle orientation.

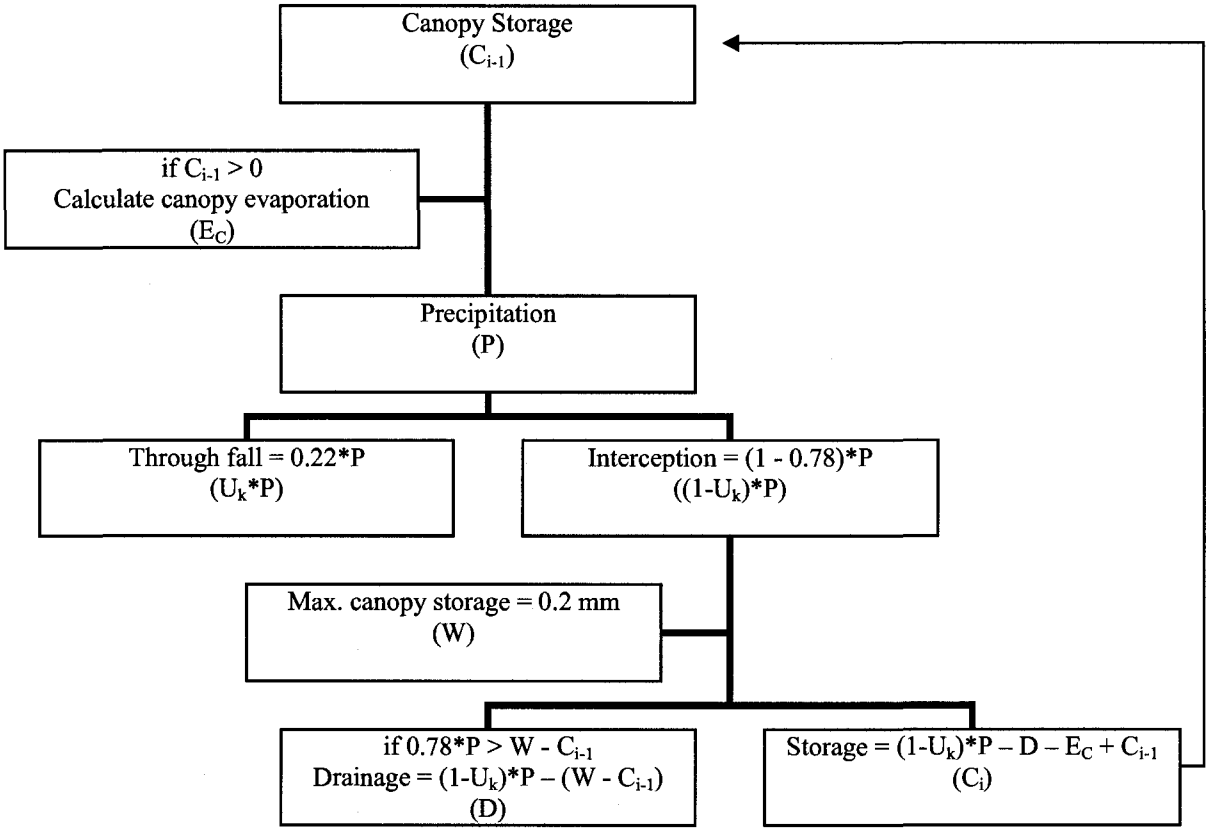

Figure 4.4: General flow chart of the canopy wetness model used to estimate when the canopy was saturated, partially wet, and dry based on measured precipitation, wind speed, specific humidity, and values derived from the literature for throughfall and canopy storage capacity for conifer species with similar stand statistics. Example values are from Kuchment and Demidov (2006)

The canopy gap fraction reported above is much higher than that reported in Kuchment and Demidov (2006) for a jack pine stand (Fig. 4.4). The value was based on a jack pine stand located near Nipawin, SK (53°54'58.82"N, 104°41'31.29" W; elevation 579.3m) (Baldocchi el al., 1997a) with comparative stand characteristics listed in Table 4.2. Differences in LAI and the overestimation of U_k could account for the difference.

The value for maximum canopy storage capacity was taken from Kuchment et al. (2006) being 0.2 mm. According to Chapin et al. (2002) canopy interception storage capacity can be related to LAI, but differs among species. Using the linear regression from Aston (1979), which relates W and LAI ($W = 0.094 + (0.065 \pm 0.012)*LAI$) for a conifer species (*Pinus radiata*), an estimate was obtained of 0.20 ± 0.02 mm. A review of canopy storage capacity by Llorens and Gallart (2000), however, indicates that W estimates for conifers range from 0.1 to 3.0 mm.

A simple sensitivity analysis was performed to see what effect an error in the estimate of maximum canopy storage capacity and free throughfall coefficients had on the modelled length of time the canopy remained wet. Values chosen for the sensitivity analysis were W = 0.1, 0.2, 0.4, 0.8, 1.6 and 3.0 mm, and U_k = 0.22, 0.4, 0.6, and 0.87.

The results can be seen in Table 4.3 where the values represent the total percent of half hours where the canopy was modelled to be wet. It should be noted that over the study period precipitation occurred on just over 3% of all half hours. A significant portion of partially wet canopy conditions are attributable to an extended period of time later in the study period, with very low VPD.

The percentage of time the canopy was modelled to be wet varied greatly, ranging from 9 – 82 % of all half hours (Table 4.3), based on the range of values of W and U_k

reported in the literature. It was assumed that an estimated W of 0.2 mm was reasonable since it was corroborated by the empirical relation described by Aston (1979). Imposing this constraint on the model, when canopy wetness was taken into account for data analysis, the high U_k estimate was used to define half hours with a dry canopy, and the low U_k estimate was used to define half hours with a wet or partially wet canopy.

Table 4.2: Stand characteristics from BOREAS jack pine site (SOJP) in Saskatchewan (53°54'58.82"N, 104°41'31.29" W) and Mildred Lake site (RJP92) in Alberta (N 57° 03.916' W 111° 39.818') measured during the growing season of 1996 and 2007 respectively. With respect to LAI, 'Plant' LAI includes woody material, while 'Leaf' value is an estimate with woody material removed.

Property	**SOJP**	**RJP92**
Age (y.o)	75-90	15
Mean height (m)	12.7	4.5 ± 0.7
d.b.h (cm)	12.9	6.5 ± 1.3
stand density (stems ha^{-1})	1320	~ 2500
'Plant' LAI (m^2 m^{-2})	2.5	1.38 -1.6
'Leaf' LAI (m^2 m^{-2})	2.3	--

Table 4.3: Results of sensitivity analysis on canopy wetness model. Values indicate the fraction of half hours where the canopy was modelled as being wet or partially wet.

W	U_k			
	0.22	0.4	0.6	0.87
0.1	0.09	0.09	0.12	0.20
0.2	0.13	0.14	0.17	0.31
0.4	0.17	0.19	0.24	0.40
0.8	0.24	0.28	0.34	0.54
1.6	0.34	0.38	0.46	0.71
3.0	0.46	0.51	0.59	0.82

4.4.5 Flux footprint

It is important to have an understanding of the size of the contributing flux source area and distance of maximum potential influence, especially where extensive uniform fetch is not present in all directions. Depending on estimates of footprint size, flux data may be rejected based on mean wind direction because of inadequate fetch.

The one-dimensional analytical solutions (Schuepp et al., 1990) for the flux footprint based on measurements made at a height z under neutral stability can be expressed as:

$$\frac{1}{Q_0}\frac{dQ}{dx} = (-)\frac{U(z-d)}{u_* k x^2} e^{-U(z-d)/ku_* x} \qquad (4.11)$$

where the l.h.s is the relative flux contribution at an upwind distance x, and U is the average wind speed between $d + z_o$ and z based on a log wind profile, and is calculated as:

$$U = \frac{u_*[\ln((z-d)/z_0) - 1 + z_0/(z-d)]}{k(1 - z_0/(z-d))} \tag{4.12}$$

To obtain the distance for which measurements are most sensitive, the first derivative of Equation (4.11) is taken with respect to x and is set to zero (Schuepp et al., 1990):

$$x_{max} = \frac{U}{u_*}\frac{(z-d)}{2k} \tag{4.13}$$

Similarly, to obtain the cumulative flux contribution for a given upwind distance, Equation 4.11 is integrated between 0 and x. According to Schuepp et al. (1990) footprint analysis produces adequate estimates under neutral stability, being within 20% of numerical simulations. However, corrections should be made for stability since footprints contract under unstable, and expand under stable conditions. The U/u_* ratio was multiplied by a stability correction factor (ϕ_m) with parameterization suggested in Campbell and Norman (1998). Similar to results presented in Blanken et al. (2001), the mean value of the stability parameter ζ was assessed for daytime and nighttime conditions, where the effect on the flux footprint can be seen in Figure (4.5).

Results indicate that measurements are most sensitive to areas relatively close to the tower during all stability conditions, where according to Equation (4.13), x_{max} is about 11 m, 8 m, and 28 m under neutral, unstable, and stable conditions respectively. Fetch is considered adequate when its boundaries extend to an upwind distance equivalent to at least 80% of the contributing flux footprint. Based on Figure (4.5 - lower panel), 80% of the flux is contributed from a distance up to 100 m, 76 m, and 250 m from the tower

under neutral, unstable, (daytime $\overline{\zeta} = -0.12$), and stable (nighttime $\overline{\zeta} = 0.34$) conditions. This implies that under unstable conditions, fetch is adequate in all directions. For neutral and stable conditions, fetch would be adequate from the north and south, with east-west fetch being questionable for neutral conditions and inadequate for stable conditions because of inadequate distance for a fully adjusted boundary layer to form. As a result of inadequate fetch based on the modelled flux footprint, data from periods when the mean wind direction was from the east or west quadrant was flagged for further analysis.

Measured half hourly average wind direction was not uniformly distributed (not shown), with relatively little wind coming from the north. With approximately 58% of all wind measurements coming out of either the east or west quadrant, and 24% and 36% of those measurements being neutral or stable respectively, up to 14% of all measured fluxes would have questionable fetch and 21% would have inadequate fetch. These values are likely overestimates since the east and west quadrants depart ±45° from 90° and 270°, with fetch increasing as wind direction moves away from due east and west.

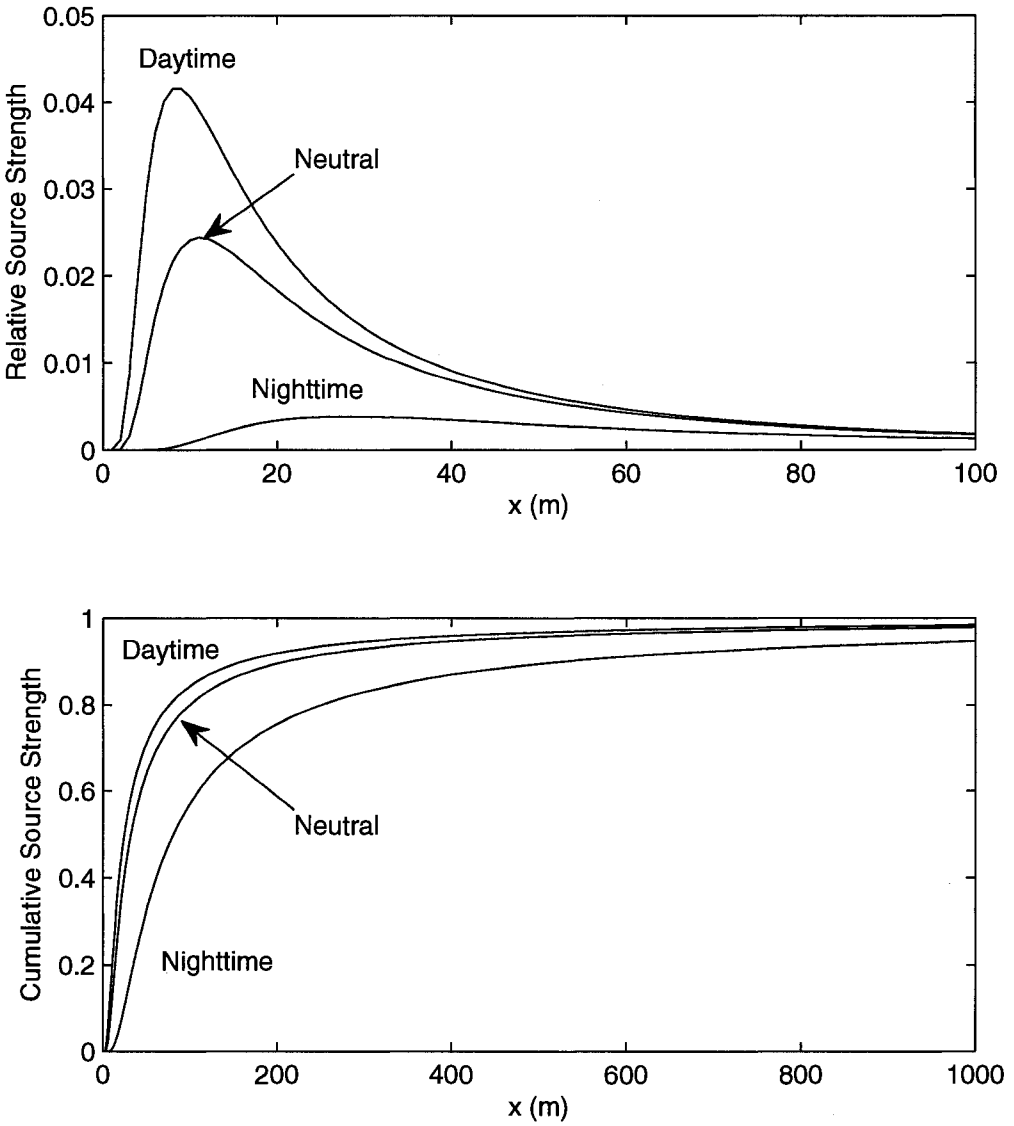

Figure 4.5: Relative (upper panel) and cumulative (lower panel) flux footprint predictions for a measurement height of 8.8 m during neutral stability, mean daytime ($K\downarrow > 0$ W m^{-2}), and nighttime ($K\downarrow = 0$ W m^{-2}) stability conditions ($\zeta = -0.12$ and 0.34 respectively).

4.5 Quality Control and Assurance

An extensive flagging system was employed to examine suspected problem data based on simple turbulent statistics such as standard deviation, skewness, and kurtosis. As well, high frequency spiking, requirements of steady-state and developed turbulence, a friction velocity threshold, and spectral characteristics were examined. A 'hard' and 'soft' flagging system, modelled after Vicker and Mahrt (1997), was used where data with hard flags were removed outright and soft flagged data were subject to further inspection. Relations between soft flagged data and periods of rain, low u_*, or different stability conditions were examined to try to simplify data screening criteria to a minimum number of variables affecting data quality.

Hard flagged data was processed by a combination of automated routines and manual inspection with resulting single half hour gaps being filled by linear interpolation and gaps of up to a few hours in length being filled using mean diurnal variation according to Falge et al. (2001).

4.5.1 Evaluation of statistics

Simple procedures for removing physically unrealistic data involved comparing data to predefined maximum and minimum limits such as 0 – 65 g m^{-3} for water vapour density and -20 – 50°C for summer temperature, where data outside of these ranges was hard flagged. As part of the overall quality assurance flagging system, higher moment statistics were evaluated such as skewness and kurtosis. According to Vickers and Mahrt (1997) skewness and kurtosis can be used to detect instances of poor instrument performance and statistically unusual behaviour. Empirically determined threshold values

for soft and hard flags used were respectively (-1,1) and (-2,2) for skewness, and (2,5) and (1,8) for kurtosis (Vickers and Mahrt, 1997).

Table 4.4 shows the results of soft and hard flagging for u, v, w, T, ρ_v and ρ_c based on skewness and kurtosis criteria. All wind speed components and ρ_v follow the same pattern where, compared to overall results (n = 6570), soft and hard flags decrease under unstable conditions ($\zeta < 0$, n = 3399) and increase under stable conditions ($\zeta > 0$, n = 3162) for both skewness and kurtosis. T only follows this pattern for hard flags. For soft flags, a greater portion of temperature data is identified as unusually skewed and kurtotic while $\zeta < 0$, but still considered physically possible, compared to $\zeta > 0$. This is potentially due to the effect of significant partitioning of energy to sensible heat during daytime convective conditions. The increase in hard flags under stable conditions can be attributed to the more intermittent nature of turbulence under stable conditions.

Table 4.4: Summary of the percentage of data soft and hard flagged based on skewness and kurtosis according to empirically determined thresholds (Vickers and Mahrt, 1997).

			u	v	w	T	ρ_v	ρ_c
Skewness	[-1, 1]	Total	0.9	1.0	0.2	6.1	8.4	15.0
		$\zeta < 0$	0.6	0.7	0.1	8.3	6.1	14.7
		$\zeta > 0$	1.3	1.2	0.3	3.7	10.8	15.3
	[-2, 2]	Total	0.1	0.0	0.0	0.4	1.7	4.8
		$\zeta < 0$	0.1	0	0	0.3	1.1	5.4
		$\zeta > 0$	0.1	0.0	0.1	0.4	2.2	4.2
Kurtosis	[2, 5]	Total	1.4	2.2	7.5	6.1	13.4	20.4
		$\zeta < 0$	0.7	1.5	2.4	6.3	8.8	17.7
		$\zeta > 0$	2.1	2.9	12.9	5.7	18.3	23.2
	[1, 8]	Total	0.2	0.2	1.1	1.0	3.6	9.1
		$\zeta < 0$	0.1	0.1	0.2	0.7	2.4	9.2
		$\zeta > 0$	0.3	0.3	2.0	1.2	4.8	8.9

4.5.2 Spike detection and removal

Spikes are typically characterized as large amplitude departures from the time series resulting from random noise or non-ideal weather conditions (Brock, 1986; Law et al., 2004). As such, only spikes of 0.1 s length were identified for removal from the high frequency time series. Values not falling within a realistic range for a given variable (e.g. $0 > \rho_v > 65$ g m^{-3}) were removed prior to spike identification and removal, as well as error values corresponding to NaN or -9999. Spikes were identified using a methodology similar to Vickers and Mahrt (1997), with spikes considered points in a time series with an amplitude greater than several standard deviation from the mean. The mean was constructed as a recursive digital filter (Kaimal and Finnigan, 1994):

$$\widetilde{c}_k = \left(1 - \frac{\Delta t}{\tau_f}\right)\widetilde{c}_{k-1} + \frac{\Delta t}{\tau_f} c_k \tag{4.14}$$

where c is an arbitrary variable, Δt is the incremental time step between measurements, and τ_f is the RC filter time constant. Equation 4.14 is obtained through a simplification that assumes that $\Delta t << \tau_f$; which were 0.1 s and 60 s respectively. Cut-off values for spike identification were chosen such that the exceedance probability was 10^{-4} in order to minimize false positives. This level of exceedance probability corresponds to a SD of about 3.9, where typical cut-off values range between 3 and 5 (Baldocchi et al., 1997a; Vickers and Mahrt, 1997; Humphreys, 2006). Gaps produced by spike removal in the high frequency time series were filled by linear interpolation between adjacent points.

During nighttime, or otherwise stable conditions, variability in turbulent time series can be suppressed. As a result of potentially low variance, relatively large deviations from the mean could be incorrectly identified as spikes despite being driven by

real physical phenomena. Therefore, a threshold algorithm was employed to accept/reject the initial results of the spike filter. In addition to evaluating each point with respect to the local mean and standard deviation, potential spikes had to exceed adjacent measurements by a predefined threshold; so long as said points were not themselves identified as spikes. Thresholds were determined by evaluating the ensemble first-order moments of the difference time series of the respective variables for all half hours, every second day of June 2007 (total 720 half hours). Though the original time series may not all have had good normal distributions, the difference distributions did. As such, spikes were identified when they exceeded adjacent points by four times the S.D. of the respective difference distribution. When the half hour spiking rate exceeded a given threshold, chosen as 5 spikes per half hour, the half hour was flagged for removal (Law et al., 2004; Humphreys, 2003).

Table 4.5: Threshold by which a data point identified as a spike must exceed its neighbouring values to be accepted as a spike.

Variable	Threshold (3.9* SD)
u	1.34 ms^{-1}
v	1.24 ms^{-1}
w	1.12 ms^{-1}
CO_2*	3.75 mg m^3
H_2O*	0.55 g m^3
T	0.53 °C

* sample depth is 719 instead of 720

Spikes were detected in a significant portion of half hours based on the algorithms used. For any given criteria listed in Table (4.6), there is a lot of variability between variables for the percent of the data set that contains spikes, where spiking tended to be greatest for ρ_c, and least for T. Overall, the spiking rate for ρ_v was lower than T, however ρ_v spiking was higher during precipitation and high RH compared to T. Furthermore, results presented in Table 4.6 tend to indicate that periods of precipitation and high RH adversely affect the spiking rate for IRGA measurements more than sonic data. Among variables, though, high RH does not seem to have a significant effect on the spiking rate when compared to precipitation.

Table 4.6: Percentage of half hours with spikes in the high frequency time series. Results are binned into all half hours (n = 6575), half hours with precipitation (n = 183), and those with high relative humidity (n = 747).

	Total	Precip.	RH ≥ 0.9	Total	Precip.	RH ≥ 0.9
	% with >= 1 spike ½ hr^{-1}			% with >= 5 spike ½ hr^{-1}		
u	25.0	32.2	8.6	2.4	4.9	0.5
v	16.1	19.7	5.4	1.9	2.2	0.9
w	32.3	41.5	8.7	5.3	11.5	1.2
ρ_c	31.3	70.0	27.4	11.2	48.6	5.6
ρ_v	9.3	55.2	3.4	1.4	13.1	0.8
T	15.5	13.1	1.6	1.5	4.9	0.0

4.5.3 Assessment of steady-state requirements and developed turbulence

In order to asses the steady state requirement for half hour averaging periods, the average covariance of several shorter time intervals (5 minutes length) (Eq. 4.15) were compared with the covariance for the entire half hour. The average covariance of the N periods was calculated as:

$$\begin{aligned} \left(\overline{x'w'}\right)_i &= \frac{1}{N-1}\left[\sum_j x_j w_j - \frac{1}{N}\sum x_j \sum w_j\right] \\ \overline{x'w'} &= \frac{1}{M}\sum_i \left(\overline{x'w'}\right)_i \end{aligned} \tag{4.15}$$

where x is an arbitrary variable, N is the number of samples corresponding to 5 minutes and M is the number of segments (M = 6) calculated per half hour.

Foken and Wichura (1996) suggest that steady state conditions are generally met when the relative difference between both measures of covariances is less than 30%. Test results indicate steady state conditions for u, T, ρ_v, and ρ_c following coordinate rotation 89.3%, 92.1%, 83.7%, and 80.4% of the time respectively, where coordinate rotation increases the number of half hours considered stationary by 11.4 ± 1.0 %. Similar to the results of Section 4.5.2, diagnostics indicate that covariances associated with only sonic variables are more stationary than IRGA variables. Because of this link, the effect of precipitation on the measure of stationarity was assessed. Precipitation had very little effect on the proportion of half hours considered stationary for sonic variables (~93%), whereas the proportion of ρ_v and ρ_c considered stationary decreased to 71.7% and 59.8% respectively.

To test for developed turbulent conditions, flux variance similarity is used with the general form (z/L < 0):

$$\frac{\sigma_x}{X_*} = c_1\left(-\frac{z}{L}\right)^{c_2} \tag{4.16}$$

where σ is the variance of a wind component, temperature, or other scalar, X_* is their dynamical parameter (u_* for wind components and $T_* = -\overline{(w'T')}/u_*$ for temperature), and c_1 and c_2 are coefficients of integral turbulence formulated by Folken and others, and are dependent on stability (Foken and Wichura, 1996; Law et al., 2004). According to Kaimal and Finnigan (1994) the wind velocity components u and v do not follow Monin-Obukhov similarity, therefore the test was performed for w and T only.

Similar to the test for stationarity, an integral turbulence characteristic parameter (ITC), which is simply the relative difference between the measured flux-variance ratio and the modelled ratio of Equation (4.16), is evaluated. For any given half hour, if the test parameter is less than 30%, it is assumed that turbulent conditions are well developed (Foken and Wichura, 1996).

According to the ITC for w, this test indicates that well developed turbulent conditions are present 96.7% (n = 6013) of the study period with 74.3% of poorly developed turbulent conditions occurring at night or periods of low radiant forcing ($K\downarrow$ < 50 W m^{-2}). Figure (4.6) shows that the relation between ϕ_w and ζ = (z-d)/L conforms better to the predicted values within the stable region ($\zeta > 0$) while turbulence seems to be suppressed, although within acceptable error bounds, during unstable conditions ($\zeta < 0$). The ITC test performs much worse for T, where well developed turbulent conditions are indicated 17.5% and 59.8% of the study period based on ϕ_T parameterization from

Kaimal and Finnigan (1994), and Foken and Wichura (1996) respectively. Among the main differences in the two parameterizations is that c_1 and c_2 in Equation (4.3) are not defined for $\zeta \geq 0$ in Foken and Wichura (1996). ITC is particularly poor during stable conditions for T based on a comparison of $\square_T$ and ζ (not shown). Nevertheless, ITC_T is successful only 34.6% of time while $\zeta < 0$ for the parameterization of Kaimal and Finnigan (1994).

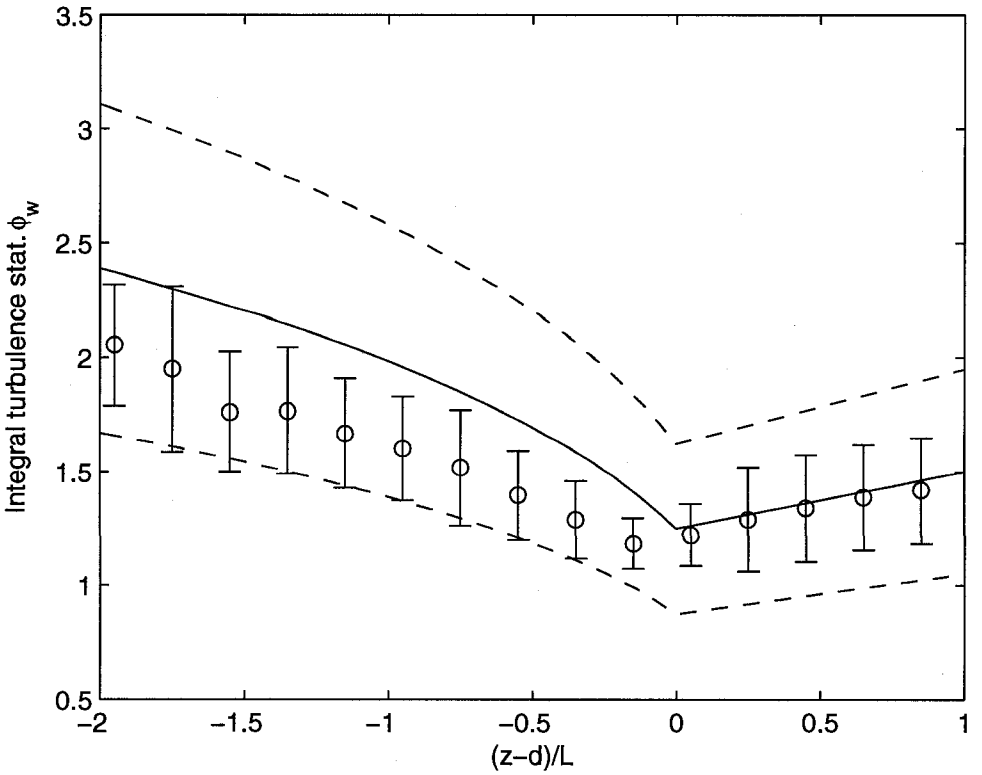

Figure 4.6: Integral turbulence statistic ($\phi_w = \sigma_w / u_*$) versus stability over the range defined by the modeled parameters of Kaimal and Finnigan (1994). Mean and ±1 standard deviation of ITC corresponds to circles (○) and error bars. Modeled similarity function and 30% cutoff range are shown as solid and dashed lines respectively.

4.5.4 Flux corrections

When using eddy covariance, it has been found that there is a systematic underestimation of turbulent fluxes on the order of 10-30% when mixing is suppressed and wind speeds are low such as during the nighttime (Lavigne et al., 1997; McCaughey et al., 1997). The degree of energy balance closure is typically assessed by taking the slope of the relation described as follows:

$$(H + LE) = a \cdot (R_n - G) + b \tag{4.17}$$

where a and b are the slope and y-axis intercept parameters, respectively, for the linear regression between available energy and the sum of turbulent fluxes. However, unless otherwise stated, this study grouped G with H and LE. This is because the ordinary least square (OLS) fit assumes all error is in the dependent variable. Because G was determined from a single heat flux plate, it was assumed to have significant relative error due to spatial variability in canopy cover and distribution of understory vegetation. In addition, the basis for evaluating energy balance closure assumes that there is a relative degree of accuracy in the R_n measurement. Without this modification, closure is likely systematically underestimated unless a weighted least squares regression is used. S was not measured, in part, because it was assumed to be negligible for the relatively short jack pine stand, where S values for relatively tall forests tend to be of a similar magnitude or smaller than G on a half hourly basis, and near zero on a daily basis.

Table 4.7: Linear least square regression of R_n v. H+LE+G

Period	a	b	R^2
Total	0.866 ± 0.003	15.1 ± 0.5	0.94
Daytime	0.859 ± 0.004	17.6 ± 0.7	0.93
Nighttime	0.730 ± 0.018	5.65 ± 0.44	0.46

Linear regression parameter estimates include uncertainty corresponding to 95% confidence interval.

Other studies correct for the underestimation of turbulent fluxes by multiplying both H and LE by $(a)^{-1}$ to maintain proportionality between the two fluxes (Blanken et al., 1997; Barr et al., 2006). Table 4.7 summarizes the results of the energy balance closure based on the linear regression of half hour data for the entire study period. Results indicate that, on average, turbulent fluxes are underestimated by 11% at a typical midday summer R_n value of 600 w m^{-2} under fair weather conditions. Because turbulent mixing is suppressed at night, daytime and nighttime closure is compared. Daytime closure is very similar to overall closure, however nighttime closure is both lower and has significant scatter based on an R^2 value of 0.46.

The cause of the residual error term in the energy budget can be broadly divided into instrument limitations, experimental design, and violation of assumptions regarding point measurement of turbulent fluxes (Finnigan et al., 2003). The difference between daytime and nighttime closure suggests that atmospheric stability and turbulent mixing play an important role. To examine the effects of stability and turbulent mixing on closure, the relation between u_* and closure was assessed under different stability conditions (Fig. 4.7). Only closure values with a sample size no less than 20 were included.

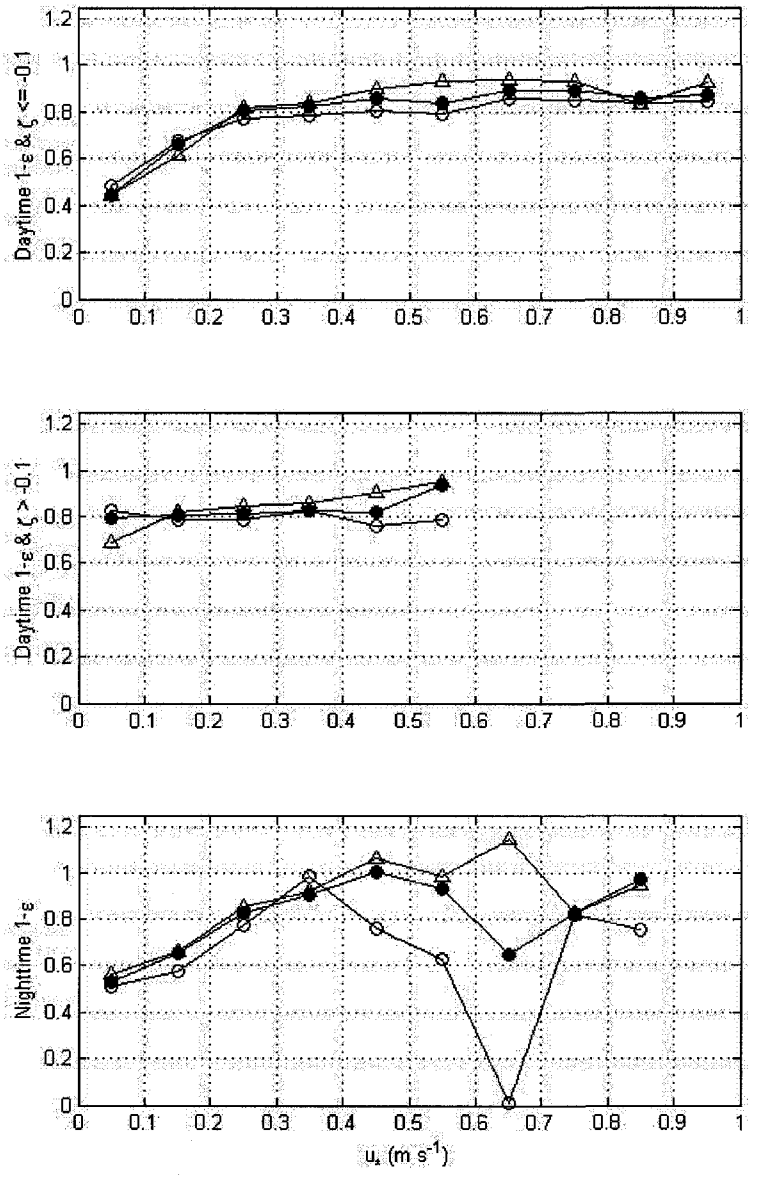

Figure 4.7: Relation between friction velocity and energy balance closure for daytime unstable (upper panel), neutral-stable (middle panel), and nighttime (lower panel) conditions. Closure estimates obtained from ordinary least square fit (○), mean average deviation (●), and the assumption of Cauchy distributed errors (Δ).

These results indicate that for this site and instrument configuration turbulent fluxes are systematically underestimated during unstable conditions when u_* is below 0.25 m s^{-1}. Depending on the method of linear regression for daytime neutral-stable conditions, closure remained relatively stable over the range of u_* with closure increasing for OLS and mean average deviation, and decreasing under the assumption of Cauchy distributed errors. The primary difference between the three methods is how they deal with outlier values, where OLS is most sensitive to outliers and the Cauchy method least sensitive. The results of the three linear regression methods differs the most for nighttime conditions because, although spikes have been filtered, the relative difference between dependent and independent variables is amplified due to the small magnitude of nighttime fluxes.

The energy balance closure was used to identify periods of poor closure but not for flux correction, where fluxes were removed outright when $u_* < 0.1$ m s^{-1} due to particularly bad closure, while measurements made when $u_* < 0.2$ m s^{-2} were soft flagged. Instead, spectral analysis was used to determine appropriate flux corrections.

Since high frequency data was retained (30 minute blocks at 10 Hz) it was possible to examine spectra/cospectra for flux loss resulting from high frequency attenuation or inadequate sampling frequency. Spectral analysis was performed by applying a fast Fourier transform to complete high frequency time series' (n = 18000) after the following conditioning steps: (i) despiking by removing data more than 3.9 S.D. from the digital recursive mean and filling by linear interpolation; (ii) rotation of the wind vectors based on the method described in Section (4.4.1); and (iii) linear detrending and

application of a Hamming cosine filter, suggested by Kaimal and Finnigan (1994) as a suitable choice for reducing red noise.

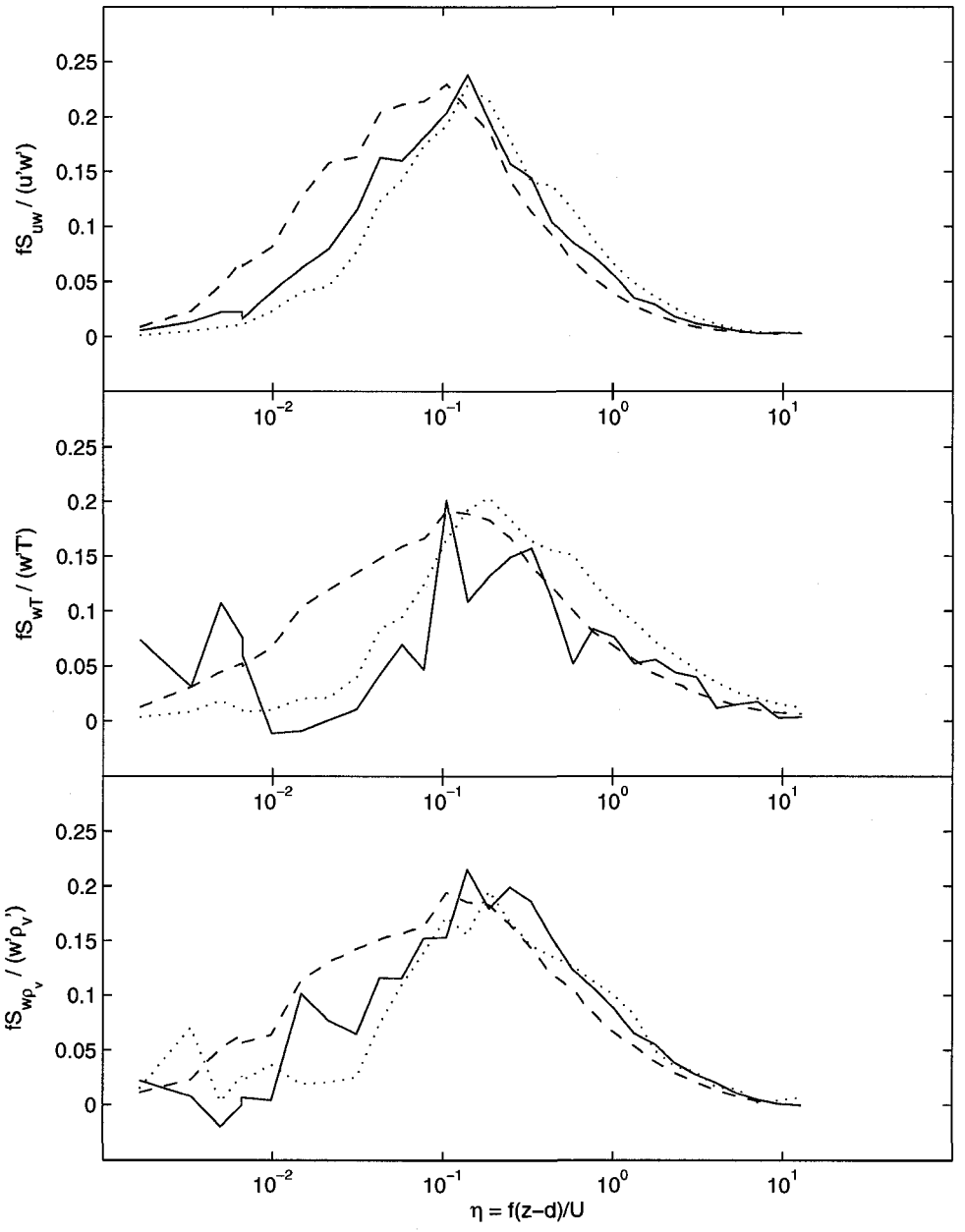

Figure 4.8: Semi-log cospectra for $\overline{u'w'}$ (upper panel), $\overline{w'T'}$ (middle panel), and $\overline{w'\rho_v'}$ (lower panel) normalized by their respective covariance against non-dimensional frequency. Cospectra are for daytime with U = 2 ± 0.2 m s^{-1} during unstable (dashed line), neutral (solid line), and stable (dotted line) conditions

Figure (4.8) shows the cospectra uw, wT, and $w\rho_v$, where the area under the curve in the semi-log plot is proportional to covariance (Stull, 1988). The non-dimensional frequency, η, was obtained by normalizing frequency by (z-d)/U, where U is cup wind speed taken at a median value of 2 m s^{-1}. Cospectra were determined from 348, 45, and 89 half hours for unstable, neutral, and stable conditions, respectively. With respect to flux loss due to inadequate sampling frequency, all three cospectra under each stability regime approach the zero asymptote at the non-dimensional Nyquist frequency suggesting 10 Hz was sufficient for capturing the smallest turbulent scales contributing to total covariance.

An examination of the power law relation for the cospectra can be seen in Figure 4.9, where the same data is used as Figure 4.8, except it is presented in log-log space to amplify the abscissa and so that power law relations appear as straight lines. Results show that uw cospectra most closely conform to the -4/3 slope in the inertial sub-range. Behaviour of wT and $w\rho_v$ are not as ideal where there appears to be some high frequency flux loss for $w\rho_v$, and additional unexpected turbulent energy for wT indicated by a less negative slope. For all but the stable $w\rho_v$ cospectra, the rise at the highest frequencies, where it occurs, is likely the result of white noise amplification (i.e. multiplication by f) as indicated by an approximate slope of 1.

Similar results were obtained by Kelliher et al. (1998) where the slope of normalized turbulent spectra of w, T, and ρ_v above the canopy of a Siberian pine forest were averaged over the daytime period when unstable atmospheric conditions prevailed. The slope of w in the inertial subrange approximated the ideal -2/3 slope quite closely

(equivalent to the -4/3 slope for cospectra), while T had a less negative slope and ρ_v had a more negative slope.

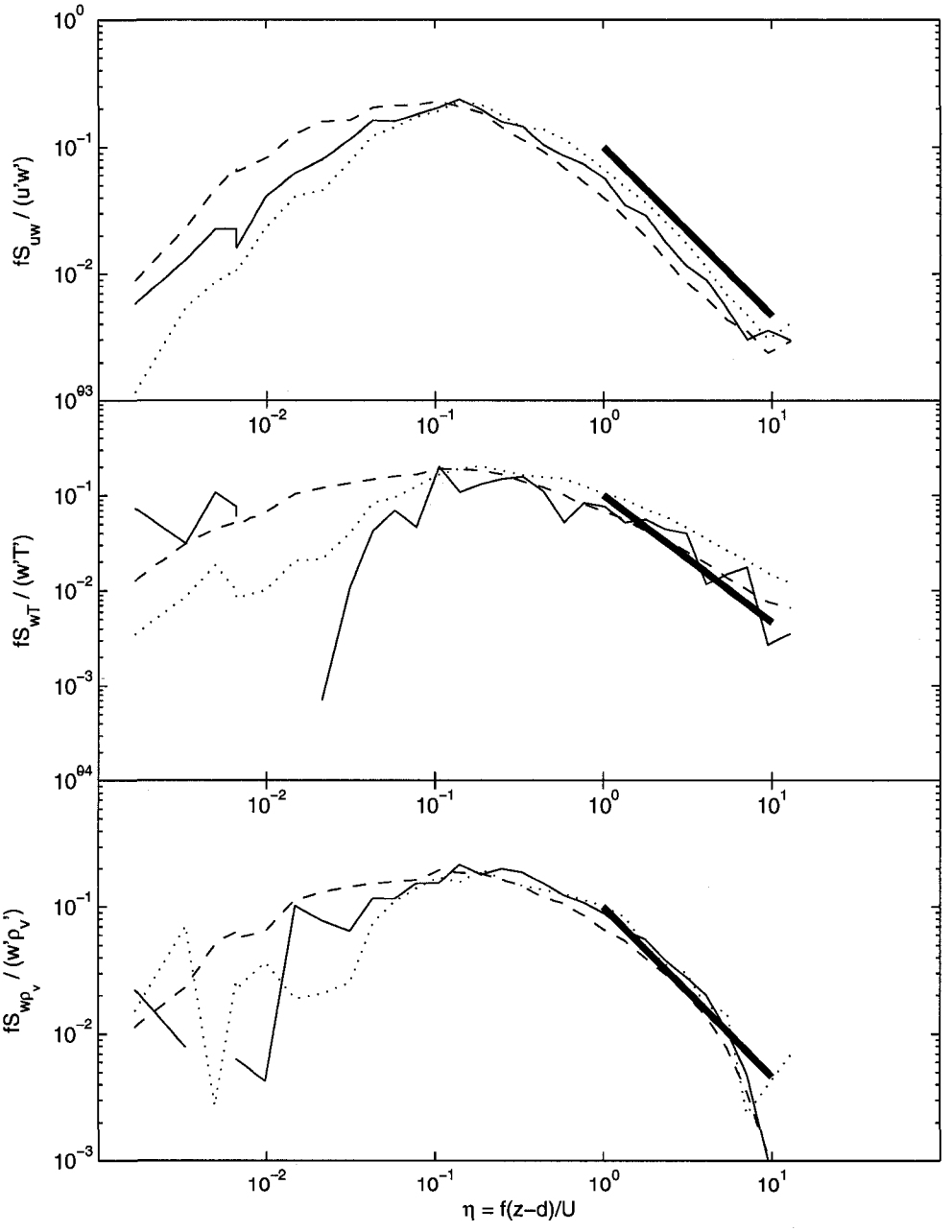

Figure 4.9: Log-log cospectra for $\overline{u'w'}$ (upper panel), $\overline{w'T'}$ (middle panel), and $\overline{w'\rho_v'}$ (lower panel) using the same conventions as Figure 4.8. The expected power law relation in the inertial sub-range is shown as a thick black line with -4/3 slope.

Law et al. (2004) present an analytical method for estimating flux loss from spectral attenuation. An estimate of flux loss resulting from high frequency attenuation only is obtained as follows:

$$\frac{\overline{w'x'}}{(\overline{w'x'})_m} = 1 + (2\pi \cdot f_x \tau_e)^{\alpha} \tag{4.18}$$

where f_x is the peak frequency of the cospectrum, τ_e is the equivalent time constant for all sources of high frequency attenuation, and α is a broadness parameter associated with stability conditions.

Using τ_e determined according to instrumentation type and configuration, and parameterization of time constants from Massman (2000), estimates were derived for high frequency corrections. Table 4.8 reports estimated high frequency correction factors for several values of f_x (0.10, 0.14, and 0.18) which loosely correspond to cospectral peaks of unstable, neutral, and stable conditions. Different values of f_x were evaluated because the cospectral peak tends to shift based on stability (Fig. 4.9).

Estimates of the flux correction factor suggests that the closure method of correcting fluxes may be inappropriate since the correction factor for LE is an order of magnitude greater than that for H. Additional error reported for the LE flux correction factor is due to uncertainty in the precise lateral separation distance between the IRGA and sonic sensors (0.15 ± 0.05 m).

By applying corrections according to results in Table 4.8, daytime closure when $u_* > 0.2$ (n = 3405) improves from 0.911 ± 0.003 ($R^2 = 0.94$) to 0.935 ± 0.004 ($R^2 = 0.94$) when forced through zero. In order to facilitate comparison with uncorrected fluxes, this corresponds to an average increase in H and LE by 0.58% and 6.1% respectively, given the distribution of stability conditions over the study period.

Table 4.8: Estimated flux correction factors based on high frequency spectral attenuation. The correction factor was calculated using Eq. 4.18 and f_x of 0.10, 0.14, and 0.18 for unstable, neutral and stable atmospheric conditions respectively.

	Stability		
	$\zeta < -0.02$	$\lvert\zeta\rvert \leq 0.02$	$\zeta > 0.02$
$u'w'$	1.018	1.023	1.029
$w'T'$	1.0049	1.0058	1.0068
$w'\rho_v'$	1.045 ± 0.014	1.063 ± 0.020	1.080 ± 0.030

5 Results and Discussion

Comparisons are made between the study site and a chronosequence of three jack pine stands growing in Saskatchewan in the Canadian boreal region. A comparison of stand statistics between the study site (hereafter referred to as RJP92) and the three Saskatchewan sites can be seen in Table 5.1, and climate normals of temperature and precipitation in Figure 5.1. It should be noted that there is no intention to make direct comparisons of temporal variability, but rather the intention is to examine biophysical and climatic controls on ET, where all else being equal, there is an expectation of similar responses based on long term limitations imposed by climate. Therefore, Figure 5.1 serves to point out that the two locations, on average, experience very similar temperature and precipitation regimes, both in terms of magnitude and seasonal variability. The two locations have a typical dry continental climate with less than 500 mm of annual precipitation with relatively wet, warm summers, and cold, dry winters.

The three sites in the chronosequence, a mature site (OJP), and two sites harvested in 1975 (HJP75) and 1994 (HJP94), respectively, are the closest jack pine forests studied on a continuous basis using the eddy covariance methodology to RJP92. The site identifiers refer to stand origin, dominant tree species, and recruitment age; where R, O, and H represent 'reclaimed', 'old', and 'harvested', respectively. Stand characteristics for RJP92 lie between the young and more mature Saskatchewan sites. The influence of different stand characteristics on microclimatological conditions and subsequently on the controls on ET will be compared to RJP92.

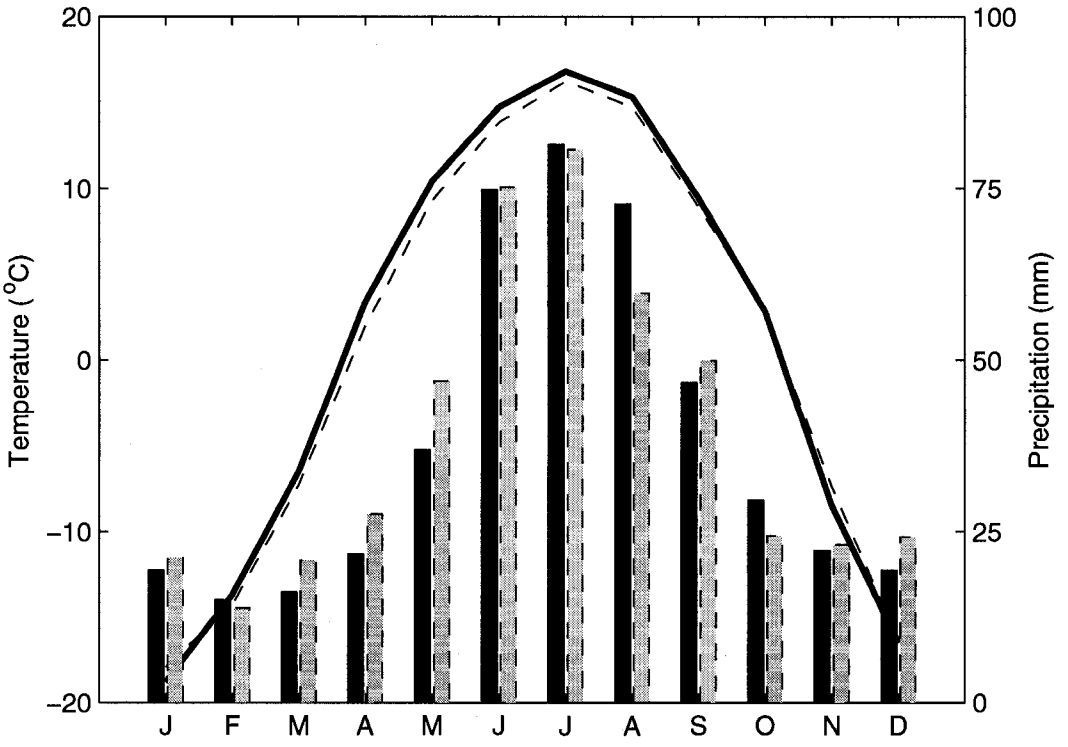

Figure 5.1: 1971 – 2000 climate normals for temperature (lines) and precipitation (bars) from the Fort McMurray airport (solid black) and Waskesiu Lake (dashed). Data from Environment Canada (http://www.climate.weatheroffice.ec.gc.ca/climate_normals/index_e.html).

Half hourly flux and meteorological data were obtained through the Flux Canada Research Network (BERMS project leaders – Barr, A., Black, T.A., McCaughey, J.H), where data availability differs between the sites. All sites had meteorological data spanning 2004 – 2005, with OJP and HJP94 beginning in 1998 and 2001 respectively. Availability of flux data was far more limited, with OJP, HJP75, and HJP94 spanning 1999 – 2005, 2004 – 2005, and 2001 – 2002, respectively.

Table 5.1: Comparison of select site and stand characteristics for jack pine growing in the boreal region of Central and Western Canada. Stand statistics for the three chronosequence sites is based on 2005 data, whereas RJP92 is based on 2007 data.

	Sites			
	RJP92	OJP	HJP75	HJP94
Species	Jack pine	Jack pine	Jack pine	Jack pine
Latitude	57° 03.916'	53° 54.980'	53° 52.549'	53° 54.505'
Longitude	111° 39.818'	104° 41.522'	104° 38.717'	104° 39.353'
Elevation a.s.l.(m)	310	579.27	533.54	580
Age	15	75-90	29	11
LAI (m^2 m^{-2})	1.38 – 1.6	2.3*	3.1	0.6 – 1.0*
Precipitation (mm yr^{-1})	455.7[a]	467.3[b]	467.3[b]	467.3[b]
Mean annual temp. (°C)	0.7[a]	0.4[b]	0.4[b]	0.4[b]
Tree height (m)	4.5 ± 0.7	12.7	7.6	3.7
d.b.h. (cm)	6.5 ± 1.3	12.9	-	3.2
Density (stems ha^{-1})	2175 - 2500	1320	-	4056

HJP94 and OJP compiled from Kalyn and Van Rees, 2006. Agr.For.Met; HJP75 data compiled from Mkhabela et al., 2008. 28th conf. on Agr.For.Met.; * denotes data from Amiro et al. 2006a. Agr.For.Met.; Precipitation and temperature data from Environment Canada climate normals from Fort McMurray[a] and Waskesiu Lake[b].

5.1 Leaf Area Index

Due to the limited number of LAI measurements (12) per field campaign (approximately every other week throughout the study period) the values in Figure 5.2 are by no means an extensive survey of LAI for RJP92. LAI measurements are intended for use as part of long term monitoring to assess if significant intra or inter-annual change occurs. The apparent drop, albeit small, in LAI around mid-summer could be in response to moisture stress incurred from limited precipitation and high near-surface soil suction. However, since the change in LAI over the study period was small in comparison to the measurement errors, it is also possible that the variation was not statistically significant. As previously mentioned (Chapter 4.3), LAI measurements can be underestimated when taken under clear sky conditions near midday due to the effect of needles reflecting direct beam radiation. This is not thought to be the cause of the drop in LAI on doy 179 because it was the only period of LAI measurements taken under overcast conditions.

Bliss (1980) indicates that strong soil suction values less than -3500 to -4000 kPa can result in needle loss, particularly young needles. Photographs indicate a degree of browning of needles, but it is uncertain whether this correlates with moisture stress in the 2007 growing season and consequently on LAI. Comparison of mean LAI values to the jack pine chronosequence indicates that the reclamation site has intermediate values. Due to the open nature of the canopy, effective LAI values measured by the LAI-2000 are just as much a function of the planted stand density as the foliage density of the jack pine.

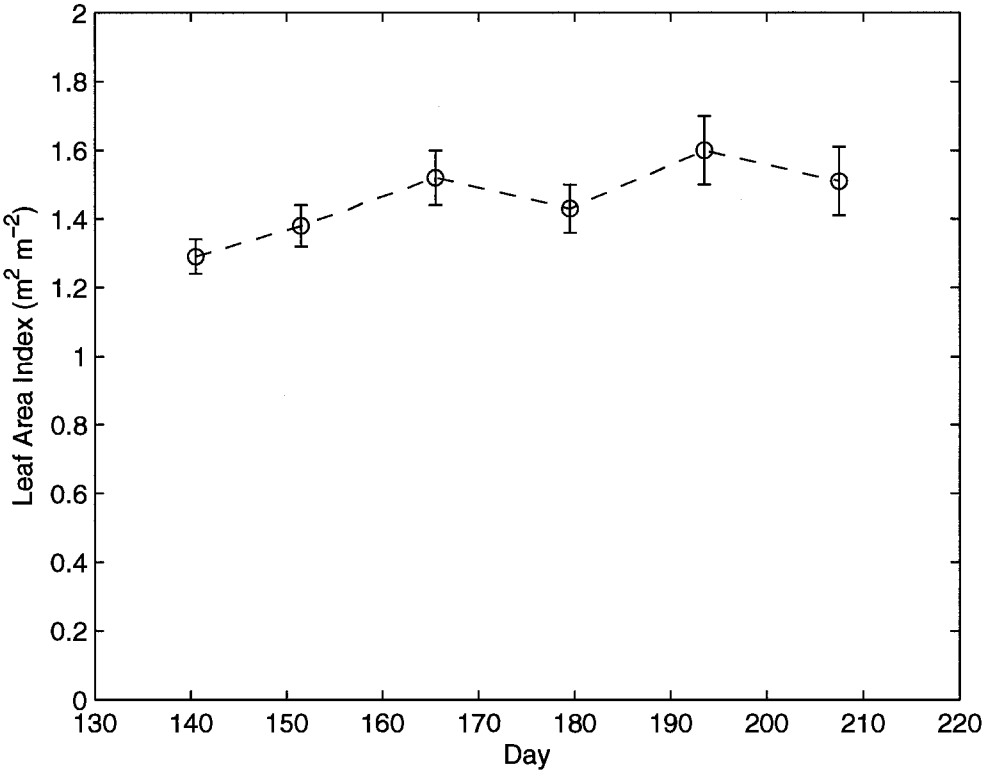

Figure 5.2: The mean leaf area index ± 1 S.D. measured every other week at RJP92 during the 2007 growing season.

5.2 Aerial and Soil Microclimate

5.2.1 Temperature

Increasing air and soil temperature signals the onset of vegetation productivity in addition to having an impact on ET through increasing vapour pressure deficit. Temperature itself is not a variable that describes system processes, but rather is a state variable that is the product of various energy and mass transfer mechanisms and pathways. Figure 5.3 shows the mean daily air temperature at RJP92 at EC height over the study period having a distinct seasonal trend, peaking nearly a month after the summer solstice, where the derivative of the polynomial fit indicates a peak at day 195 (14 Jul). In addition to seasonal variability, there is significant daily variation that is the

result of changes in the amount of solar radiation received which is linked to cloudiness on a daily basis. However, daily variation in receipt of solar radiation explains just over 30% of daily temperature variations. In addition to the change in mean air temperature as a result of varying characteristics of synoptic scale air masses that move through the area, variability in temperature is also the result of surface wetness and the availability of soil moisture for ET and subsequently on the partitioning of available energy between H and LE.

Also shown in Figure 5.3 is the difference between air temperature at EC height and soil temperature at a depth of 3 cm. Shading has been added to highlight periods when air temperature is greater than soil temperature and vice versa. Because of the conservative nature of soil temperature which results from heat transfer being largely limited to conduction, day to day variability in soil temperature is less than air temperature, with daily amplitude decreasing with depth. Furthermore, soil thermal properties cause it to have more thermal inertia than the air above so that there tends to be a lag between heating and cooling. In general, this causes the soil to be an energy sink following snow melt until past mid summer, after which it becomes a source (see also Fig. 5.11). Figure 5.3b shows that up until about day 220, average daily air temperature exceeds soil temperature with one particularly large exception during cloudy, wet conditions for several days around day 160. Following day 220, temperature differences start alternating between positive and negative depending on daily variability, with values becoming progressively more negative.

Though not shown, soil profile data for temperature, VWC, and soil suction were available starting in December of the previous year. These data indicate that ground thaw

was complete down to a depth of 15 cm by day 106 (16 Apr), and down to a depth of 50 cm two days later. At the lowest measured depth of 80 cm, the minimum winter temperature only reached -0.5°C, and therefore the thaw period was less distinct, where it oscillated around zero from day 81-108 (22 Mar – 18 Apr). Soil moisture data suggests that snow melt began around day 89 (30 Mar) and ended around day 106 (16 Apr). The date of snowmelt onset corresponds well with air temperature data from the Fort McMurray airport (Environment Canada) where mean daily air temperature remained above 0°C from day 81 (22 Mar) on with the exception of the first week of April. The return to sub zero mean daily air temperatures results in a cessation of increase in VWC in the till layer and net draining of the sand layer (not shown). This indicates that up to a month of potentially significant stand ET and productivity were not measured as part of this study.

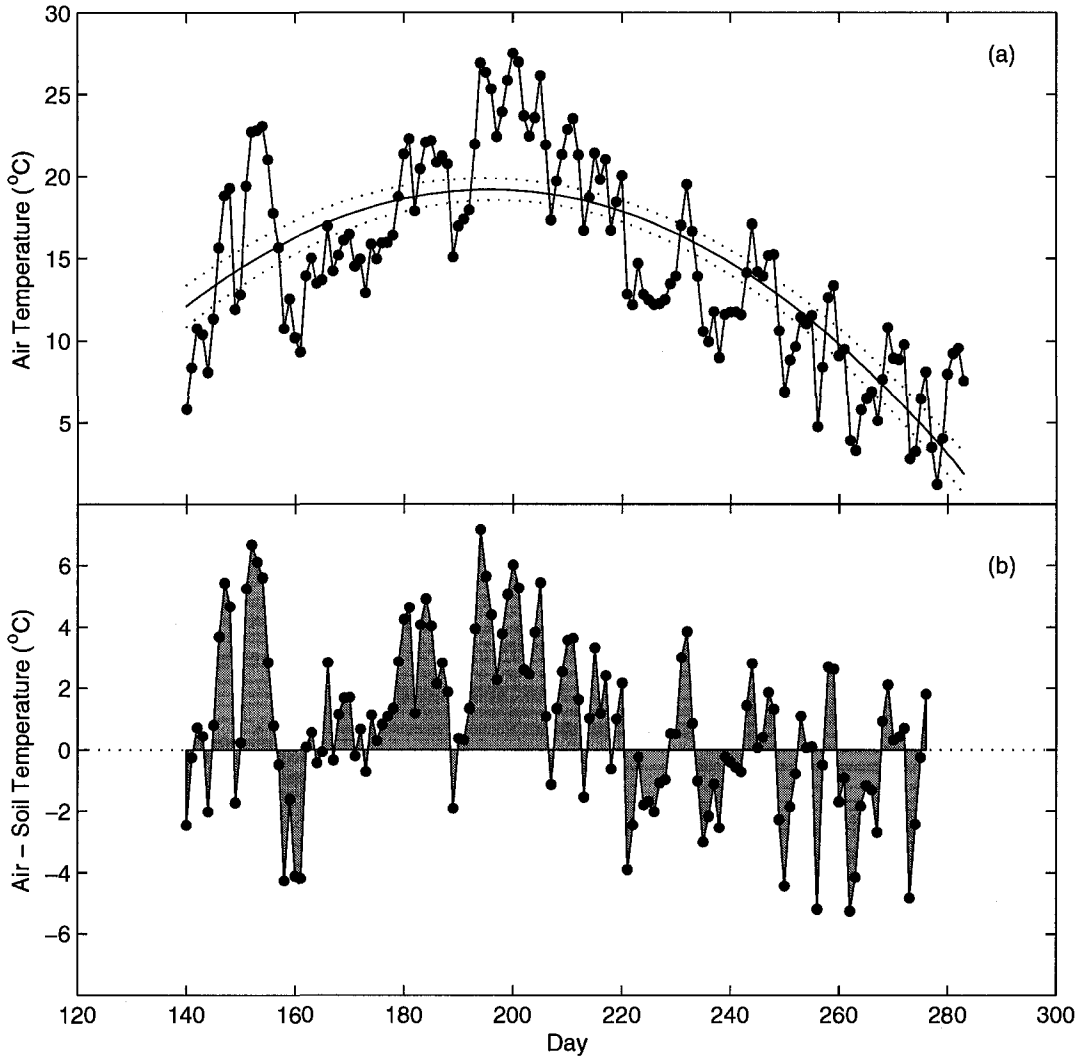

Figure 5.3: Variation of daily mean air temperature at EC height (a), and the difference between air and soil temperature at a depth of 3 cm (b) for RJP92 during the 2007 growing season. A 2nd order polynomial regression is shown in (a) to highlight the seasonal trend, where dashed lines are 95% confidence intervals.

5.2.2 Precipitation

Figure 5.4 shows that rainfall intensity in the first and last 25 days of the study period never exceeded 2 mm hr^{-1}. More intense rain events occurred between days 160 and 255 (roughly June though August). The greatest rain event based on half hour measurements occurred on day 200, being equivalent to 13.2 mm / 30 min, with greatest daily total precipitation being 23.6 mm on the same day. The largest rainfall event based on consecutive half hours with measured precipitation began on day 233, ending early on day 234 with a total of 23.9 mm. Both of these major rain events coincide with significant changes in either VWC or soil suction in the top 15 cm of the soil profile (see Fig. 5.5 and 5.6).

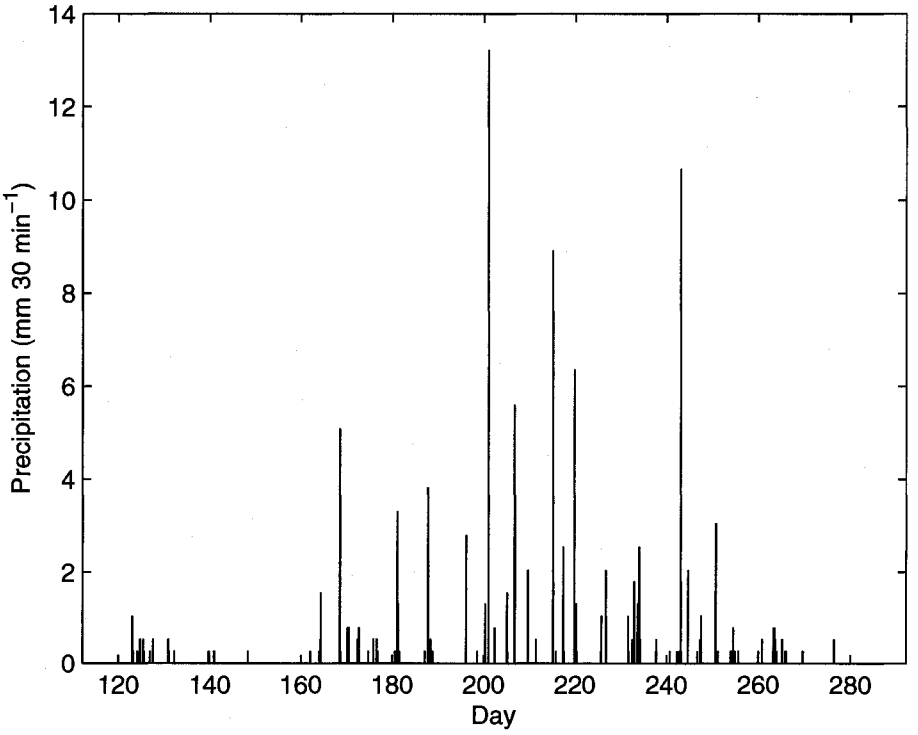

Figure 5.4: Variation of half-hourly total precipitation measured <1km to the east of the jack pine stand over the 2007 growing season. Data was acquired from Syncrude Canada Ltd.

5.2.3 Soil Moisture

According to Chapin (2002), in general 80% of boreal tree species roots are in the top 50 cm with a maximum rooting depth of between 1.5 and 3 m. This is corroborated by Bannan (1940), where it is demonstrated that jack pine tend to have tap roots that can easily exceed 1.2 m depth for large specimen (3 – 12 m) in sandy soil. Baldocchi et al. (1997) further indicate that the fine root zone for a mature jack pine stand growing in sandy soil (OJP) is within the top 15 cm of the soil profile. As such, the depth over which soil moisture and matric potential were measured (down to 80 cm) should encompass the bulk of the root zone for jack pine.

The study period began with soil moisture content (θ_s) in the till layer being near field capacity (Figure 5.5). The magnitude of θ_s at 5 and 15 cm were similar over the study period, ranging from 0.13 – 0.22 m^3m^{-3}. There is an apparent change in porosity and/or texture within the soil profile by 30 cm, with θ_s on average being about 0.07 m^3m^{-3} greater over the entire study period. Following the beginning of the study period, soil moisture was initially depleted within the till layer by ET, with apparently little water being lost to drainage since θ_s in the sand layers changed very little (Fig. 5.5). Significant precipitation events on day 201 and 207 had disproportionately small effects on θ_s. Soil moisture content was largely replenished from several days of modest yet persistent precipitation over days 232-234.

Near-surface soil texture at RJP92 differs from typical soils where jack pine forests grow, which usually have a sandy texture. The soils at the chronosequence sites are well-drained sandy soils (Baldocchi et al., 1997a), with maximum θ_s between 0.14 – 0.17 m^3m^{-3} in the top 30 cm of soil and an apparent wilting point of about 0.05 m^3m^{-3}.

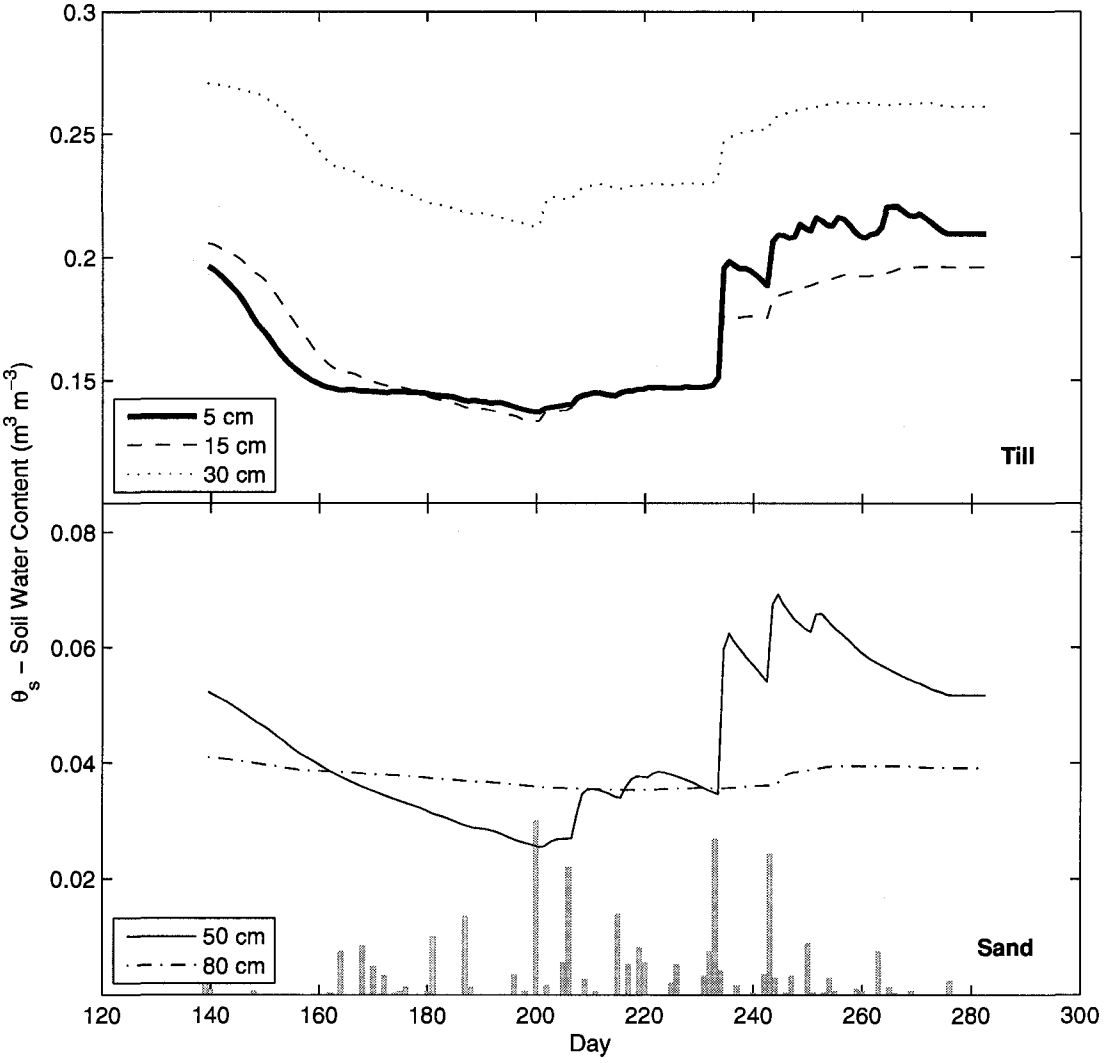

Figure 5.5: Variation in the daily mean volumetric soil water content at several depths (5, 15, 30, 50, and 80 cm) in the till and sandy soil layers for the jack pine stand over the 2007 growing season. Daily total precipitation (unitless) is shown as shadowed bars in the lower panel.

Significant change in soil suction in the top 15 cm occurred over the study period, with daily mean values ranging from -10 to -1595 kPa (Figure 5.6). The large negative near surface Ψ_s values were the result of warm temperatures, low levels of precipitation, and evapotranspirative loss prior to day 201. Though the maximum daily Ψ_s value reached -1595 kPa, the greatest measured value was approximately -3700 kPa. This is significant because the maximum xylem tension that can be supported by jack pine is between 3500 and 4000 kPa (Bliss, 1980). However, if subjected to this level of suction repeatedly, or for an extended period of time, the tree would experience significant moisture stress and there would be a preferential loss of young needles (Bliss, 1980).

The large precipitation event on day 201 had the effect of alleviating the extreme soil suction in the upper 15 cm of soil. Rainy conditions over the following 50 days continued to increase soil suction as soil moisture content increased. The significant change in $\Psi_{s,5cm}$ from -1595 to -542 kPa over days 200 – 232 was not accompanied by a significant change in θ_s (0.137 – 0.147 m^3m^{-3}), suggesting that the soil was near wilting point. This is supported by soil moisture characteristic curves for a silt loam soil (Ward and Robinson, 2000). Soil suction at 30 cm was much more conservative, reaching a maximum suction of -428 kPa. Similarly, soil suction in the sand layer was small, not decreasing below -15 kPa.

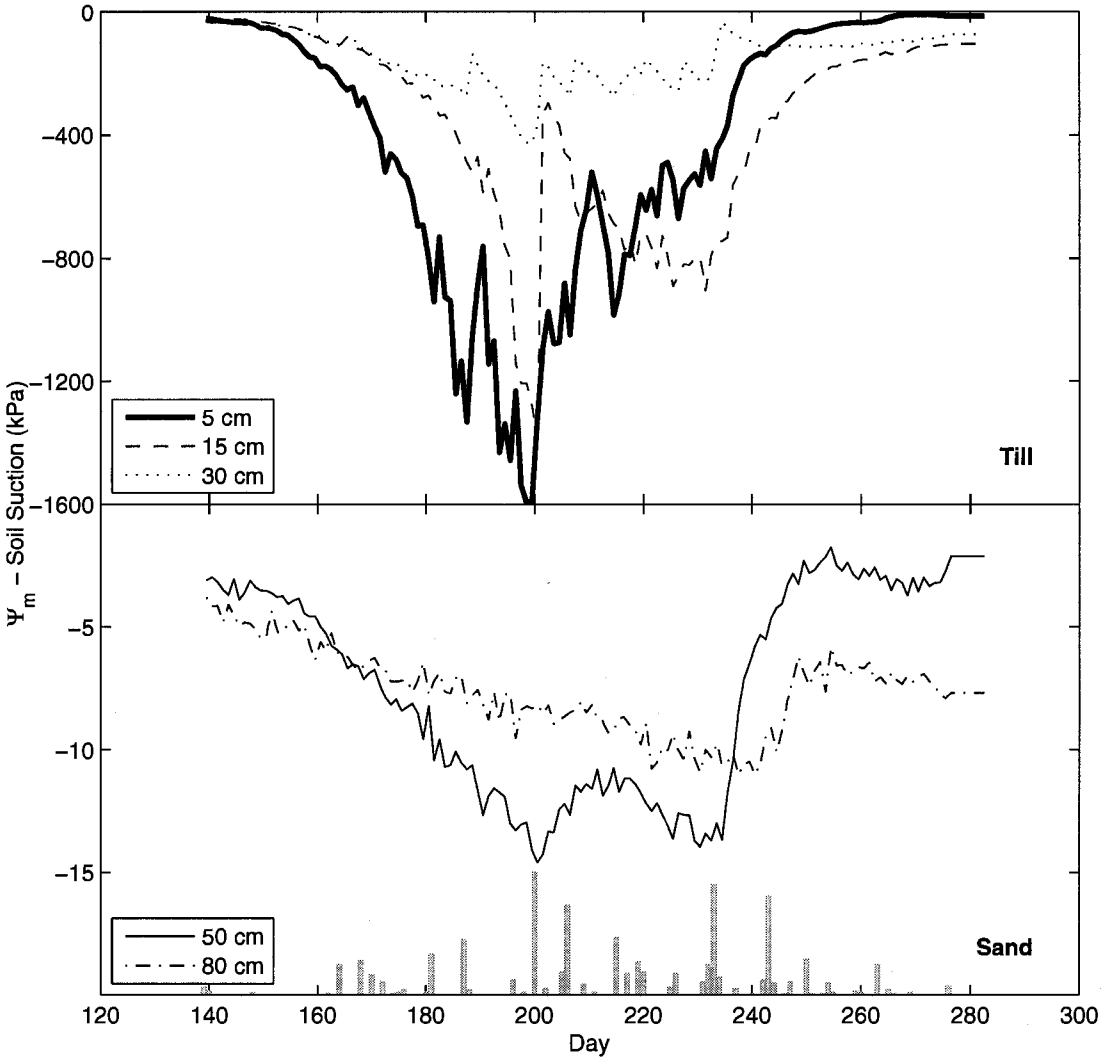

Figure 5.6: Variation in the daily mean soil suction at several depths (5, 15, 30, 50, and 80 cm) in the till and sandy soil layers for RJP92 over the 2007 growing season. Daily total precipitation (unitless) is shown as shadowed bars in the lower panel.

5.3 Mass and Energy Fluxes

5.3.1 Surface Reflectivity to Shortwave Radiation

Surface reflectivity to shortwave radiation (albedo) as measured by the ratio of incoming to outgoing daily sums (Figure 5.7) averaged 0.168 ± 0.008 over the study period. This value for albedo is high in comparison to values reported in the literature for jack pine stands which have summer values of 0.09-0.136 as summarized by Baldocchi et al. (2000a). Values for a young jack pine stand with a mean height of 2.27 m growing near Thompson, Manitoba (55.9°N, 98.29°W) ranged between 0.126-0.140 depending on sky conditions (McCaughey et al., 1997). Comparison to the BERMS chronosequence shows similar results (Table 5.2). However, although the mean albedo for RJP92 is greater than HJP94, the difference does not seem to be a statistically significant. Albedo from the BERMS data seems to indicate that young sites have lower summer albedo compared to mature sites, including HJP02 (not shown) which has a similar albedo to HJP94. This is not simply the result of differing methods of calculation, though the methods may in fact be different between studies. Since the lowest average daily values for RJP92 (Figure 5.7) were 0.150 ± 0.021 with similar minimum average half hourly values, the relatively low albedo reported in the literature could not be obtained using RJP92 data by any sensible means.

With respect to seasonal variability, albedo exhibits a slight positive trend over the study period ($\alpha = 0.000089*doy + 0.15$; $R^2 = 0.99$). However, a more stepwise change seems to occur around day 215-225, possibly due to increased precipitation and increased soil moisture availability. Although the albedo of wet soil is lower than dry soil, it is being suggested that the optically brighter understory vegetation responded to

increased soil moisture availability. There is photographic evidence which shows an increase in understory vegetation when comparing pictures taken on doy 207 and 222.

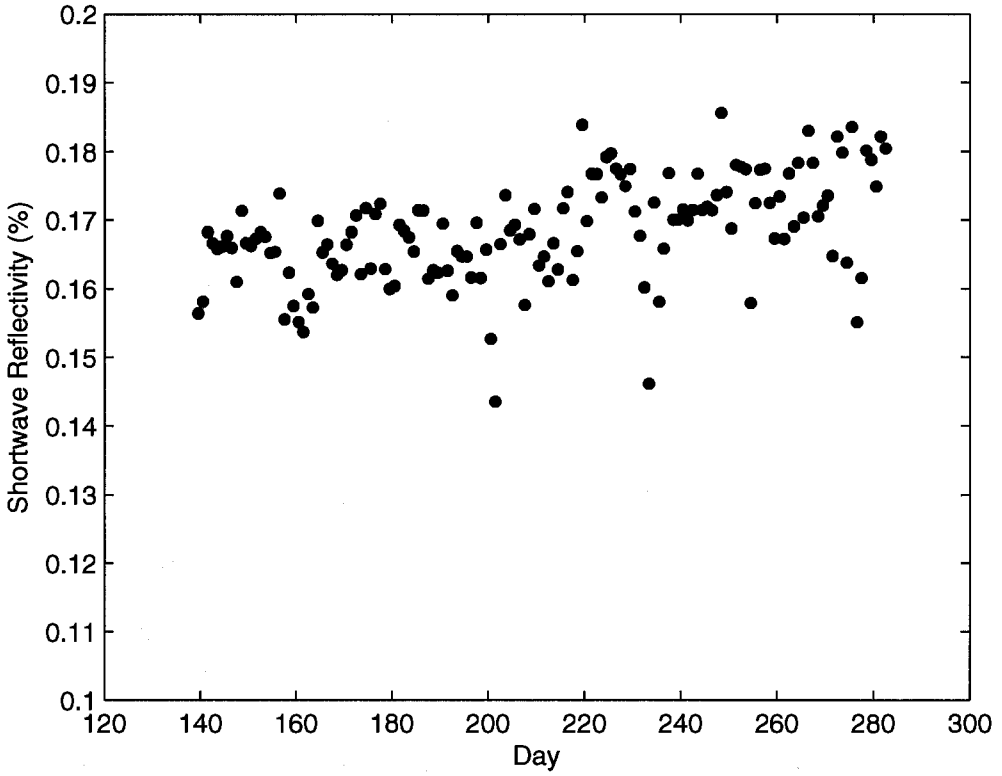

Figure 5.7: Seasonal variation of the ratio of daily sum of incoming to outgoing shortwave radiation over RJP92 during the 2007 growing season.

Figure 5.8 shows an increase in mean daily albedo between the first and last 60 days of the study period, where minimum midday values were 0.150 ± 0.021 and 0.159 ± 0.008 respectively. In addition to the previously mentioned change in the understory vegetation, the increase in midday albedo could also be the result of increased cloudiness associated with greater precipitation, or simply the result of the changing solar elevation angle. The difference in temporal variability between the two periods, particularly in the morning and early evening is likely the result of a difference in mean solar elevation between the two periods where summer solstice occurs on doy 172. Furthermore, there is

a significant difference in mean day length between the two periods, as defined by K↓>0, where daylight lasts on average 19.3h and 14.7h for the early and late periods respectively.

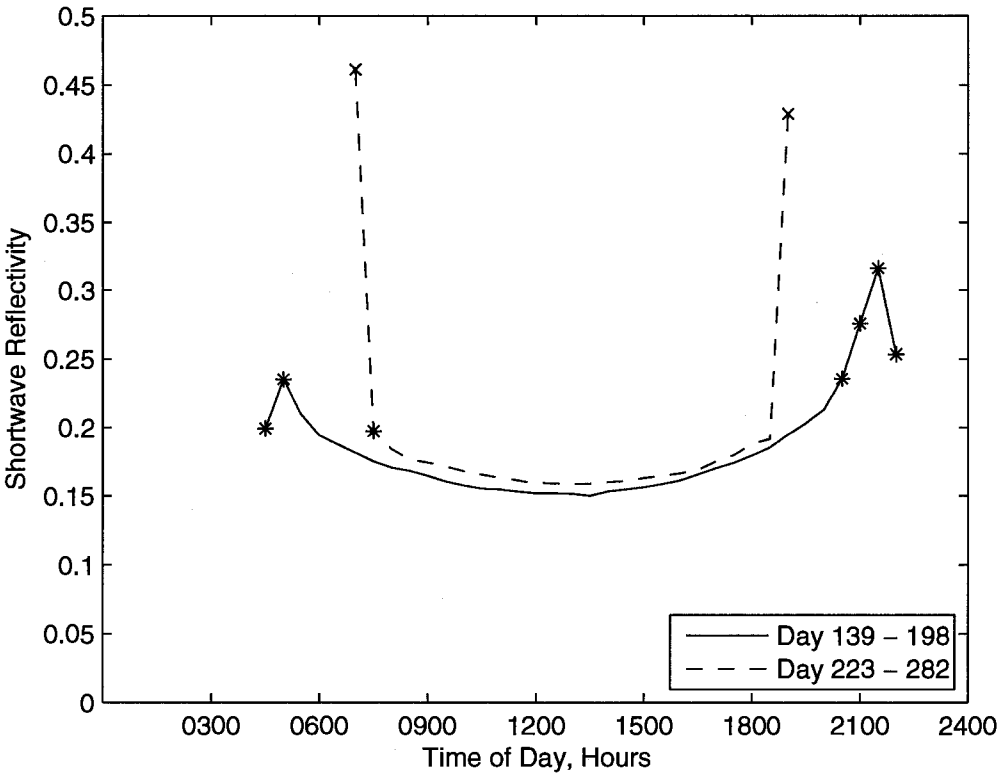

Figure 5.8: Mean diurnal variation of albedo for a 60 day period at the beginning (solid line) and end (dashed line) of the 2007 study period. Markers indicate albedo values whose S.D. is significantly greater than midday values and either less than (*) or greater than (x) the respective albedo value. Midday (0900 – 1700) S.D. ranges between 0.005 – 0.02 for both time periods.

Betts and Ball (1997) suggest that, all else being equal, higher albedo values for a given site are associated with cloudy conditions. This is because under cloudy conditions shortwave radiation is coming from all sectors of the sky, resulting in an increased probability of reflection of incoming radiation with a large angle of incidence. The effect of cloudiness on albedo for the RJP92 site was assessed to see if it had a significant effect. In order to assess cloudiness, an index was derived which was computed as the ratio of the sum of daily measured incoming shortwave radiation to a modelled value for clear sky conditions. The model was adapted from Stull (1988) where daytime values were calculated as:

$$K\downarrow = S \cdot T_K \sin \Psi \tag{5.1}$$

where S is solar irradiance taken to be 1370 W m^{-2}, Ψ is the solar elevation angle, and T_K is the net sky tansmissivity. T_K was calculated as follows for clear sky conditions:

$$T_K = 0.6 + 0.2 \sin \Psi \tag{5.2}$$

When $\sin\Psi$ is negative (i.e. at night), Equation (5.1) is set to zero.

Based on the modelled cloudiness index, albedo had a very weak correlation and slight positive linear relation ($\alpha = 0.006 * I_{cloud} + 0.165$; $R^2 = 0.03$) to cloudiness. Since the relation proposed by Betts and Ball (1997) does not seem to apply to RJP92 during the summer, it cannot account for the site's relatively high albedo.

The increased roughness of the surface resulting from the open nature of the canopy and spacing of planted rows could lead to increased radiation trapping due to complex geometry which would result in a lower albedo (Oke, 1987). However, since albedo from this study tends to be higher than values for jack pine reported in the

literature, the lack of canopy closure inherently suggests that the spectral characteristics of the forest floor and understory vegetation play a significant role.

This difference in average albedo can have an effect on the energy balance through the effect on R_n. Although there is a negative feedback between net shortwave radiation and outgoing longwave radiation due to its effect on surface temperature, Oke (1987) indicates that the net result of an increase in albedo of an unvegetated surface is a decrease in net radiation. The situation for vegetated surfaces is more complex, but in general it still results in a decrease in daytime net R_n. These results have important practical implications for parameterization of coupled energy and mass balance models and cover failure risk assessment for oil sands reclamation since standard values for albedo would tend to overestimate daytime R_n, at least prior to canopy closure.

Surface reflectivity to PPFD is also examined because it has a more direct link to changes in the vegetation since it represents the radiation bandwidth that is absorbed by chlorophyll. The average daily surface reflectivity to PPFD for RJP92 calculated over the entire study period is 4.7 ± 0.5 % (Table 5.2).

This compares well with results from a young jack pine site, where surface reflectivity to PPFD ranged from 5.1 – 5.4% depending on sky conditions (McCaughey et al., 1997). A few points can be made regarding comparisons of surface reflectivity to PPFD between RJP92 and the chronosequence (Table 5.2). First, average surface reflectivity to PPFD for RJP92 is not higher than all other sites, such as with shortwave albedo, but rather the value lies between the young and mature sites. Secondly the reflectivities to different bandwidths do not have a constant proportionality between the chronosequence sites. Overall, there seems to be a relation between surface reflectivity to

PPFD and LAI associated with the jack pine needles, which would explain why HJP75 had a higher surface reflectivity to PPFD than OJP despite being younger and shorter.

Table 5.2: Comparison of daily albedo and maximum net radiation between RJP92 and chronosequence sites. Values are calculated from the period doy 139 – 282, where values in parentheses are the standard deviation.

Site	RJP92	OJP	HJP75	HJP94
Albedo	0.168	0.098	0.093	0.148
	(0.008)	(0.009)	(0.010)	(0.013)
Reflected fraction	0.047	0.041	0.029	0.066
of incoming PPFD	(0.005)	(0.002)	(0.002)	(0.008)
Max. R_n	16.86	19.35	18.98	17.56
($MJ\ m^{-2}d^{-1}$)				

OJP and HJP94 2002 data; HJP75 2005 data

5.3.2 Shortwave Radiation and PPFD

Figure 5.9 shows both the seasonal and daily variability of shortwave radiation at RJP92. Measurements of shortwave radiation can also be considered a surrogate for PPFD (not shown) since they have a strong linear relation over the study period (R^2 = 0.984 and 0.972 for downwelling and upwelling respectively) where downwelling PPFD is on average 37% of K↓, and upwelling PPFD is on average 11% of K↑. K and PPFD were converted to the same units using Planck's law and the average photon energy for light with a wavelength of 550 nm. The difference is attributable to the bulk surface reflectivity to the different wavelength ranges.

The mean incoming shortwave radiation about which daily values vary ranged from about 245 W m^{-2} (PPFD – 415 μmol $m^{-2}s^{-1}$) near summer solstice (day 155) to 60 W m^{-2} (PPFD – 100 μmol $m^{-2}s^{-1}$) by the end of the study period. Daily variation in response to variable cloud conditions resulted in short term variability of a similar magnitude. In comparing measured daily receipt of shortwave radiation to modelled values based on location and time of year (Stull, 1988), it is evident that very few days had 'ideal' clear sky conditions. Approximately 25% of days had relatively cloud free clear skies, with measured daily shortwave radiation being ≥ 80% of maximum potential values.

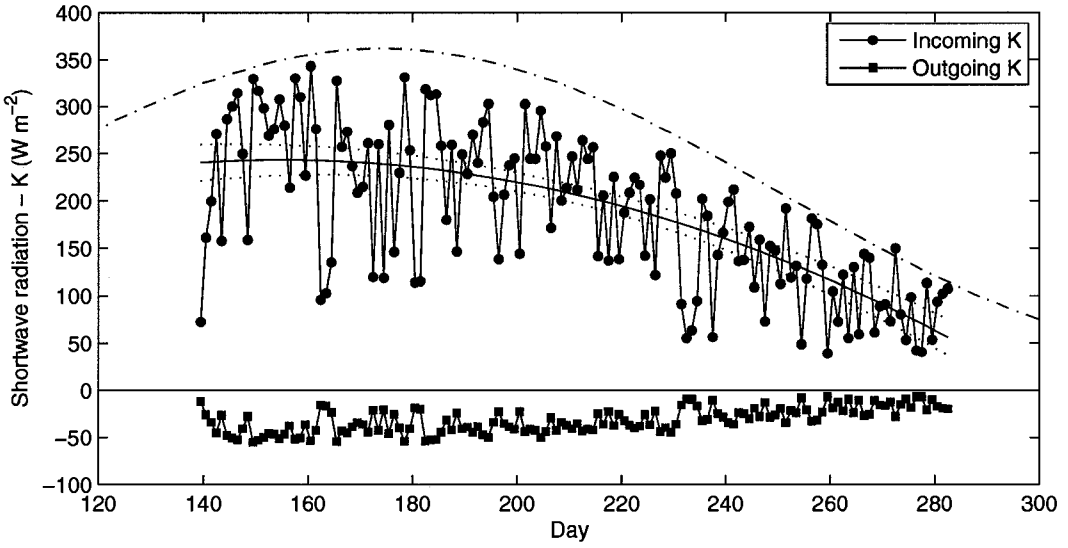

Figure 5.9: Variation of mean daily incoming and reflected shortwave radiation for RJP92 during the 2007 growing season. Positive and negative values denote direction, where positive is downwards. A 2nd order polynomial regression is shown to highlight the seasonal trend, where dotted lines are 95% confidence intervals. Dash-dot line represents the modelled maximum incoming K based on latitude, longitude, time of year, estimated solar constant, under cloudless conditions (Stull, 1988).

5.3.3 Net Radiation

Net radiation constitutes the major energetic input of the system to drive surface heating, ET, and photosynthesis, which in turn has impacts on water balances and net ecosystem productivity. Mean daily R_n experienced a seasonal trend, peaking prior to the summer solstice, where the derivative of the polynomial fit indicated a peak at day 163 (12 Jun.) (Figure 5.10). Maximum daily R_n values were between 175 – 200 Wm^{-2} (15.1 – 17.3 MJ m^{-2}) during midsummer, decreasing to maximum daily values of about 50 Wm^{-2} (4.3 MJ m^{-2}) by the end of the study period. The magnitude of daily variability is of a similar magnitude to the seasonal trend which is the result of variable cloud conditions.

Peak R_n values are of a similar magnitude to those measured for the jack pine chronosequence (Table 5.2). Comparing maximum daily R_n values and albedo for the respective sites suggests a correlation with albedo, where albedo decreases as the stand matures, resulting in greater absorption of radiation. Furthermore, data for HJP94 from 2001 – 2005 (not shown) demonstrates a concurrent decrease in albedo from 0.148 ± 0.013 to 0.092 ± 0.026 and increase in maximum measured R_n from 17.56 – 19.13 MJ $m^{-2}d^{-1}$ as the stand ages. LAI measurements were not available in all years for comparison. Therefore, the higher albedo of RJP92 does in fact seem to reduce maximum potential daily receipt of R_n below that of both mature and other similarly aged young jack pine stands. However, daily cloud cover conditions still play a larger role in day to day variability. The higher albedo of RJP92 resulting in lower potential R_n would, all else being equal, serve to reduce surface heating and VPD, thus reducing evaporative potential and water loss over the growing season.

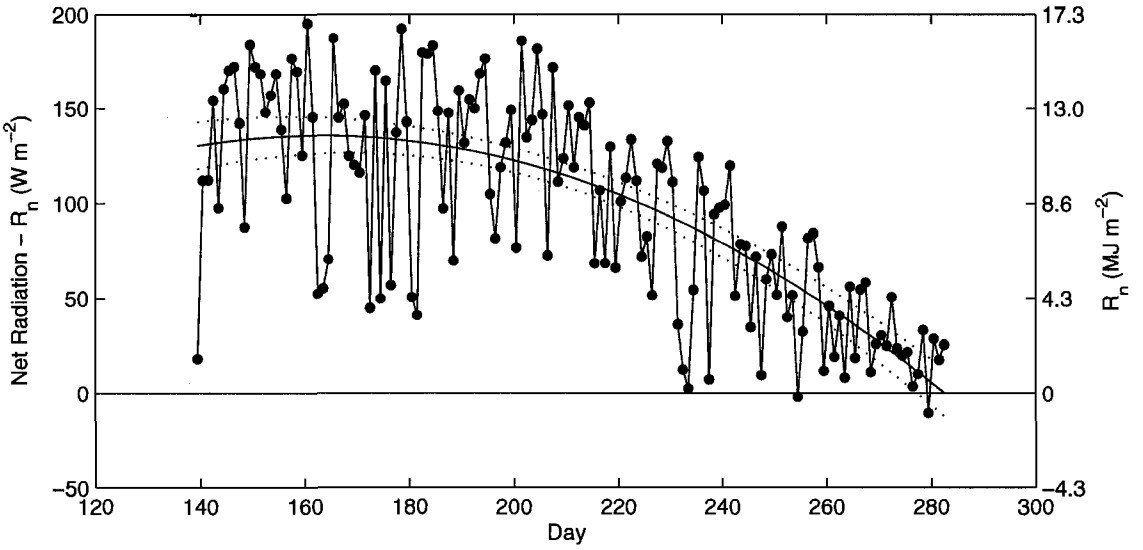

Figure 5.10: Variation of mean daily net radiation for the jack pine stand during the 2007 growing season. Positive values of R_n represent net flux towards the surface. A 2nd order polynomial regression is shown to highlight the seasonal trend, where dotted lines are 95% confidence intervals.

5.3.4 Ground and Sensible Heat Flux

Figure 5.11 shows the seasonal and daily variability of the soil heat flux, measured as the heat flux at 5 cm depth and the change in heat storage in the top 5 cm. Soil heat flux is by far the smallest of the measured components of the energy balance on a daily basis. As a result of the conservative nature of the soil environment due to the lack of turbulent exchange mechanisms and the influence of soil moisture, the seasonal trend appears much more linear than the other fluxes over the study period.

Similar to Figure 5.5b, G remains largely positive from the beginning of the study period until around day 210 as it becomes progressively more negative, although the seasonal trend line does not reach zero until day 235. During the positive period (day 139 – 210), daily average G does not exceed 10% of daily average R_n, ranging from -2.5 –

16.7 W m^{-2} (-0.2 – 1.4 MJ $m^{-2}d^{-1}$). By the end of the study period, there is nearly the opposite situation, with daily average G ranging from -13.1 – 3.9 W m^{-2} (-1.1 – 0.3 MJ $m^{-2}d^{-1}$). This is reflected in the seasonal trend line which beings at 7.6 W m^{-2} (0.7 MJ $m^{-2}d^{-1}$) and decreases in a near linear fashion to -4.6 W m^{-2} (-0.4 MJ $m^{-2}d^{-1}$). This is similar to results presented by Baldocchi et al. (1997a) who examined OJP data from 1994 between days 140 and 260, where the average daily G values had a sink strength of 10 W m^{-2} and ended with daily G values with a source strength of 5 W m^{-2}.

Following day 210, when G becomes progressively more negative, G as a proportion of R_n tends to become larger and more variable. This is a result of R_n and air temperature decreasing at a faster rate than the energy loss from soil heat storage. The switch to G/R_n being negative is the result of the convention that G is negative when the surface is a heat source. This implies that energy released from soil heat storage adds to available energy for sensible or latent heat exchange, instead of removing it as is the case for typical midsummer conditions. Although midsummer daily soil heat flux was small, maximum values reached just less than 150 W m^{-2} on a half hourly basis.

Canopy heat storage (S) has been ignored in this study (not measured). The rationale for ignoring S is that, on a daily basis, S varies about zero at a smaller magnitude than G during the growing season (Baldocchi et al., 1997a). Even on an hourly basis, S rarely ever exceeded 50 W m^{-2} for both OJP and HJP75 for all of 2004 and 2005. BERMS biomass heat storage was calculated using biomass estimates of Gower et al. (1997). H and LE storage terms were calculated by respectively taking the integral of the temperature and specific humidity gradients over the height of EC measurements (Barr et al, 2006).

Comparison of S between OJP and HJP75 for 2005 suggests that S is on average 10% less for the younger, shorter stand. Since the RJP92 canopy is shorter than both OJP and HJP75, and therefore has a smaller volume for heat storage, S would likely be smaller. Furthermore, with a higher albedo, less energy would be absorbed for surface heating.

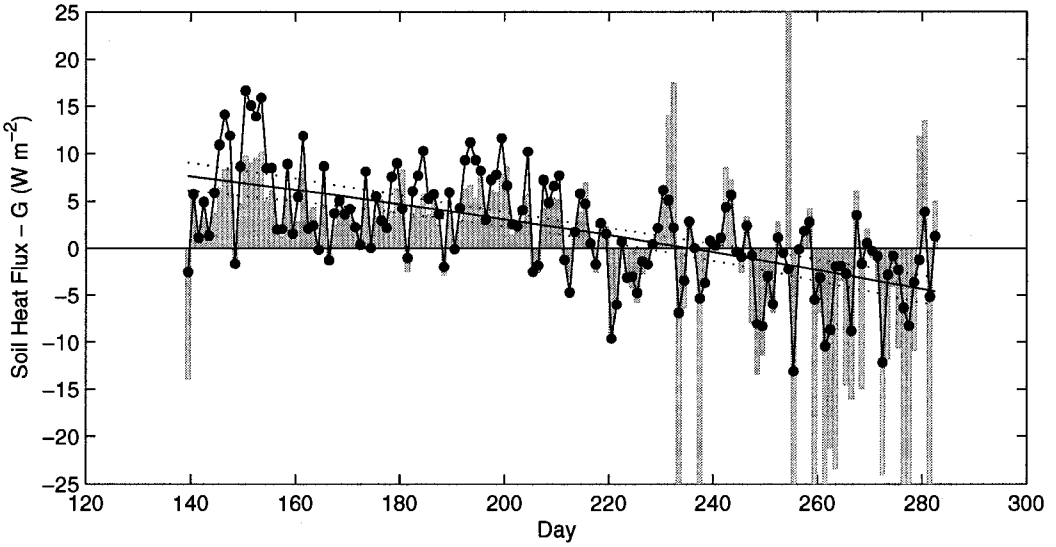

Figure 5.11: Variation of mean daily soil heat flux for the RJP92 during the 2007 growing season. Positive values of G represent heat flux into the ground. Shaded bars indicate ratio of G to R_n, scaled so that the y-axis can also be interpreted as percent.

Sensible Heat Flux

Figure 5.12 shows the daily and seasonal variability of the sensible heat flux above the canopy. The seasonal trend of H is similar to R_n ($R^2 = 0.81$), with differences which largely result from changes in daily energy partitioning due to available moisture conditions. Daily average H values tended to be positive throughout the study period where they ranged from -10 – 195 W m^{-2} (-0.9 – 16.8 MJ m^{-2} d^{-1}). Similar to other fluxes, large day to day variability, up to 105 W m^{-2} (9.1 MJ m^{-2} d^{-1}), was the result of cloud conditions, where seasonal changes were tied to decreasing R_n.

During midsummer, when fluxes were large and G positive, typical values of H/R_n were 50-75% until around day 200, with the onset of more rainy conditions, when the H/R_n value remained below 50% while G was positive. The intermittent large values of H/R_n towards the end of the study period were the result of small daily R_n values combined with the energy source from G that was large in relation to R_n.

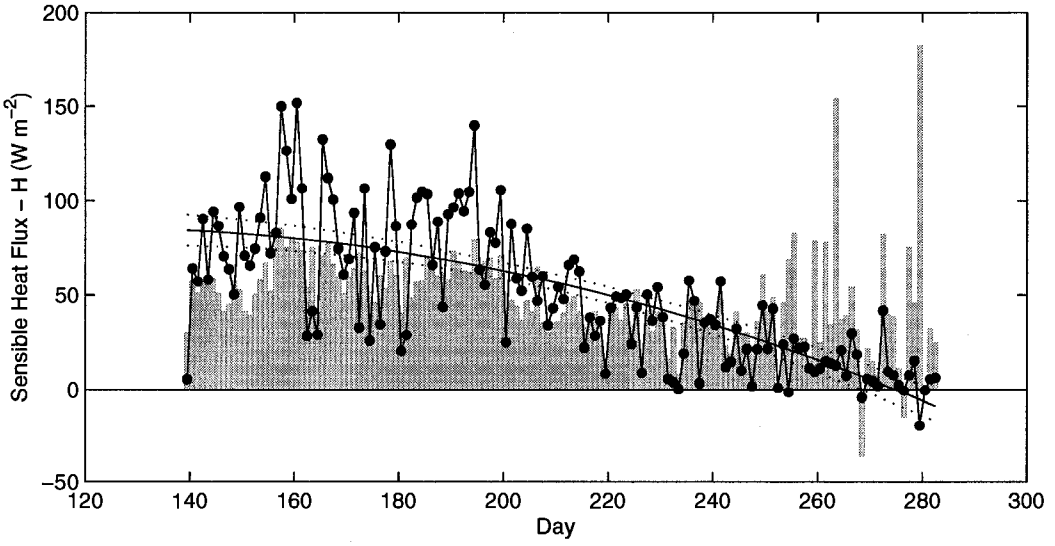

Figure 5.12: Variation of mean daily sensible heat flux for RJP92 during the 2007 growing season. Positive values of H represent turbulent flux away from the surface. Shaded bars indicate ratio of H to R_n, scaled so that the y-axis can also be interpreted as percent.

5.3.5 Latent Heat Flux

Figure 5.13 shows the daily and seasonal variability of LE above the canopy. The seasonal trend for LE is distinct from the other measured fluxes. The polynomial fit to daily average LE data has a smaller range of variability compared to H, being 35 W m^{-2} versus 95 W m^{-2}. The peak in the seasonal trend, according to the derivative of the polynomial fit, occurred on day 196, 33 days after peak R_n. In reality, minimum LE values occured during this period and corresponded with minimum θ_s. Actual peak measured values occurred even later, falling between days 201 and 227.

Over the entire study period, the polynomial fit shown in Figure 5.13 does not seem to be a robust representation of seasonal variability in LE. The correlation between Rn and LE ($R^2 = 0.33$) is not as strong compared to H because of the additional biological control on ET during dry canopy conditions, and because of a change in rainfall frequency/intensity throughout the study period.

Following day 200, with increased rainfall, smaller negative soil suction in the upper 15 cm, and gradual recharge of soil moisture storage, daily LE seemed to be more closely coupled to R_n on a daily basis; likely as a result of increased free evaporation and lower surface resistance.

During the relatively dry conditions prior to day 200, LE was typically equal to, or less than 50% of R_n. Exceptions during this period, where LE/R_n tended to equal or exceed R_n were the result of days with heavy cloud cover, small daily average R_n, and negative daily G values. Following day 200, with increased rainy conditions, LE/R_n typically exceeded 50%, being up to about 75% while G was positive. The frequency of LE exceeding daily R_n increased towards the end of the study period as R_n became

progressively smaller, with G supplying additional energy. On occasion H also supplied additional energy, with H values more negative than R_n or negative H values while R_n still remained slightly positive near dusk.

Over the study period, daily LE ranged from 6 – 101 W m^{-2} (0.5 – 8.7 MJ $m^{-2}d^{-1}$ or 0.2 – 3.6 mm), where typical daily LE was 50 ± 21 W m^{-2} (4.3 ± 1.8 MJ m^{-2} d^{-1} or 1.75 ± 0.74 mm). In comparison to the daily chronosequence data over the same time of year, OJP data ranges from 0.1 – 3.5 mm with typical values of 1.34 ± 0.73 mm, HJP75 ranges from 0.0 – 3.4 mm with typical values of 1.32 ± 0.78 mm, and HJP94 range from 0.0 – 3.4 mm with typical values of 1.29 ± 0.74 mm. LE between RJP92 and the chronosequence sites falls within the same range, where average LE values at RJP92 tend to be slightly higher for the respective years examined.

It was thought that LE at RJP92 might be systematically different than the more extensive chronosequence sites because of advective effects along the relatively short east-west axis; where advection of drier air from the surrounding area may increase LE, while advection of more moist air would suppress LE. Particular attention was paid to the potential effect of advection from the east due to the sparse nature of the spruce trees directly adjacent to RJP92 to the east, and the large tailings pond less than a kilometre to the east. Based on the temporal distribution of wind direction (not shown), a significant portion of wind from the east occurred at night when LE was low. Therefore, although advection and edge effects may have biased LE measurements at night, the effect on daily values would be negligible.

As pointed out by Baldocchi et al. (1997a) peak LE values tend to occur during the midsummer following significant rainfall when sky conditions are clear. Such is the

case on day 201, following 23.6 mm of rain on day 200, with relatively clear sky conditions ($K\downarrow$ 90% of maximum modelled value), where daily LE is approximately 3.3 mm. Since a significant portion of LE under these conditions is the result of free evaporation, all else being equal, one would expect similar maximum daily LE values for jack pine within the boreal region.

Similar results are found for the chronosequence sites, where OJP tended to require more consecutive days with rain so that soil moisture availability would not be limiting on ET. Since soil moisture availability seems to have an impact on daily total LE on sunny days following significant rainfall events, this suggests that jack pine have a relatively small canopy water holding capacity. With rapid depletion of water stored in the canopy, ET when soil moisture is not limiting should be a function of LAI. Since RJP92 and the chronosequence sites have similar LAI, this helps to explain why maximum daily LE under the above mentioned conditions is similar.

Finally, although below canopy measurements were not made, other studies suggest that the contribution to LE from the forest floor ranges between 10 to 40% on a daily basis as a result of the relatively open nature of jack pine canopies (Baldocchi et al., 1997a). The significant contribution to LE from the understory is directly related to a combination of relatively low LAI and shoot clumping common for jack pine, which allows significant incoming radiation to reach the forest floor allowing for both direct soil evaporation and transpiration from the understory vegetation (Baldocchi et al., 2000b).

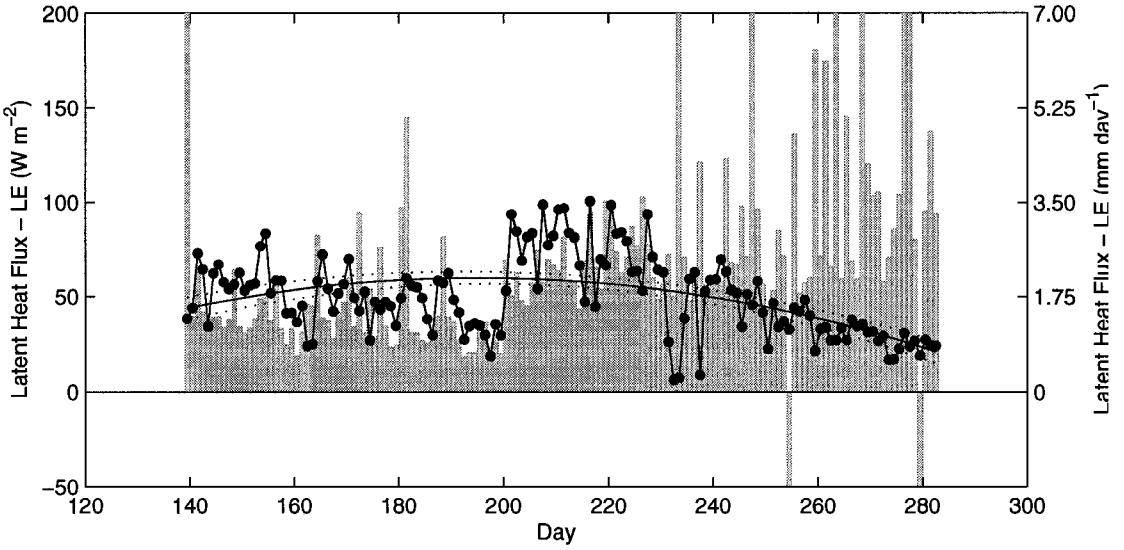

Figure 5.13: Variation of mean daily latent heat flux for RJP92 during the 2007 growing season. Positive values of LE represent turbulent flux away from the surface. Shaded bars indicate ratio of LE to R_n, scaled so that the y-axis can also be interpreted as percent.

5.3.6 Mean Diurnal Variation of Energy Balance

Figure 5.14 shows the mean diurnal variation of R_n, H, LE, and G for 5 separate periods from day 138 – 282 (mid-May – Oct.). Values presented in Figure 5.14 were calculated by averaging half hourly flux values over the specified period. Mean daily flux values for the specified periods and their standard deviation can be seen in Table 5.3, where standard error commonly reported for mean diurnal variation can be obtained by dividing by the following ($\sqrt{n}$; n = 18, 43, 31, 33, 18).

Unlike other studies which tend to divide mean diurnal variation in an unbiased fashion, such as by month (Blanken et al., 2001; Restrepo and Arain, 2005) or by field campaigns (Jarvis et al., 1997; McCaughey et al., 1997), the choice of periods was made based on differing synoptic microclimatic conditions which are summarized in Table 5.3.

Table 5.3: Climate statistics and mean energy budget terms for select periods for RJP92 during the 2007 growing season. Shaded values in brackets represent ± 1 S.D.

	Period				
	139 – 157	157 – 200	200 – 231	231 – 264	264 – 282
T (°C)	15.3	18.0	18.4	11.2	6.7
	(6.9)	(6.0)	(6.0)	(4.7)	(4.2)
VPD (kPa)	1.15	1.00	1.01	0.46	0.36
	(0.82)	(0.77)	(0.75)	(0.33)	(0.26)
Precipitation (mm day^{-1})	0.16	1.03	2.59	2.38	0.20
$-\Psi_{m,5cm}$ (kPa)	49.0	789.4	756.4	141.0	13.2
	(23.4)	(646.7)	(296.7)	(146.0)	(3.6)
R_n (MJ day^{-1})	11.84	11.19	10.17	4.80	2.31
	(3.61)	(4.00)	(3.04)	(3.08)	(1.62)
H (MJ day^{-1})	6.29	7.33	4.12	1.99	0.84
	(2.03)	(3.04)	(1.58)	(1.47)	(1.19)
LE	5.15	3.96	6.74	3.65	2.4
(MJ day^{-1})	(0.98)	(1.18)	(1.36)	(1.45)	(0.56)
G (MJ day^{-1})	0.67	0.42	0.11	-0.15	-0.24
	(0.51)	(0.30)	(0.38)	(0.38)	(0.33)
Residual	-0.27	-0.53	-0.79	-0.69	-0.71
β	1.22	1.85	0.61	0.55	0.35
$\alpha = LE/LE_{eq}$	0.54	0.43	0.74	0.83	0.84

The primary divisor was based on moisture availability, both in terms of intercepted precipitation allowing for free evaporation, and soil suction limiting loss from transpiration. Period 1 (day 139 – 157) is considered warm, with relatively high VPD, minimal precipitation, but ample soil moisture as a result of moisture stored from spring snowmelt. Period 2 (day 157 – 200) is considered hot, with relatively high VPD, moderate precipitation, and high soil suction. Period 3 (day 200 – 231) is considered hot, with relatively high VPD, significant precipitation, and high yet decreasing soil suction. Period 4 (day 231 – 264) is a warm to cool period, with relatively low VPD, significant precipitation, and low soil suction. Finally, Period 5 (day 264 – 282) is a cool period, with low VPD, little precipitation, and minimal soil suction due to moisture stored from previous rainy period and reduced ET losses.

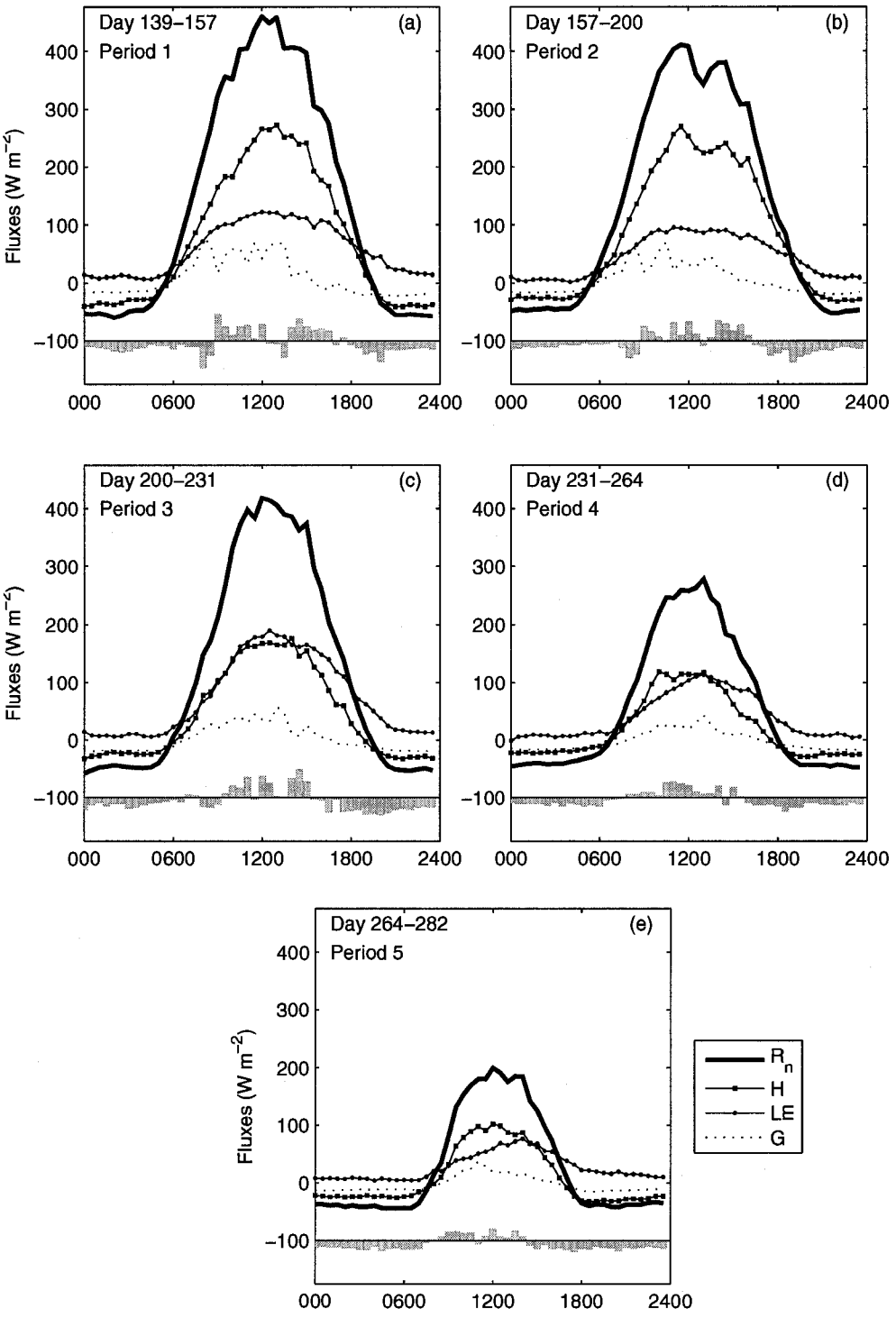

Figure 5.14: Mean diurnal variation of energy balance components (R_n, H, LE, and G) for RJP92 over several successive periods during the 2007 growing season. Shaded bars indicate energy balance residuals with a base value offset of -100 for better viewing. Negative residuals indicate flux underestimation when R_n is negative, and flux overestimation when R_n is positive. Summary of mean climatic conditions during the separate periods are summarized in Table 5.3:

The largest partitioning of energy during the daytime throughout the study period was to H. However, because LE remained slightly positive at night, daily averaged LE was greater than H following Period 2. The daily Bowen ratio increased from 1.22 to 1.85 from Period 1 to 2 as a result of limited precipitation and greater negative Ψ_m in the upper 15 cm and its resulting effect on stomatal closure. According to Chapin (2002) low soil moisture produces abscisic acid in the roots which, when transported to the needles, causes stomatal closure resulting in a reduction in g_s (increase in r_s). Furthermore, although the mechanism of the sensitivity of stomatal conductance to atmospheric humidity is poorly understood, there is a feedback from increased VPD, which creates greater evaporative potential, that results in stomatal closure, thus limiting LE under dry conditions. Following Period 2, daily Bowen ratios remained below unity, decreasing progressively from 0.61, to 0.55, to 0.35. These values are comparatively low viewed against peak daytime Bowen ratios which averaged 2.2, 2.9, 1.2, 1.6, and 2.0. Peak Bowen ratios for Periods 1 – 3 are fairly representative of midday energy partitioning. However, for Period 4 and 5, the increased Bowen ratio is more the result of increasing asynchrony between peak H and LE, with LE peaking later in the day.

Period 3 had the greatest total LE because of wet conditions and high daily R_n, where LE exceeded equilibrium values, approaching typical values (1.26) reported for free evaporation from well watered short vegetation. LE is thought to be able to exceed equilibrium values because of the entrainment of warmer, drier air from above the capping inversion maintaining a non-zero VPD as the surface boundary layer grows under convective daytime heating conditions. Despite high LE values in both absolute terms and with respect to equilibrium rates, the Bowen ratio was higher than in

subsequent periods because soil moisture had not fully recovered, with high soil suction limiting LE at the beginning of Period 3.

VPD in Periods 4 and 5 were much less than the preceding periods, potentially reducing stomatal closure. Precipitation in Period 4 continued to increase soil moisture content, resulting in near zero Ψ_s. Over the last two periods, there was increasing partitioning to LE on a daily basis, as expressed by a decreasing Bowen ratio, and a concurrent increase in LE above equilibrium rate. High θ_s and Ψ_s were maintained in Period 5 despite low levels of precipitation because of a drastic reduction in daily R_n in Period 4, resulting in reduced evaporative potential.

With respect to daily variability throughout the study period, H remained closely coupled to R_n, while LE tended to peak near midday for the first three periods and decreased less rapidly, remaining positive despite negative R_n (not shown). LE in Periods 4 and 5 tended to peak after midday, suggesting a stronger control of VPD on LE since VPD also peaked later in the day (Figure 5.15). G remained small yet significant on a half hourly basis, with mean values not exceeding 100 W m^{-2}. Nighttime fluxes of G were small and relatively constant throughout the study period ranging from 14 – 20 W m^{-2} on a diurnal basis. Mean daytime G became progressively smaller in each subsequent period along with R_n, resulting in G being a net energy sink in Periods 1 – 3 and a net source in Periods 4 and 5.

Also shown in Figure 5.14 is the mean diurnal course of the energy balance residual ($\varepsilon = R_n - H - LE - G$), with the daily average residuals summarized for the separate periods in Table 5.3. The first observation regarding residuals is that they are consistently negative when summed on a daily basis, ranging from -0.27 MJ $m^{-2}d^{-1}$ to -

0.79 MJ $m^{-2}d^{-1}$. Comparing these results to the diurnal course of residuals, where negative values represent closure greater than unity, it can be seen that there is a consistent small negative residual at night throughout the study period. During the daytime, residuals are more variable on a half hourly basis and between periods. The daily sum of residuals seems reasonably small, where they correspond to an average half hourly imbalance of -3.1 W m^{-2} to -9.1 W m^{-2}. In addition, the average maximum half hourly imbalance was on the order of ± 50 W m^{-2}.

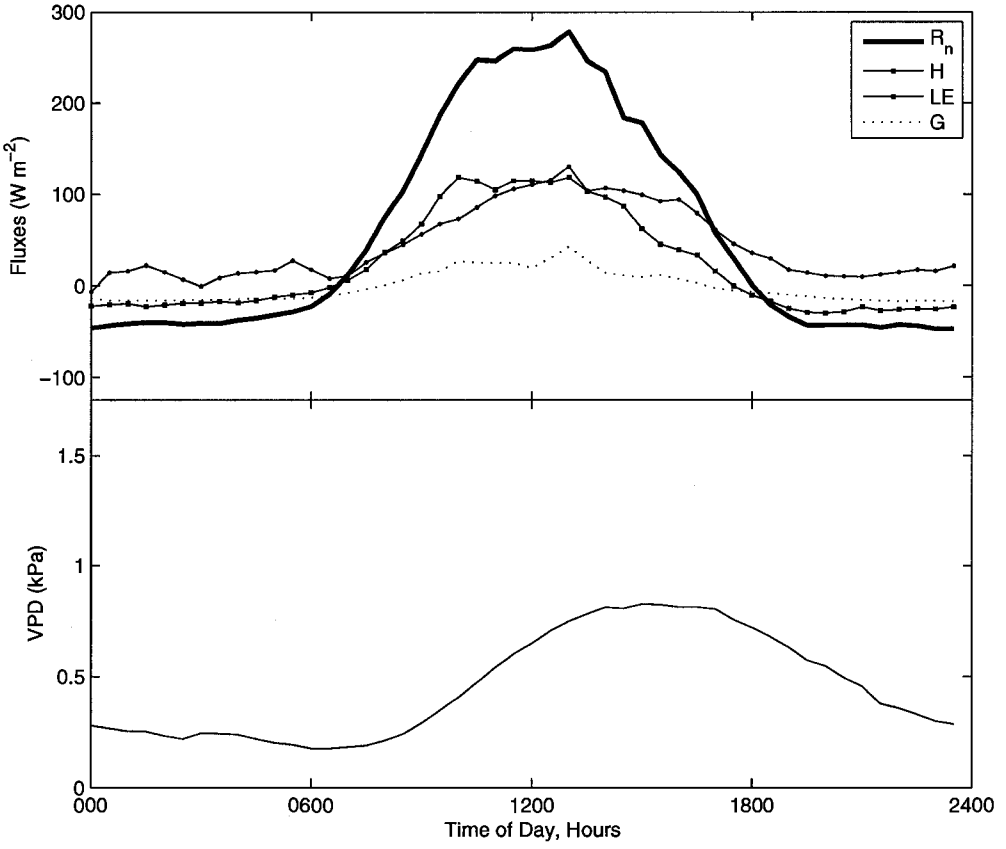

Figure 5.15: Comparison of diurnal variability of energy balance components (R_n, H, LE, and G) with vapour pressure deficit for RJP92. Data is based on the mean diurnal variation for day 231 – 264 (19 Aug. – 21 Sept.) of the 2007 growing season.

Although the CO_2 flux has not been identified as a central focus of this study, seasonal and diurnal variability in site productivity might elucidate links between vegetation, environmental variables, and ET. One of the questions raised regarding the increased partitioning of energy to LE in Periods 3 – 5 examined above is whether the vegetation played a significant role through increased transpiration in comparison to free evaporation. Results presented in sections 5.3.7 and 5.3.8 will be used to examine this question.

5.3.7 Seasonal CO_2 Flux

Throughout the literature, a variety of naming and sign conventions are used in describing the flux of carbon in a system. For clarification, the following conventions will be used for the remainder of this thesis. The net flux of CO_2 measured above the jack pine canopy using eddy covariance will be referred to as net ecosystem exchange (NEE). NEE is sometimes used interchangeably with net ecosystem production (NEP), where it is assumed that, as is the case herein, the loss of carbon through soil leaching or other non-gaseous pathways or CH_4 loss is negligible. Gross ecosystem production (GEP) represents total carbon fixation via photosynthesis, and is considered essentially equivalent to gross primary production (GPP). Ecosystem respiration (R) is the sum of respiration from the soil and plant tissues and is reported as a positive value. NEE is reported as negative when there is net uptake/assimilation of carbon ($|GEP| > |R|$) and positive when there is net efflux ($|GEP| < |R|$).

Commonly, nighttime fluxes are rejected when there is not adequately developed turbulence which results in a lack of energy balance closure due to an underestimation of turbulent fluxes. A threshold value is used to assess nighttime NEE to determine at what

value of friction velocity NEE reaches an asymptote. Values below the friction velocity threshold are rejected and are modelled for gaps greater than one hour.

Since photosynthesis stops at night without incoming PAR, nighttime NEE is actually a measure of respiration. Soil respiration is primarily modelled as a non-linear function of soil temperature, such as with all Fluxnet-Canada Reasearch Network (FCRN) sites (Amiro et al., 2006a), where the influence of soil moisture is sometimes included. The relation between soil temperature and nighttime NEE is subsequently used to model daytime R. The exponential model used by FCRN was found to poorly model nighttime respiration for RJP92 as it was not particularly sensitive to decreasing R when temperature was below 8°C.

For R values presented in Figure 5.16 the sum of square residuals indicated that a quadratic fit in comparison to linear, natural logarithmic, exponential and multiple linear regressions was best. Although the sum of squares is minimized in an absolute sense for the second order polynomial fit, the statistical significance of this result over the other results is questionable.

When nighttime relations were used to derive daytime R estimates, the values produced during peak temperature periods were suppressed using the quadratic fit. Daily average soil respiration values based on chamber measurements (unpublished Cabin data) were used to assess the reliability of modelled respiration based on nighttime relations. Again, although minimization of the sum of square residuals did not point to any specific model as being superior, when compared to daytime chamber measurements, the covariance between daily mean R from chamber measurements and multiple linear

regression incorporating soil moisture was significantly better compared to other methods examined.

Missing daytime NEE was modelled based on the non-linear relation to PPFD. When diurnal NEE is examined, it often tends to be a skewed bell shape as opposed to the more rectangular hyperbolic shape of PPFD. This suggests a significant controlling influence by temperature and stomatal conductance, both of which were combined for model purposes using VPD.

Over the study period, RJP92 was a net carbon sink, with average daily uptake of less than 1 gC $m^{-2}d^{-1}$ (Figure 5.16). However, there was significant day to day variability over the study period. Peak daily carbon uptake occurred early in the study period, with values greater than 3 gC $m^{-2}d^{-1}$ around days 144 and 157. Large day to day variability early in the season, when soil suction was not high, was closely coupled to daily incoming PPFD. However, during the days 180 – 210 when NEE fluctuated about zero, daily PPFD values were still high with peak daily values regularly exceeding 1000 μmol $m^{-2}s^{-1}$ on a half hourly basis. This seems to coincide with increasing soil suction and surface resistance. Alleviation of these limitations on NEE in the period immediately following day 200 resulted in a return to RJP92 being a net sink. Towards the end of the study period, decreasing temperatures resulted in a decrease in daily respiration. This was accompanied by decreasing daily PPFD such that over the last 20 days of the study period respiration balanced production.

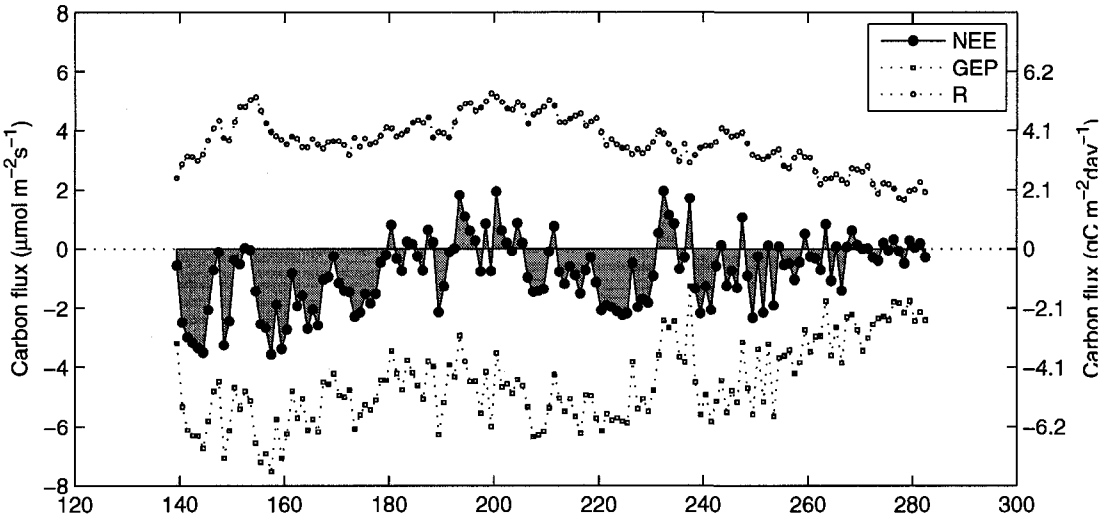

Figure 5.16: Variation of mean daily flux of CO_2 for RJP92 during the 2007 growing season. Positive and negative NEE values represent a net source and sink respectively.

5.3.8 Diurnal CO_2 Flux

Figure 5.17 shows the mean diurnal course of NEE measured above the canopy using eddy covariance. Values were computed as the mean half hourly value for the respective periods from data that had been gap filled as mentioned above.

The range of the diurnal course of NEE was similar to other jack pine stands reported in the literature. McCaughey et al. (1997) reported on the diurnal variability of a young jack pine stand in northern Manitoba (55.9°N) with maximum nighttime efflux of about 3 μmol $m^{-2}s^{-1}$ and maximum daytime net assimilation of less than 9 μmol $m^{-2}s^{-1}$ from June to August. In relation to other conifer species, the magnitude of diurnal NEE is similar to mature black spruce (Jarvis et al., 1997) and less than mature Douglas fir (Humphreys et al., 2006).

As discussed above, changes in nighttime efflux are largely controlled by soil temperature and moisture conditions. The highest nighttime efflux occurred in Period 3

which was also the warmest, and the lowest nighttime efflux occurred during the coldest, Period 5.

There was significant change in the magnitude and temporal variability of daytime NEE. The highest daytime values, which occurred in Periods 1,3, and 4, coincided with periods with a combination of near zero Ψ_s in the top 15 cm; and high peak PPFD. Despite daily R_n in Period 4 being 40 – 50 % of Period 1 and 3 values (see Table 5.3), mean peak daily incoming PPFD (823 ± 279 μmol $m^{-2}s^{-1}$) was about 60% of the corresponding values for Period 1 and 3 (1409 ± 229 μmol $m^{-2}s^{-1}$ and 1253 ± 166 μmol $m^{-2}s^{-1}$). The discrepancy between the two is the result of the dual role of day length and solar elevation angle on daily sums of radiation receipt. Although Ψ_s values in Period 3 were significantly more negative compared to Periods 1 and 4, Period 3 experienced high peak incoming PPFD, while the magnitude of Ψ_s continued to decrease throughout the period, coinciding with precipitation events. Since photosynthesis is positively correlation with PPFD and leaf water potential, and leaf water potential is linked to Ψ_s, this results in a degree of offset between the two with respect to NEE.

With respect to Periods 2 and 5, peak PPFD was high in Period 2 (1284 ± 263 μmol $m^{-2}s^{-1}$), but near surface Ψ_s attained its most negative value during this period, and although soil moisture suction was low throughout Period 5, incoming peak PPFD was small (575 ± 181 μmol $m^{-2}s^{-1}$). The contribution of the understory flora to daytime assimilation may also have decreased in Period 5 due to plant senescence. Some browning of the edges of aspen leaves and a slight yellowing had already occurred by day 224 at other sites at the same elevation within a 15 km radius. Furthermore, as temperatures decline towards autumn, frost at night can lead to reduced photosynthetic

capacity and stomatal conductance, though these effects are reversible (Baldocchi et al., 2000a). In fact, negative nighttime temperatures measured at EC height began after day 261, with several occurrences before the end of the study period.

With respect to temporal variability, there was a peak in daytime net uptake before noon in all but the last period, which peaked near or after noon. The peak in NEE prior to noon preceding a significant drop in net uptake is particularly evident in Period 2 which was relatively dry, with high near surface Ψ_m. This behaviour is often seen in the diurnal course of g_c for conifer systems (see Figure 5.20). As VPD increases, g_c drops (r_c increases) dramatically when moisture is limiting.

Due to the shared stomatal limitations to CO_2 assimilation and H_2O loss via transpiration, the changing diurnal course of NEE indicates that the increase in LE as a proportion of R_n or in comparison to its equilibrium rate following day 200 was at least, in part, attributable to transpiration. Despite high daily average and peak PPFD values in Period 2, peak daytime net uptake was low in conjunction with having the lowest value of α. In the two subsequent periods, despite a decrease in peak incoming PPFD, peak daytime net uptake increased, in conjunction with LE exceeding equilibrium rates.

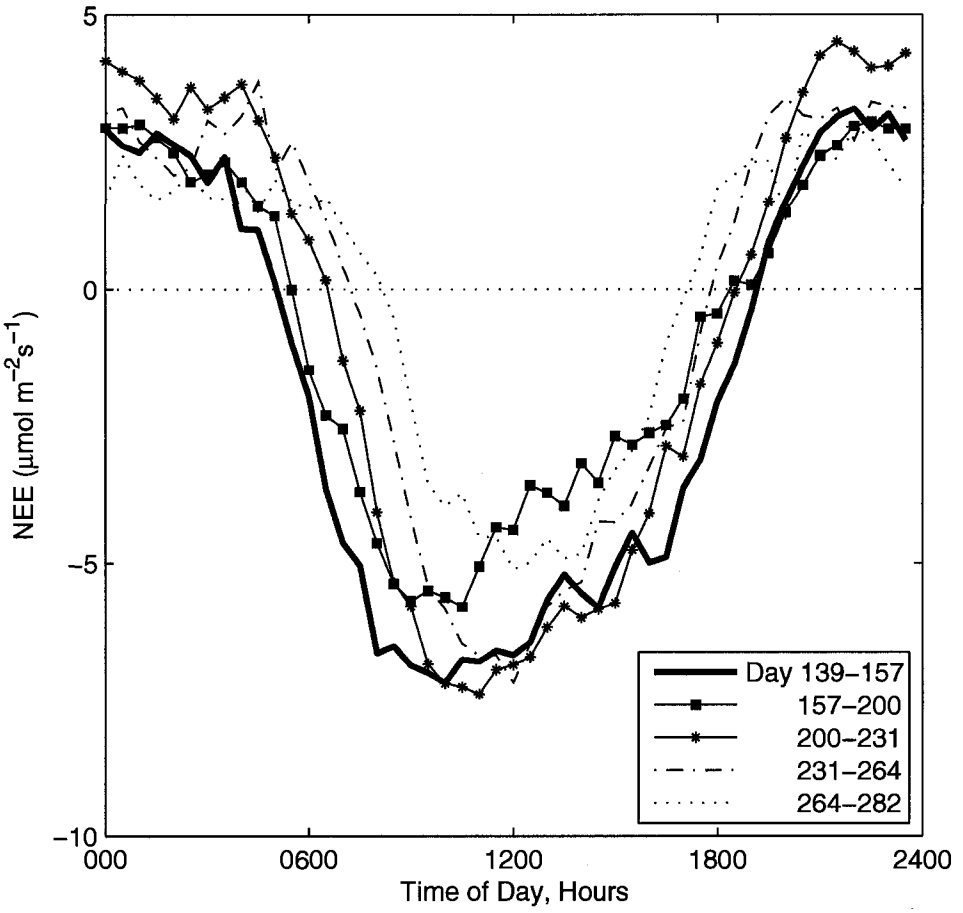

Figure 5.17: Mean diurnal variation of half-hour NEE measurements for several successive periods for RJP92 during the 2007 growing season. S.E. ranges from ± 0.39 – 0.52 (not shown).

5.4 Water Balance

For a relatively dry site where water balances are predominantly vertical (i.e. runoff and/or stream flow are negligible) and depending on the thickness of the soil profile measured, $\Sigma(P-E)$ should approximately equal the cumulative change in soil moisture storage. Referring to Figure 5.18, it can be observed that, overall, there is a moisture deficit ($E>P$) throughout the field season on a daily basis, with the exception of days with large precipitation events. When comparing the $\Sigma(P-E)$ deficit to the change in soil moisture storage, Figure 5.18 shows that the slope of the deficit is steeper than the change in soil moisture storage. Looking at days 140-160, during which less than 2 mm of rainfall occurs, ET exceeds precipitation by approximately 41 mm, whereas soil moisture storage over the profile measured was reduced by less than 19 mm.

The above observation may suggest that the jack pines at this site tap into water sources deeper than 80 cm. As previously mentioned, jack pine growing in sandy soils have been found to have tap roots at depths greater than 80 cm (Bannan, 1940). Spatial heterogeneity in the subsurface could be expected to account for some variance between the different components of the water balance. Interpolation issues might also exist due to the spacing of the soil moisture sensors. Furthermore, most rain gauges systematically underestimate rainfall with increasing wind speed. Over the range of wind speeds measured at the site, rainfall may have been underestimated by 0-15% and on average by 6% at mean wind speed.

The second major observation is that prior to the large rainfall event on day ~236, the water surplus was not captured in the soil moisture storage term. For moderate precipitation events preceded by dry periods, canopy storage could account for some of

the discrepancy. It is also possible that extended dry periods could have created slightly hydrophobic soil surface conditions affecting the ability of the soil to absorb water. Although the site is relatively flat locally, small amounts of the water budget may have been lost to overland flow where a small drainage ditch is located on the western edge of the site.

Possible evidence for the presence of hydrophobic conditions is in the difference in the change in the soil moisture storage term following doy ~236, compared to the previous period, where precipitation events are closely matched by equivalent changes in soil moisture storage. Since these rainfall events occur during 'wet' periods where R_n and VPD are concurrently low, canopy storage is more likely to be saturated and hydrophobic conditions eliminated.

Some temporal discrepancy can be attributed to the different temporal scales at which the results are recorded, where soil moisture was recorded every 4 hours, LE every ½ hour, and precipitation every 0.254 mm. Comparison of total precipitation measured over the study period against two other rain gauges located within a 10 km radius of the study site shows up to 15.5% variability in total precipitation, where in fact both of the other stations measured less precipitation than the one located closest to the study site.

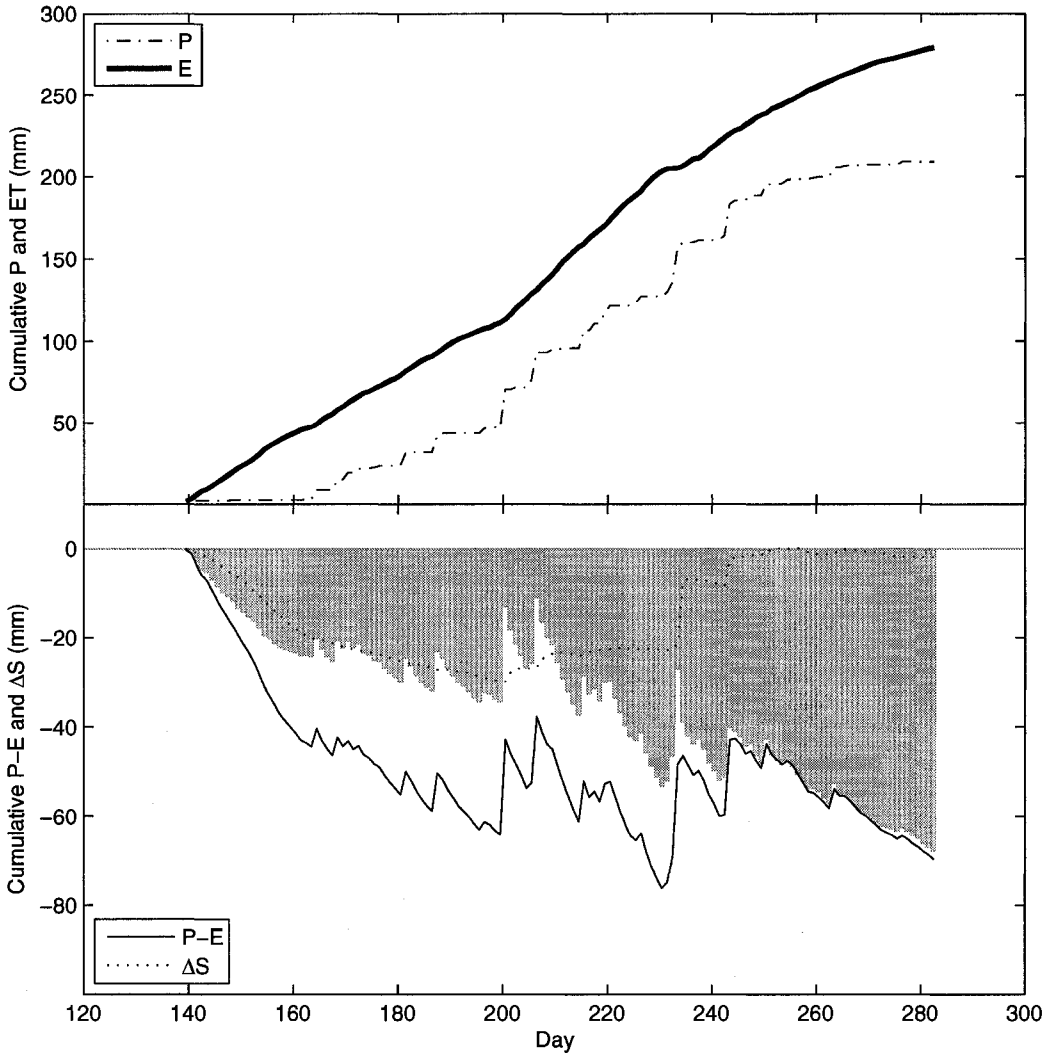

Figure 5.18: Cumulative sum of select water balance components (P, E, and ΔS) for RJP92 over the 2007 growing season. The shaded bars in the lower panel represent the difference between cumulative precipitation deficit and soil moisture storage measured between 0 and 80 cm.

5.5 Controls on LE

Long term regulation on plant growth in the western boreal region is affected by cold temperature and the relatively dry environment. These conditions limit decomposition rates within the soil, reducing the rate of nutrient cycling. Since photosynthetic capacity scales with leaf nutrition (Field and Mooney in Givnish, 1983), low nutrient availability would result in slow growth rates. Slow growth rates produce narrow growth rings with reduced hydraulic conductivity, limiting potential transpiration rates (Baldocchi et al., 2000a). This feedback between climate, growth rates, and potential transpiration cause jack pine, in general, to be conservative with respect to ET, allowing them to survive in dry environments.

ET in the short term, which is linked to ecosystem parameters such as plant productivity, nutrient and water cycling, is not simply a function of meteorological conditions but rather there is additional biophysical control by the vegetation (Shuttleworth and Calder, 1979) which will be examined in more detail. To accomplish this objective, a number of methods identified from the literature will be used.

First, normalizing measured LE by estimated rates of equilibrium LE (Equation 2.17) helps to diagnose how biotic factors control daily ET relative to the amount of available energy, where low values are associated with dry low productivity forest systems such as jack pine (Baldocchi et al., 2000a). Second, under good soil water availability, PAR and VPD are the two major environmental factors that control stomatal conductance for a variety of species (Baldocchi et al., 1991). The role of stomatal conductance in the control of water use will be examined using the decoupling coefficient

(Equation 2.18) and a multiplicative non-linear model (Jarvis, 1976; Jarvis and McNaughton 1986).

5.5.1 Equilibrium LE

Examination of the Penman-Monteith equation identifies the primary environmental and biophysical factors which control evaporation, which are available energy ($R_n - G$), the humidity concentration gradient and atmospheric demand (VPD), surface resistance (r_s), and aerodynamic resistance (r_a). It should be noted that resistance and conductance are used somewhat interchangeably in the literature, where $r_0 = 1/g_0$.

The ratio of LE to its equilibrium rate (LE/LE_{eq}) helps to diagnose the degree of biotic control on ET, with lower values implying greater biotic control and high values implying a close coupling to available energy. Figure 5.19 shows the magnitude and variability of LE/LE_{eq} over the study period, where results have been separated according to modelled periods where the canopy remained wet or partly wet.

Under dry canopy conditions prior to day 200, daytime LE remained below equilibrium levels, beginning at an average LE/LE_{eq} of 0.51 and trending downwards to 0.26. These values indicate a strong increasing biological control on LE as soil suction becomes more negative, causing stomatal closure, where LE/LE_{eq} values are comparable to values reported for OJP in Baldocchi et al. (1997a). Comparing annual precipitation in 1994 for Prince Albert, SK (100 km SW of OJP) to 1971-2000 climate normals (Environment Canada), 1994 values exceeded the norm by 16.8% and exhibited typical seasonality with a significant portion of annual precipitation occurring during the summer.

Following day 200, as soil moisture becomes progressively less limiting, LE/LE_{eq} increases to where values continuously exceed 0.60 after day 215. These results differ from those of Baldocchi et al. (1997a). It is believed that the different soil textures played an important role in modulating seasonal LE/LE_{eq}. In sandy soils common for jack pine, soil moisture is rapidly depleted following precipitation events. For RJP92, with a silt loam soil texture, high soil moisture was maintained over an extended period, allowing for greater LE/LE_{eq}.

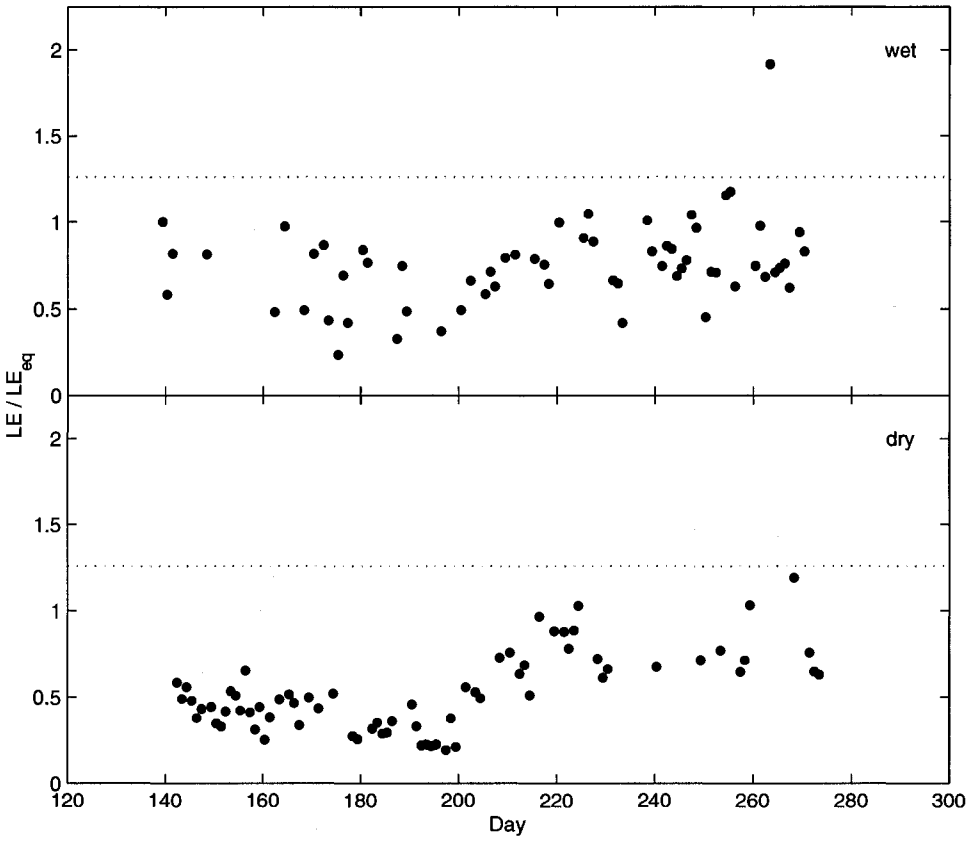

Figure 5.19: Variation of the mean daytime (0800 – 1800) ratio of LE to equilibrium LE (Priestly-Taylor α) for wet or partially wet (top panel) and dry (bottom panel) canopy conditions for RJP92 during the 2007 growing season. The dotted line in both panels represents a typical α value of 1.26 for a relatively smooth, freely evaporating surface.

During wet canopy conditions, LE/LE_{eq} in general was higher than under dry canopy conditions, with a mean daytime value of 0.78 over the entire study period and only 12% of values being equal to or greater than unity. Because of the small canopy storage capacity of jack pine and relatively high aerodynamic roughness, the canopy does not remain saturated for extended periods of time, with biological control exerting increasing influence with increasing time from rainfall events.

Figure 5.20 further examines the link between LE/LE_{eq} and surface resistance. There is a clear relation between LE/LE_{eq} and r_s, where LE/LE_{eq} decreases non-linearly with increasing r_s. Since r_s is calculated by rearranging Equation 2.16, some caution should be used in interpreting results illustrated in Figure 5.20 since there is some degree of autocorrelation with both variables being a function of LE (Baldocchi et al., 1997a). The choice of a natural logarithmic fit of the form $LE/LE_{eq} = a_1 \cdot \ln(r_s)^{-1} + a_2$ came from relations used in the literature (Wever et al., 2002) which compared well to the exponential fit of the form $LE/LE_{eq} = a_1 \cdot (a_2 - \exp(-r_s \cdot a_3))^{-1}$ (Monteith, 1995; Blanken et al., 1997) for RJP92.

Discrepancies between the two models occurred most notably at low values of r_s (< 75 s m^{-1}) where modelled LE/LE_{eq} approached a maximum value of 1.4 for the exponential fit, whereas the natural logarithmic fit approached infinity. Despite producing more appropriate estimates at low r_s, with values approaching equilibrium levels, the model seemed to be unstable under certain conditions, where modelled results for HJP75 and HJP94 were extremely poor.

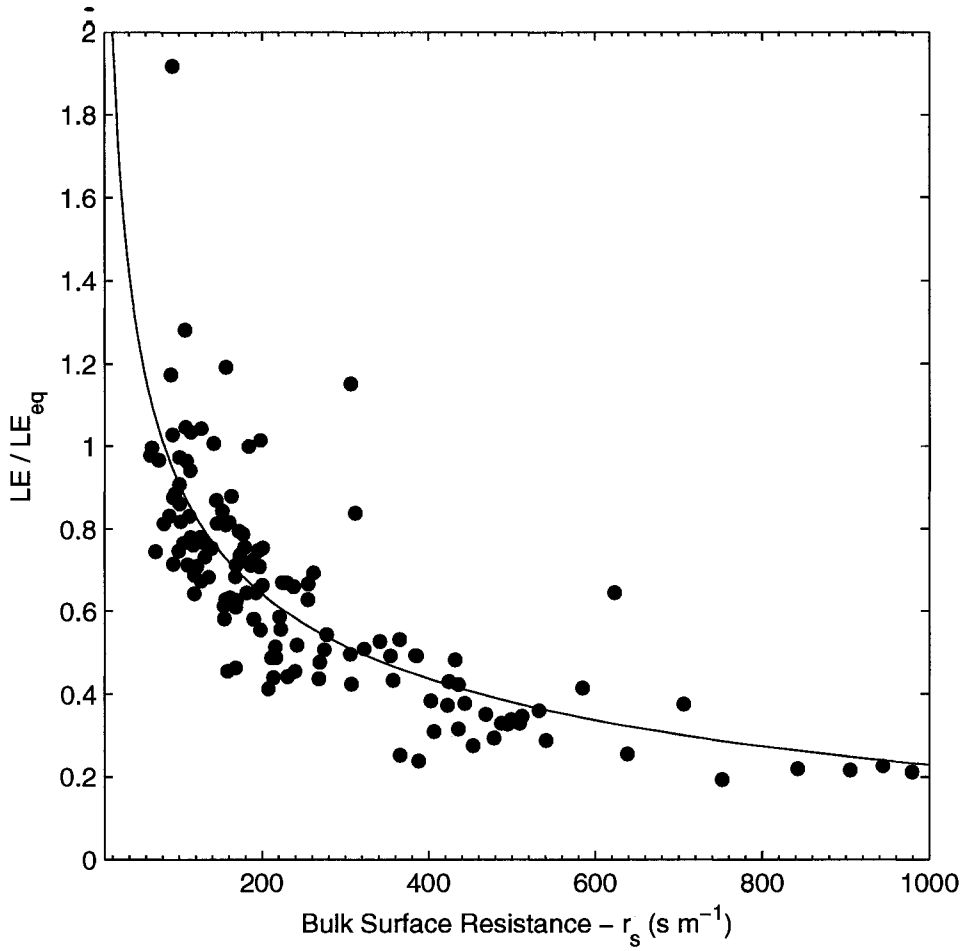

Figure 5.20: Relation between bulk surface resistance and Priestly-Taylor α. Values represent mean daytime values (0800 – 1600). The line represents the following fitted regression ($LE/LE_{eq} = 9.38[\ln(r_s)]^{-1} - 1.13$).

Figure 5.21 shows the results of the modelled LE/LE_{eq} values based on the logarithmic relation to r_s for RJP92 and the jack pine chronosequence sites. Firstly, the results indicate that the relation between r_s and LE/LE_{eq} for RJP92 lies between the young and more mature stands. Secondly, the modelled relations were very similar between OJP and HJP75, and were lower than HJP94. This implies greater biological control over LE by the more mature stands with greater LAI, which may also influence r_a. As LAI of the

jack pine stands increase, less radiation would reach the forest floor, increasing the importance of canopy LE over LE from the soil surface and understory vegetation.

The similar relation between r_s and LE/LE_{eq} for RJP92 and the 3 chronosequence sites suggests that, despite different edaphic conditions that are the result of the engineered soil cover at RJP92, the reclaimed site is behaving 'normally' or within the bounds of behaviour exhibited by the chronosequence sites for the years chosen.

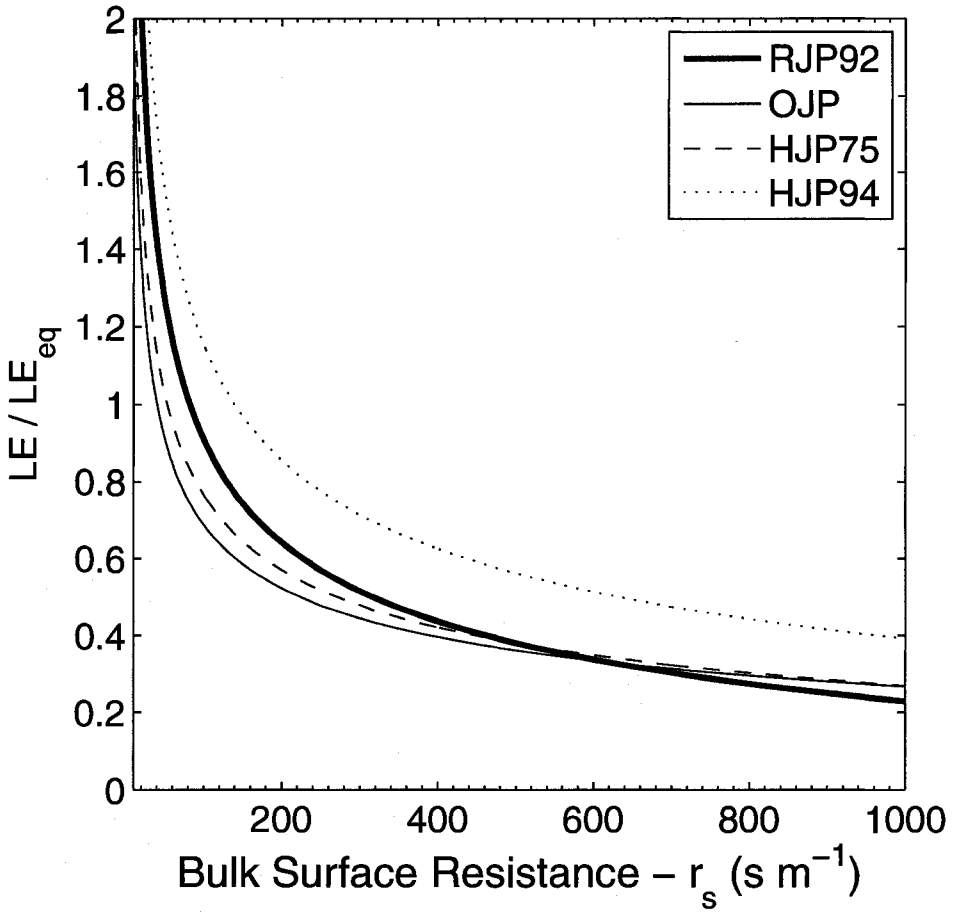

Figure 5.21: Comparison of least squares fit of $a_1 \cdot \ln(r_s)^{-1} + a_2$ to LE/LE_{eq} for select boreal jack pine stands.

5.5.2 Aerodynamic and Surface Resistance

According to Chapin (2002) aerodynamic resistance is the main way vegetation influences LE from dry canopies when there is an adequate supply of soil moisture, whereas canopy resistance imposes only some additional control with increasing importance as soil moisture declines. This implies that r_s accounts for the temporal variability in LE in response to drying soils when the canopy is dry. Examination of the Penman-Monteith equation (Eq. 2.16) indicates that when water is freely available (i.e. r_s is small) available energy (or net radiation if G is small) is the dominant control on LE for aerodynamically rough forests with relatively low r_a as unrestricted moisture supply to the atmosphere theoretically results in a VPD near zero.

Figure 5.22 illustrates the difference in the magnitude and temporal variability of daytime aerodynamic and surface resistances. It is clear that in general, r_a is less than r_s for the jack pine stand. Because of its dependence on surface roughness and wind speed, r_a remains relatively constant over the study period, with a mean daytime average of 30 s m^{-1}. This is relatively high in comparison to the typical range for forests reported by Oke (1987), 5 – 10 s m^{-1}, and actually lies within the range of values for crops. This is surprising since, in general, conifer forests are aerodynamically rougher than broad-leaved forests (Baldocchi et al., 2000a). There are two considerations to be made regarding this incongruity. First, RJP92 is not a mature forest, and therefore would likely have higher r_a values compared to a taller mature stand. Secondly, when the distribution of half hourly r_a values are examined, the peak does occur much closer to reported values, around 14 s m^{-1}, where the majority of values lie between 0 – 30 s m^{-1}.

Canopy/surface resistance is effectively an order of magnitude greater than r_a prior to increased precipitation following day 200. Prior to day 200 average daytime r_s was 466 s m^{-1}, and 210 s m^{-1} following day 200. Similarly to r_a, examination of the half hourly distributions of r_s indicates peaks in the distributions at 180 and 120 s m^{-1} for the early and late periods respectively, which are more commensurate with the typical range of values reported by Oke (1987).

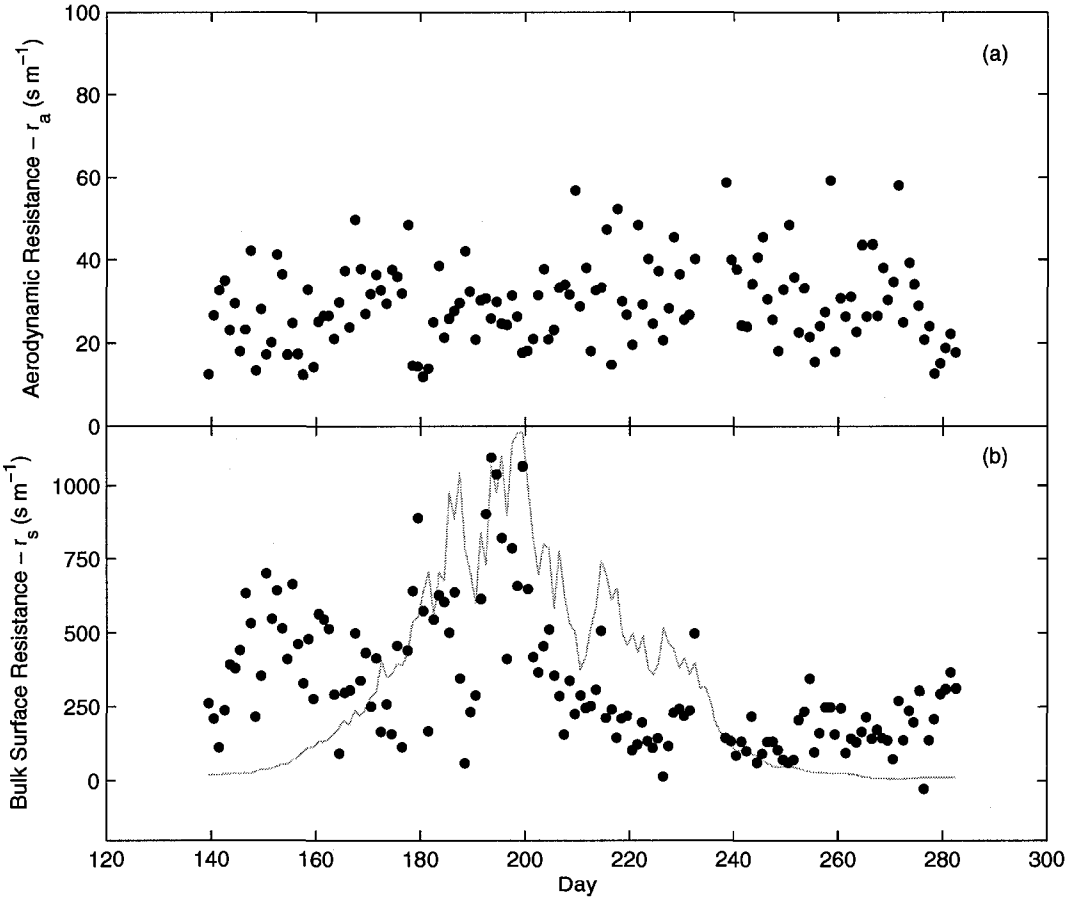

Figure 5.22: Variation in aerodynamic (a) and bulk surface resistance (b) over the 2007 growing season. Calculated values represent daytime averages, with daytime defined as $K\downarrow > 0$ W m^{-2}. r_a was calculated according to Eq. 4.8 and r_s by rearranging the Penman-Monteith equation (Eq. 2.16). Light gray line in lower panel represents daily mean soil suction measured at 5 cm depth, inverted and scaled to y-axis for visual comparison to r_s.

Comparing results to OJP presented in Baldocchi et al. (1997a) after conversion from mmol m^{-2} s^{-1} to s m^{-1} using the ideal gas law, r_a was very similar with values centered around 13 s m^{-1}. Typical values of r_s were greater than 265 s m^{-1} with values centered around 500 s m^{-1} (Baldocchi et al., 1997a). According to Baldocchi et al. (1997a) these resistance values are high compared to conifers, but agreed with independent branch level measurements.

As mentioned above, daily r_s responds to the change in precipitation regime, where increasing soil moisture storage is available for uptake by the roots. ET has been shown to be relatively insensitive to soil moisture changes when above a certain threshold, where values differ by study in relation to soil hydraulic properties and tree species. Kelliher et al (1998) gives a general threshold value of 50% for conifer forests, whereas Chapin (2002) reports a value of 25% of available water. To avoid use of threshold values, comparisons were made between r_s and soil suction because of the non-linear relation between θ_s and Ψ_s, and the more direct link between soil suction and leaf water potential.

Although the relation is not perfect, the relative change in moisture availability expressed as soil suction in the top 10 cm of soil illustrated in Figure 5.22b shows an increase in canopy resistance in response to high soil suction from day 180 – 200. Following day 200, r_s decreased as a result of increased free evaporation from a wet canopy and in response to greater moisture availability as rainfall events lowered Ψ_m. Since evaporation of intercepted water occurs fairly rapidly, given adequate R_n and VPD due to aerodynamic roughness, soil moisture availability is thought to play a significant role in drastically reducing the mean daytime values of r_s for RJP92.

Univariate analysis of surface resistance is used on a daily basis, and not on a half hourly basis, because a strong half hourly relation is not to be expected for RJP92 which has a low LAI and an open canopy. This results in significant R_n reaching the forest floor, resulting in potentially significant contributions to the energy balance by the forest floor, making it a vertically-separated dual source system (Kelliher et al., 1998). Averaged over the day, however, spatial variability becomes less important.

Based on empirically derived models of canopy conductance, potential controlling environmental variables include PPFD, air temperature, available moisture, and atmospheric moisture demand (VPD). Where daily air temperature is relatively constant and under good soil water availability, PPFD and VPD become the two major environmental factors that control stomatal conductance for a variety of species (Baldocchi et al., 1991).

Blanken et al. (1997) illustrate an additional biophysical control on canopy conductance, where g_c is linearly related to LAI for aspen. Chapin (2002), however, indicates that surface resistance is relatively insensitive to LAI because there is a trade-off between transpiration and soil evaporation. Since understory measurements were not made at RJP92, canopy and surface resistance cannot be separated. LAI was, therefore, not considered when examining resistance-conductance, coupled with the fact that measured changes in LAI were modest.

Figure 5.23 provides an example of the response of daytime surface resistance to PPFD and VPD, where mean daily temperature remains fairly constant. Under dry canopy conditions and relatively cloud free days, results are similar to those presented by Blanken et al. (1997) for a mature aspen boreal forest, where surface resistance is low in

the morning due to recharge of plant water overnight, combined with rapidly increasing PPFD. Surface resistance increases in the afternoon along with increasing VPD. Surface resistance does not begin to decrease with VPD in the early evening due to low PPFD levels.

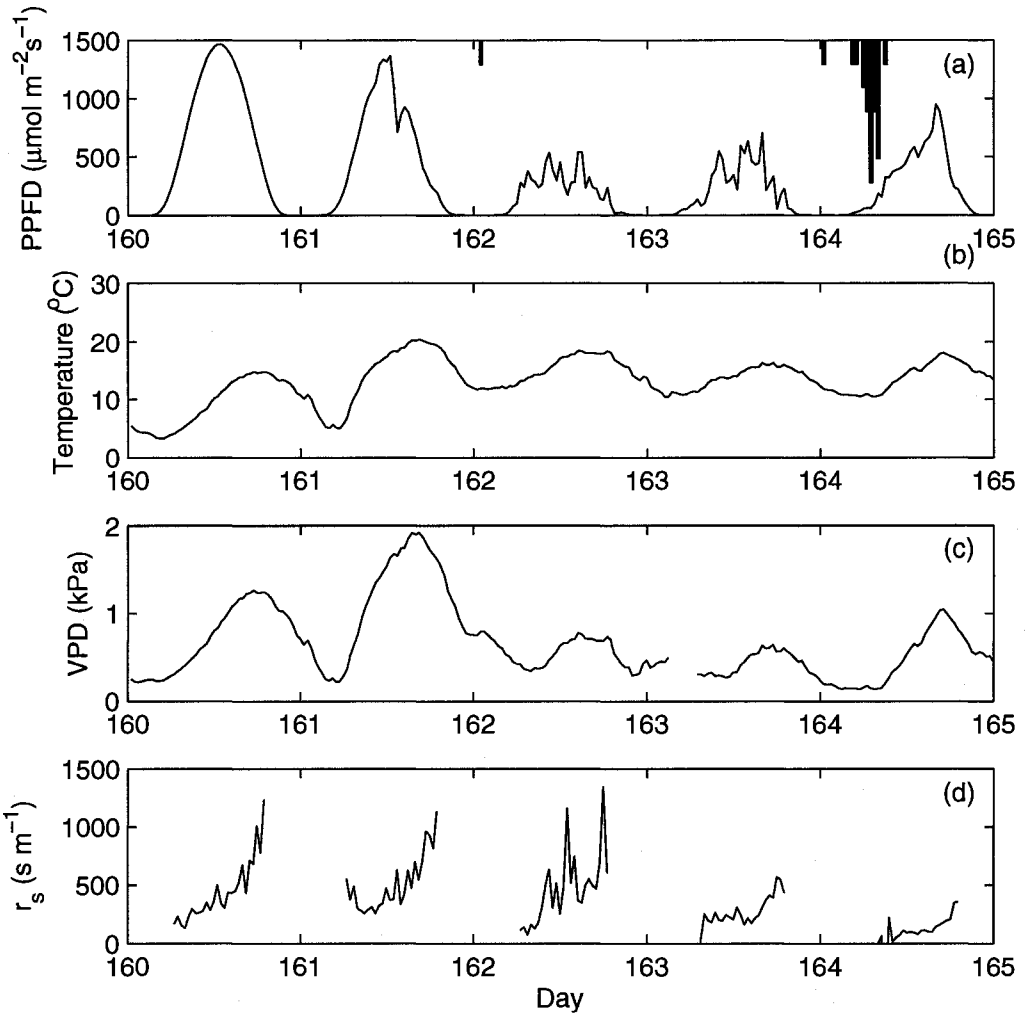

Figure 5.23: Example of half hour measurements of (d) surface resistance (r_s) and some of its environmental controls (a) PPFD, (b) temperature, and (c) atmospheric moisture deficit (VPD) for several consecutive days in June, 2007 progressing from clear to cloudy skies, to rainy conditions. Bars in panel (a) indicate timing and relative magnitude of precipitation with a maximum half hour value of 1.5 mm.

For the cloudy days shown, r_s was of a similar magnitude to sunny days as a result of low PPFD values throughout the day, where r_s values on day 163 were lower due to a slight decrease in VPD and increase in PPFD compared to day 162. The pronounced effect of wet canopy conditions on r_s can be seen for day 164, where median r_s was 98 s m^{-1} compared to the preceding days where values ranged from 240 – 480 s m^{-1}.

The dramatic effect that canopy wetness and decreased r_s have on energy partitioning can be examined by contrasting the midday Bowen ratio over the sample period in Figure 5.23. On the days with relatively clear skies, average daytime Bowen ratios exceeded 2.8, on cloudy days they were approximately 2, and on the final day with wet canopy conditions, the Bowen ratio was about 0.8.

As previously suggested above, increasing VPD throughout the day tended to cause an increase in r_s during dry conditions, and was exacerbated when soil moisture was limiting, with the effect of causing a drop off in net CO_2 uptake following noon (Figure 5.17). Although LE did not decrease as markedly in the afternoon, the diurnal variability was nonetheless affected, where LE peaked near noon while gradually decreasing instead of maintaining elevated LE levels later in the day (Figure 5.14).

Figure 5.24 shows the general relation between daytime VPD and bulk surface resistance, which encapsulates canopy resistance, for periods with contrasting soil moisture conditions on days with a dry canopy. The linear regression lines do not imply a physically based linear relation between the two variables, but rather serve to highlight the potential effect of soil moisture availability. As expected, r_s increases with increasing VPD. However, of note is that over the range of measured VPD, mean daytime r_s in the

relatively dry period (day 139 – 201) was significantly greater than that of the relatively wet period (day202 – 282).

Interestingly, it is pointed out by Grantz (1990) that if plants are to respond directly to atmospheric humidity by somehow 'sensing' it, it would have to be at the leaf ('needle') surface and that, particularly in dense canopies, the humidity conditions at the plant surface need not be similar to that prevailing in the atmosphere as measured above the plant canopy. With RJP92 having a relatively low LAI, an open-canopy, and relatively high aerodynamic roughness, the canopy space should be well mixed with the air above, particularly during daytime convective conditions.

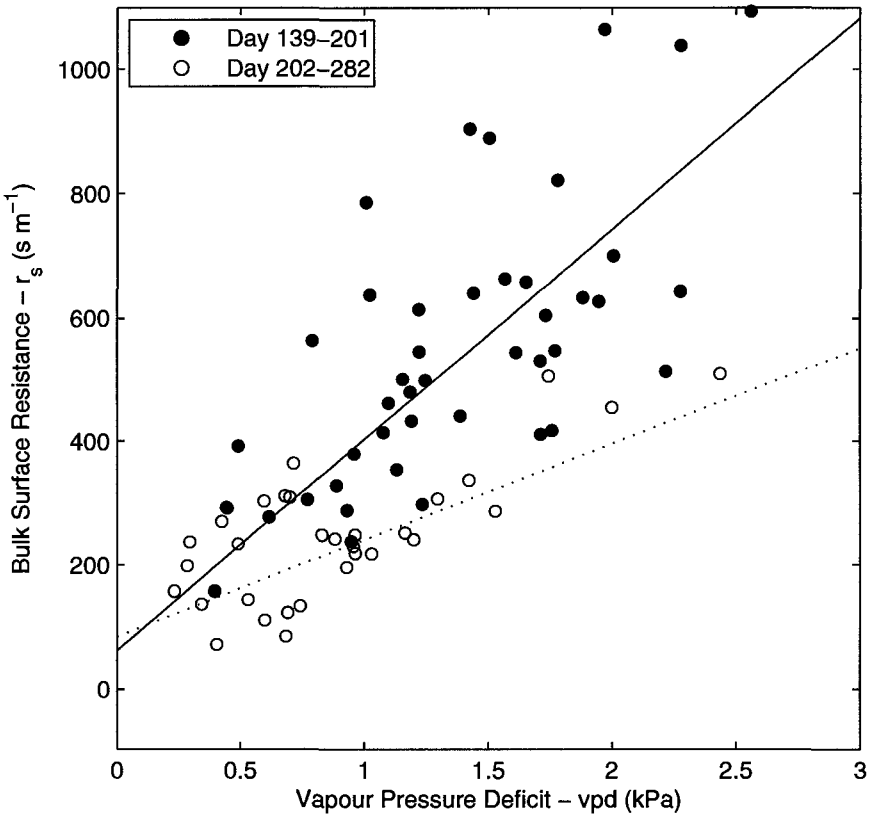

Figure 5.24: Mean daytime vapour pressure deficit versus bulk surface resistance over the 2007 growing season. Average daytime soil suction at 5 cm depth during the early and late period are -535 kPa and -344 kPa respectively.

Different models have been developed to assess the response of r_s to various environmental variables. Commonly used is an empirically based non-linear phenomenological model (Marcelo et al., 1999; Wever et al., 2002; Humphreys et al., 2003) of the general form described by Jarvis (1976) where:

$$r_s^{-1} = a_1 f(PPFD) f(VPD) f(A_w)$$

$$f(PPFD) = \frac{PPFD}{a_2 + PPFD}\left(\frac{1000}{1000 + a_2}\right)$$

$$f(VPD) = \frac{1}{1 + a_3 VPD}$$

$$f(A_w) = 1 - (1 + A_w)^{-a_4}$$

where $a_{1\text{-}4}$ are fitted parameters, PPFD is in μmol m^{-2} s^{-1}, VPD is in kPa, and A_w is available water calculated as a percentage of VWC. Generally, a_1 is considered to be the maximum conductance under non-limiting conditions. Parameter estimates for the model were obtained using a Nelder-Mead simplex algorithm (MathWorks, 2007). The model was applied to RJP92 and only two of the chronosequence sites since soil moisture data was not available for HJP94, with comparisons of model results presented in Figure 5.25.

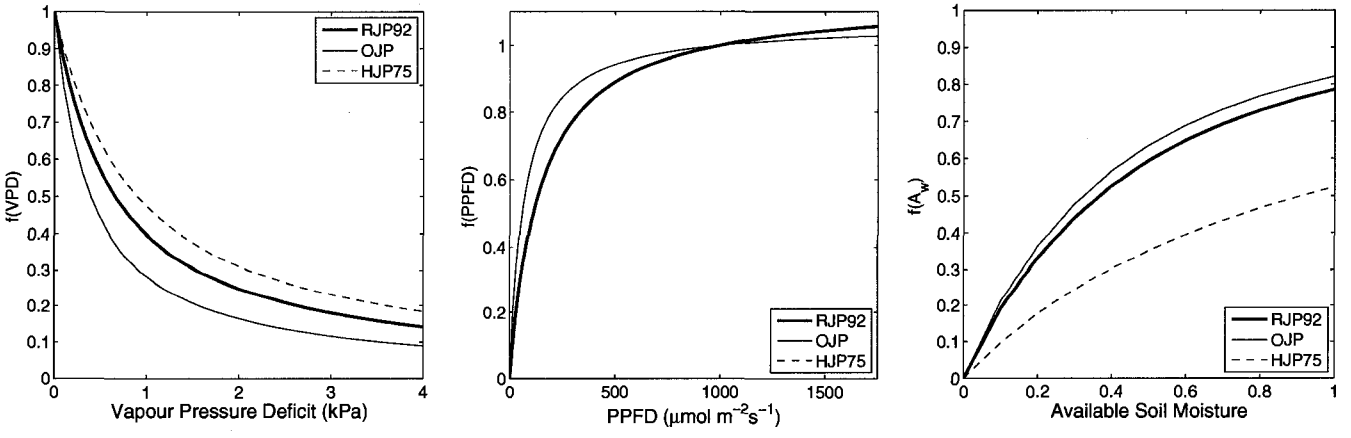

Figure 5.25: Comparison of functions of the r_s^{-1} model for RJP92, OJP, and HJP75 for daytime (0800 – 1800 h) for the entire growing season.

Results from Figure 5.25 show that the response of r_s^{-1} to PPFD is fairly similar across all three sites, likely because it is a function of the physical light response of chlorophyll (i.e. it is species dependent and not age dependent). The respective responses to VPD and available soil moisture are, however, more variable. Compared to their respective monthly climate normals for precipitation RJP92 (2007) and OJP (2002) were more than 15% below average totals, while HJP75 (2005) was more than 15% above average. When results are examined for OJP (2005), when precipitation is greater, the response to available moisture is decreased such that the relation is very similar to RJP92. Consequently, the response of OJP to VPD increases slightly. Although the modeled relations shown are for different years, the response of r_s to available moisture for OJP and HJP75 still remains large when both are evaluated for 2005 (not shown). Over the entire soil profile measured, θ_s at HJP75 exceeded OJP by between 0.02 – 0.04 m^3 m^{-3}, or on the order of 20% of field capacity. This difference in mean θ_s between OJP and HJP75 could account for the differing response of r_s to θ_s since θ_s is systematically higher at HJP75 with presumably less negative soil suction since both stands grow in sandy soil. These results, if nothing else, serve to demonstrate that the response of the biophysical control, r_s, on LE for RJP92 lies within the range of variability experienced for natural jack pine stands.

5.5.3 Decoupling Coefficient and WUE

In order to evaluate the relative importance of r_s over available energy and VPD on LE, Figure 5.26 examines the diurnal variability of Ω over the Periods 1 – 4. The value of Ω ranges from 0 to 1 with the control of ET by surface conductance increasing

as Ω approaches 0 (Jarvis and McNaughton, 1986). Conversely, high values imply a decoupling of ET response to changes in the overlying air steam.

Similar to the results of Wever et al. (2002), in general, Ω was highest in the morning, and gradually decreased throughout the day as stomatal closure exerted a stronger control on water loss. Average peak daytime values of Ω were relatively low at RJP92, ranging from 0.19 to 0.35. Low values of Ω are indicative low r_a and high r_s which may be the result of moisture stress. However this is relative to the plant species, where Ω values for jack pine and other conifers tend to be low. For perspective, average dry-canopy Ω for Douglas fir was reported as 0.24 ranging from 0.15 – 0.35 (Humphreys et al., 2003). The distributions for daytime half hourly Ω were also examined for the three chronosequence site. Median values over the summer were even lower with 0.14, 0.17, and 0.18, for OJP, HJP75 and HJP94, with standard deviations of a similar magnitude to their respective median values.

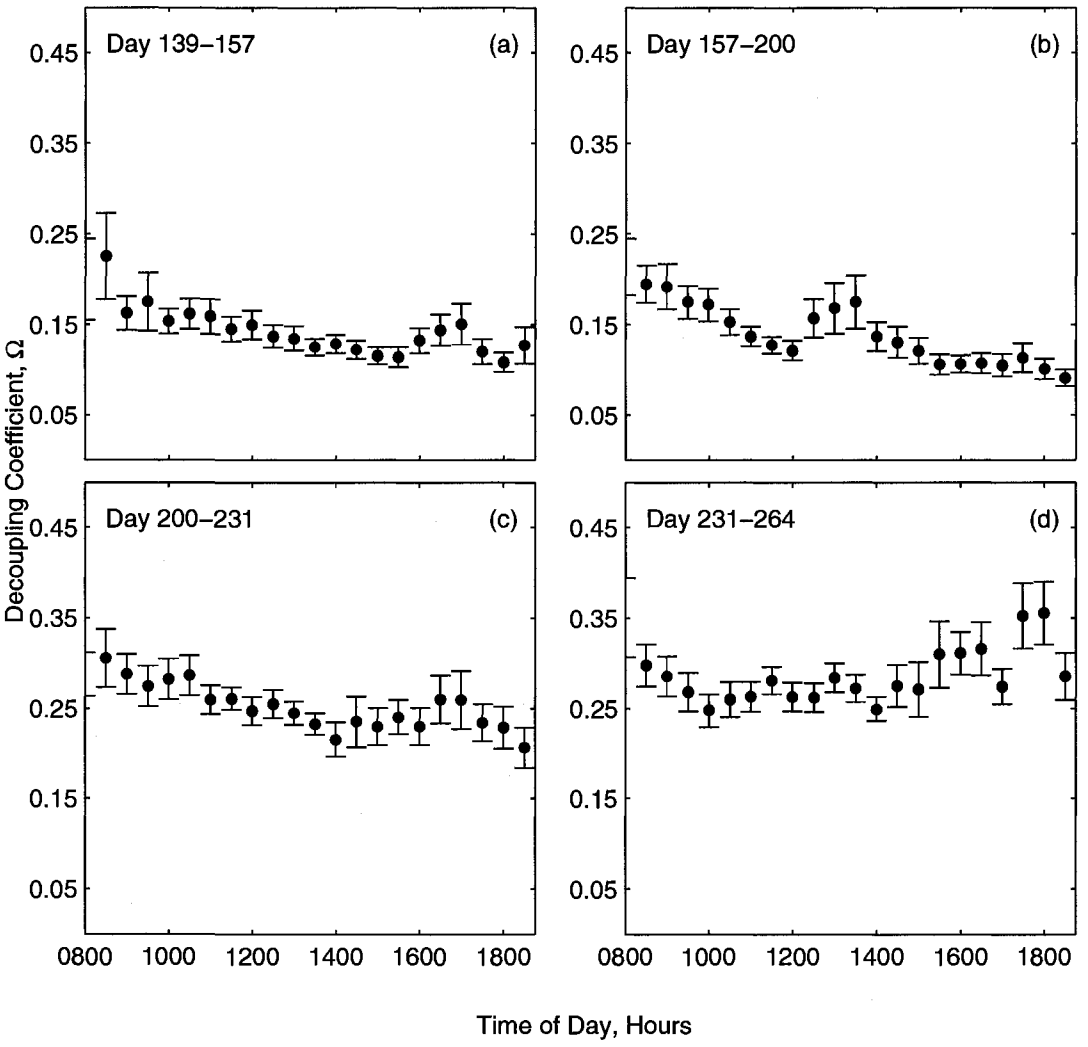

Figure 5.26: Daytime half-hour variation of decoupling coefficient for several consecutive periods at RJP92 during the 2007 growing season. Vertical bars indicate ± S.E.

With surface resistance imposing greater control on LE over the growing season for OJP and HJP75 compared to RJP92, it was examined whether this had any discernable effect on water-use efficiency (WUE = dGEP/dE). All else being equal, higher stomatal control (i.e. surface resistance) of LE should reduce the water cost of carbon gain (Wever et al., 2002). In addition, higher LAI would reduce water loss from soil evaporation. Despite these factors, WUE (slope of the regression line in Figure 5.27) for RJP92 and the two chronosequence sites is quite similar with values of 2.27, 2.21, and 2.19. Because wet canopy conditions were not removed from the analysis of WUE, the higher LAI of OJP and HJP75 implies greater potential water loss from evaporation of intercepted water. Wet canopy conditions were not removed because data from a leaf wetness sensor was not available for HJP75.

These values of WUE are low in comparison to other values for boreal species. Kljun et al. (2006), reporting on mature aspen, black spruce, and jack pine, gives WUE values of 4.62, 3.12, and 3.12 g C kg^{-1} H_2O, which compares to values for the same aspen and black spruce stand by Arain et al. (2002) of 2.85 and 2.82 g C kg^{-1} H_2O. WUE for a northern grassland ranged from 1.68 – 2.09 g C kg^{-1} H_2O (Wever et al., 2002). The discrepancy between results in Figure 5.27 and OJP in Kljun et al. (2006) could be the result of the choice of averaging period or the regression method. WUE in Kljun et al. (2006) is based on monthly averages as opposed to weekly averages herein. Furthermore, the regression used to obtain results in Figure 5.27 was a weighted least-squares fit which incorporated the error in both ET and GEP.

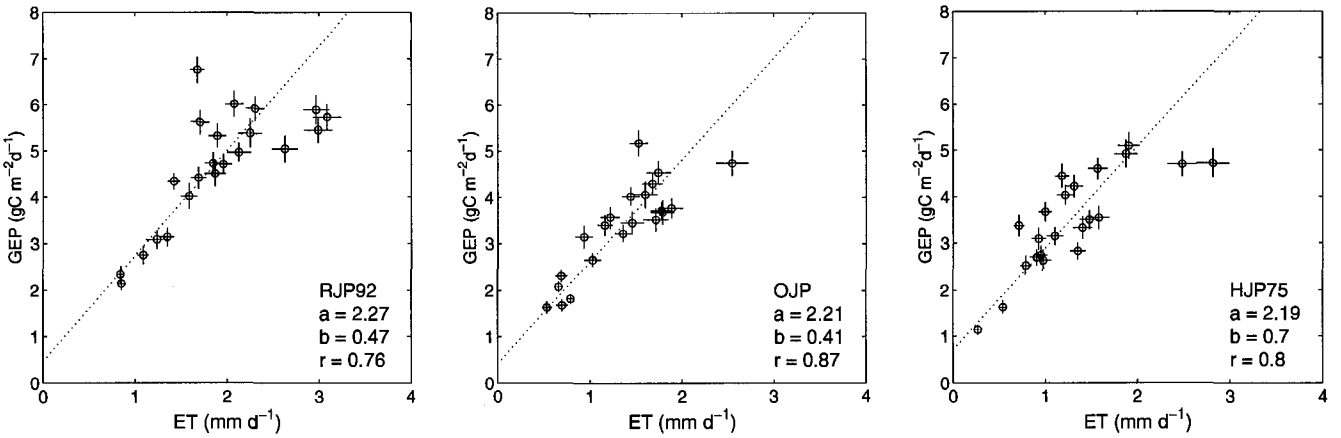

Figure 5.27: Comparison of growing season relation between ET and GEP. Data is presented as weekly averages with horizontal and vertical lines representing ± 1 S.E. for both ET and GEP. Regression parameters a and b are the slope and intercept respectively.

Conclusions

This study examined the micrometerological fluxes of mass and energy over a boreal jack pine stand growing on reclamation cover with the multiple objectives of: (a) assessing the reliability of turbulent flux data collected; (b) reporting on the magnitude and temporal variation of the components of the energy balance; (c) examining the controls on ET; and (d) comparing results from (b) and (c) to a BERMS jack pine chronosequence.

A number of methods were used to asses the reliability of turbulent flux data, which included: (a-i) using ogive curves to assess the appropriate flux averaging period; (a-ii) assessing the size of the flux footprint for coincidence with site fetch under variable stability and wind direction; (a-iii) comparing turbulent flux statistics against acceptable ranges; and (a-iv) assessing stationary and fully developed turbulent conditions.

(a-i) Results of ogive plots indicated that the common 30 minute flux averaging period was sufficient for capturing the range of turbulent covariance over the relatively short jack pine stand.

(a-ii) As a result of the relatively high median friction velocity for the site, given the height of the jack pine canopy, the modeled flux footprint was relatively small, with the maximum necessary fetch required for a fully adjusted boundary layer to develop being 250 m under stable conditions. Based on the distribution of wind direction and atmospheric stability over the study period, there was adequate fetch for up to 79% of all measurements.

(a-iii) Evaluation of turbulent flux statistics, such as skewness, kurtosis, and high frequency spiking revealed instances of poor instrument performance or simply

statistically unusual behaviour. The statistical properties of all sonic-derived variables indicated good sensor performance, with the large majority of measurements having statistical properties within expected ranges. IRGA performance was not as good, being both more skewed and kurtotic. With respect to high frequency spiking, IRGA variables were rejected more often than sonic variables. This discrepancy is at least partly attributable to the greater effect rainfall had on the spiking rate over background levels, where half hours for IRGA variables were rejected 5 – 10 times as often under rainy conditions compared to about 2 – 3 times as often for sonic variables.

(a-iv) Results of tests of stationarity showed that, in general, over 80% of half hours had adequate steady-state conditions, with slightly better performance by sonic variables. Again, rainfall had the largest effect on IRGA variables, with steady-state conditions 10 – 20% less often compared to the overall average. Results of the test for developed turbulent conditions were conflicting, with assessment based on vertical wind speed indicating turbulent conditions 96.7% of the time, yet only 59.8% under the best performing parameterization based on temperature.

The magnitude and temporal variability of energy and mass fluxes were assessed where the significant fluxes were (b-i) radiant (R_n) and (b-ii) and turbulent fluxes (H and LE). (b-i) Comparison of incoming solar radiation to modeled maximum potential values revealed that, despite being a relatively dry year, 'ideal' cloud free, clear sky conditions rarely ever occurred as a result of atmospheric transmissivity and prevalence of scattered clouds. Solar radiation, temperature, H, and G exhibited a clear parabolic trend, peaking near summer solstice, with LE having a less pronounced seasonal trend as a result of the additional variable biological control imposed on LE.

(b-ii) During the relatively dry, warm period that prevailed during the first half of the study period, midday energy portioning was predominantly to sensible heat with a common Bowen ratio of about 2. On a daily basis, however, energy partitioning between H and LE was more equal as a result of small yet consistently positive LE values at night. In the second half of the study period, with increased precipitation and available soil moisture, midday partitioning was fairly equal, with daily LE exceeding H.
Daily ET ranged from 0.2 – 3.6 mm d^{-1}, with mean values over the study period of 1.75 ± 0.75 mm d^{-1}.

Long term regulation on plant growth in the boreal region is affected by cold temperature and the relatively dry environment. Feedbacks between climate, growth rates, and potential transpiration cause jack pine, in general, to be conservative with respect to ET, allowing them to survive in dry environments (Baldocchi et al., 2000a). However, in order to effectively model ET for jack pine, short term controls on ET must be parameterized. Therefore, in addition to examining the magnitude and temporal variability of the mass and energy fluxes of RJP92, the biotic and abiotic factors which control LE were assessed: primarily (c-i) available soil moisture; (c-ii) VPD; and (c-iii) r_s.

(c-i) Soil moisture availability was found to have a significant effect on ET, where LE measured during periods with greater soil moisture availability approached equilibrium levels. The link between soil moisture and ET could be seen in the weak relation between daily r_s and Ψ_s (Fig. 5.22), where the strength of the relation was affected by multiple controls on r_s, and potential threshold behaviour described by Kelliher et al. (1998) and Chapin (2002).

(c-ii) The control of VPD on LE varied throughout the season, where LE was more closely coupled to available energy when soil moisture was less limiting as demonstrated by increasing Ω values (Fig. 5.26). As expected, r_s increased with increasing VPD, where higher r_s values were associated with smaller negative Ψ_s for a given value for VPD (Fig. 5.24).

(c-iii) A number of studies for jack pine point to the dominance of r_s in regulating water loss. Examination of bulk surface parameters such as LE/LE_{eq} and Ω indicated that ET was strongly controlled by surface conductance, particularly when soil moisture was limiting.

(d) In order to place these results in context, comparisons were made between RJP92 and 3 jack pine sites in Saskatchewan. With respect to surface radiative properties, albedo for RJP92 was higher on both a daily and seasonal basis compared to the three chronosequence sites (Table 5.2). The higher albedo of RJP92 is thought to be a result of the influence of the soil surface, understory vegetation, and the open nature of the canopy as a result of relatively low LAI (Fig. 5.2 and Table 5.1). The higher albedo of RJP92 was found to result in lower maximum daily R_n values under clear sky conditions near mid summer compared to the chronosequence sites.

The relatively dry, warm conditions that dominated the first half of the study period showed good agreement with other jack pine stands with respect to low levels of daily ET ($\leq 2mm\ d^{-1}$), relatively high r_s, and LE rates significantly less than equilibrium rates. Following several significant rainfall events and a recharge of near surface soil moisture, average daily ET rates for RJP92 tended to be somewhat greater than values for the three chronosequence sites, with values approaching and exceeding equilibrium rates.

These high LE rates were not solely the result of wet canopy evaporation, where r_s would no longer be limiting. Even during periods were the canopy was modeled as being dry, high LE levels were maintained because of the available water holding capacity of the till soil cover. This discrepancy in soil cover between RPJ92 and other jack pine stands which tend to grow on well drained sandy soils could account for its ability to maintain LE rates above those commonly reported.

Despite a stronger biological control on ET for the chronosequence sites compared to RJP92 based on typical Ω values over the growing season, analysis of WUE indicated similar water cost of carbon gain. This could be the result of site specific adaptations of the jack pine of the nature described by Addington et al. (2006) where sapwood to leaf area and root to leaf area ratios vary according to average growing season soil moisture conditions.

In addition to the above mentioned results, the similarity in the modeled response of r_s to environmental variables such as VPD, PPFD, and available water (Fig. 5.25) seems to indicate that although differences exist between the sites such as soil texture, LAI, and albedo, RJP92 is behaving 'normally' or within the bounds of behaviour exhibited by the chronosequence sites for the years chosen

Future research at RJP92 should focus on assessing the range of inter-annual variability over the natural range of both temperature and precipitation variation. Measurements of the LE contribution by the understory would also provide a fuller picture of the role jack pine play in ET. These measurements would allow for parameterization of a dual source ET model, which would be more accurate in assessing the risk of reclamation failure based on soil cover water holding capacity and summer moisture deficits derived from historical weather data.

References

Addington, R.N., Donovan, L.A., Mitchell, R.J., Vose, J.M., Pecot, S.D., Jack, S.B., Hacke, U.G., Sperry, J.S., and Oren, R., 2006. Adjustments in hydraulic architecture of *Pinus palustris* maintain similar stomatal conductance in xeric and mesic habitats. Plant, Cell and Environment, 29: 535-545.

Amiro, B.D., and Wuschke, E.E., 1987. Evapotransipration form a boreal forest drainage basin using an energy balance/eddy correlation technique. Boundary-Layer Meteorology, 38: 125-139.

Amiro, B.D., A.G. Barr, T.A. Black, H. Iwashita, N. Kljun, J.H. McCaughey, K. Morgenstern, S. Murayama, Z. Nesic, A.L. Orchansky, and N. Saigusa., 2006a. Carbon, energy and water fluxes at mature and disturbed forest sites, Saskatchewan, Canada. Agricultural and Forest Meteorology, 136: 237-251.

Amiro B.D., A.L. Orchansky, A.G. Barr, T.A. Black, S.D. Chambers, F.S. Chapin III, M.L. Goulden, M. Litvak, H.P. Liu, J.H. McCaughey, A. McMillan and J.T. Randerson., 2006b. The effect of post-fire stand age on the boreal forest energy balance. Agricultural and Forest Meteorology (Fluxnet-Canada Special Issue), 140: 41-50.

Arya, S.P., 1988. Introduction to micrometeorology. Academic Press, San Diego, 307pp.

Baldocchi, D.D. and Vogel, C.A., 1996. Energy and CO_2 flux densities above and below a temperate broad-leaved forest and a boreal pine forest. Tree Physiology, 16: 5-16.

Baldocchi, D.D., Vogel, C.A., and Hall, B., 1997a. Seasonal variation of energy and water vapor exchange rates above and below a boreal jack pine forest canopy. Journal of Geophysical Research, 102(D24): 28 939- 28 951.

Baldocchi, D.D., Vogel, C.A., and Hall, B., 1997b. Seasonal variation of carbon dioxide exchange rates above and below a boreal jack pine forest. Agricultural and Forest Meteorology, 83: 147-170.

Baldocchi, D.D., Kelliher, F.M., Black, T.A., and Jarvis, P. 2000a. Climate and vegetation controls on boreal zone energy exchange. Global Change Biology. 6 (Suppl. 1), 69-83.

Baldocchi, D.D, Law, B.E., and Anthoni, P.M., 2000b. On measuring and modeling energy fluxes above the floor of a homogenous and heterogeneous conifer forest. Agricultural and Forest Meteorology, 102: 187-206.

Baldocchi, D.D., 2003. Assessing the eddy covariance technique for evaluating carbon

dioxide exchange rates of ecosystems: past, present and future. Global Change Biology, 9: 479-492.

Bannan, M.W., 1940. The root systems of northern Ontario conifers growing in sand. American Journal of Botany, 27: 108-114.

Barbour, S.L., Chapman, D., Qualizza, C., Kessler, S., Boese, C., Shurniak, R., Meiers, G., O'Kane, M., Hendry, J., and Wall, S., 2004. Tracking the evolution of reclaimed landscapes through the use of instrumented watershed – A brief history of the Syncrude Southwest 30 overburden reclamation research program. Presented at the International Instrumented Watershed Symposium, Edmonton, AB, Canada.

Barr, A.G., van der Kamp, G., Schmidt, R., and Black, T.A., 2000. Monitoring the moisture balance of a boreal aspen forest using a deep groundwater piezometer. Agricultural and Forest Meteorology, 102: 13-24.

Barr A.G., K. Morgenstern, T.A. Black, J.H. McCaughey and Z. Nesic., 2006. Surface energy balance closure by the eddy-covariance method above three boreal forest stands and implications for the measurement of the CO_2 flux. Agricultural and Forest Meteorology. (Fluxnet-Canada Special Issue), 140: 322-337.

Betts, A.K. and Ball, J.H. 1997. Albedo over the boreal forest. Journal of Geophysical Research, 102(D24): 28,901-28,910.

Black, T.A., den Hartog, G., Neumann, H.H., Blanken, P.D., Yank, P.C., Russell, C., Nesic, Z., Staebler, R., Lee, X., Chen, S.C., Staebler, R., and Novak, M.D., 1996. Annual cycles of water vapour and carbon dioxide fluxes in and above a boreal aspen forest. Global Change Biology, 2: 219-229.

Black, T.A., Chen, W.J., Barr, A.G., Arain, M.A., Chen, Z., Nesic, Z., Hogg, E.H., Neumann, H.H., and Yang, P.C., 2000. Increased carbon sequestration by a boreal deciduous forest in years with a warm spring. Geophysical Research Letters, 27: 1271-1274.

Blanken, P.D., Black, T.A., Yang, P.C., den Hartog, G., Neumann, H.H., Nesic, Z., Staebler, R., Novak, M.D., and Lee, X., 1997. Energy balance and canopy conductance of a boreal aspen forest: partitioning overstory and understory components. Journal of Geophysical Research, 102: 28,915-28,927.

Blanken, P.D., Black, T.A., Neumann, H.H., den Hartog, G., Yang, P.C., Nesic, Z., and Lee, X., 2001. The seasonal water and energy exchange above and within a boreal aspen forest. Journal of Hydrology, 245: 118-136.

Bradshaw, A. 1997. Restoration of mined lands – using natural processes. Ecological Engineering. 8, 255-269.

Brock, F.V., 1986. A nonlinear filter to remove impulse noise from meteorological data. Journal of Atmospheric and Oceanic Technology, 3(1), 51-58.

Campbell, G.S. and Norman, J.M. 1998. An introduction to environmental biophysics, 2nd ed. Springer-Verlag, New York, NY.

Carey, S.K., 2006. Energy and water exchange from a saline-sodic overburden reclamation soil cover, Fort McMurray, Alberta. Paper presented at CLRA 2006 Conference.

Carey, S.K., 2008. Growing season energy and water exchange from an oil sands overburden reclamation soil cover, Fort McMurray, Alberta, Canada. Hydrological Processes, 22: 2847-2857.

Chen, J.M., 1996. Optically-based methods for measuring seasonal variation of leaf area index in boreal conifer stands. Agricultural and Forest Meteorology, 80: 135-163.

Chorley, R.J. and Kennedy, B.A., 1971. Physical geography: a systems approach. Prentice-Hall, London, 370pp.

Chapin, F.S., Matson, P.A., and Mooney, H.A. 2002. Principles of terrestrial ecosystem ecology. New York: Springer.

Crown, P.H. and Twardy, A.G., 1975. Soils of the Fort McMurray region, Alberta (Townships 88-89, Ranges 8-11) and their relations to agricultural and urban development. Alberta Institute of Pedology, University of Alberta.

Ehman, J.L., Schmid, H.P., Grimmond, C.S.B., Randolph, J.C., Hanson, P.J., Wayson, C.A., and Cropley, F.D. 2002. An initial intercomparison of micrometeorological and ecological inventory estimates of carbon exchange in a mid-latitude deciduous forest. Global Change Biology. 8 (6), 575-589.

Elshorbagy, A., Jutla, A., Barbour, L., and Kells, J., 2005. System dynamics approach to assess the sustainability of reclamation of disturbed watersheds. Canadian Journal of Civil Engineering, 32: 144-158.

Eugster, W., Rouse, W.R., Pielke, R.A., McFadden, J.P., Baldocchi, D.D., Kittel, T.G.F., Chapin III, F.S., Liston, G.E., Vidale, P.L., Vaganov, E., and Chambers, S. 2000. Land-atmosphere energy exchange in Arctic tundra and boreal forest: available data and feedbacks to climate. Global Change Biology. 6 (Suppl. 1), 84-115.

Falge et al., 2001. Gap filling strategies for long term energy flux data set. Agricultural and Forest Meteorology, 107: 71-77.

Field, C., and Mooney, H.A., 1983. The photosynthesis-nitrogen relationship in wild

plants. In: Givnish, T.J. (Editor), On the Economy of Plant Form and Function: Proceedings of the Sixth Maria Moors Cabot Symposium, Evolutionary Constraints on Primary Productivity, Adaptive Patterns of Energy Capture in Plants, Harvard Forest, August 1983. Cambridge University Press, UK, 717pp.

Finnigan, J.J., Clement, R., Malhi, Y., Leuning, R., and Cleugh, H.A. 2003. A re-evaluation of long-term flux measurement techniques – Part 1: Averaging and coordinate rotation. Boundary-Layer Meteorology. 107, 1-48.

Foken, T. and Wichura, B., 1996. Tools for quality assessment of surface-based flux measurements. Agricultural and forest meteorology, 78: 83-105.

Garratt, J.R. 1992. The atmospheric boundary layer. Cambridge University Press, Cambridge, GB.

Grantz, D.A., 1990. Plant response to atmospheric humidity. Plant, Cell and Environment, 13: 667-679.

Greco, S., and Baldocchi, D.D. 1996. Seasonal variation of CO2 and water vapour exchanges over a temperate deciduous forest. Global Change Biology. 2 (3), 183-198.

Grelle, A. and Lindroth, A., 1996. Eddy-correlation system for long-term monitoring of fluxes of heat, water vapour and CO_2. Global Change Biology, 2: 297-307.

Grelle, A., Lundberg, A, Lindroth, A., Moren, A.S., and Cienciala, E. 1997. Evaporation components of a boreal forest: variations during the growing season. Journal of Hydrology. 197, 70-87.

Holl, K.D. 2002. Long-term vegetation recovery on reclaimed coal surface mines in the eastern USA. The Journal of Applied Ecology. 39(6), 960-970.

Humphreys, E.R., 1999. Evaporation from a Canadian west coast douglas-fir forest: Seasonal patterns and controls. M.Sc. Thesis, University of British Columbia.

Humphreys, E.R., Black, T.A., Ethier, G.J., Drewitt, G.B., Spittlehouse, D.L., Jork, E.-M., Nesic, Z., and Livingston, N.J. 2003. Annual and seasonal variability of sensible and latent heat fluxes above a coastal Douglas-fir forest, British Columbia, Canada. Agricultural and Forest Meteorology. 115, 109-125.

Humphreys, E.R., Black, T.A., Morgenstern, K., Cai, T., Drewitt, G.B., Nesic, Z., and Trofymow, J.A, 2006. Carbon dioxide fluxes in coastal Douglas-fir stands at different stages of development after clearcut harvesting. Agricultural and Forest Meteorology, 140: 6-22.

Jarvis, P.G., 1976. The interpretation of the variations in leaf water potential and stomatal

conductance found in canopies in the field. Philosophical Transactions of the Royal Society of London, 273: 593-610.

Jarvis P.G., McNaughton K.G., 1986. Stomatal control of transpiration: scaling up from leaf to region. Advances in Ecological Research, 15: 1-49.

Jarvis, P.G., Massheder, J.M., Hale, S.E., Moncrieff, J.B., Rayment, M., and Scott, S.L., 1997. Seasonal variation of carbon dioxide, water vapour, and energy exchanges of a boreal black spruce forest. Journal of Geophysical Research, 102(D24): 28,953-28,966.

Johnson, L., Gibson, D.J., Risser, P.G. 1982. Revegetation of unreclaimed coal strip-mines in Oklahoma: I. Vegetation structures and soil properties. The Journal of Applied Ecology. 19 (2), 453-463.

Kaimal, J.C. and Finnigan, J.J. 1994. Atmospheric boundary layer flows: Their structure and measurement. Oxford University Press, New York, 289pp.

Kalyn, A.L. and Van Rees, K.C.J., 2006. Contribution of fine roots to ecosystem biomass and net primary production in black spruce, aspen, and jack pine forests in Saskatchewan. Agricultural and Forest Meteorology, 140: 236-243.

Kelliher, F.M. et al., 1998. Evaporation from a central Siberian pine forest. Journal of Hydrology, 205: 279-296.

Kljun, N., Black, T.A., Griffis. T., Barr. A., Gaumont-Guay. D., McCaughey, J.H., Morgenstern, K., and Nesic, Z., 2006. Response of net ecosystem productivity of three boreal forest stands to drought. Ecosystems, 9: 1128-1144.

Krebs, C.J., 1999. Ecological Methodology, 2nd ed. Harper and Row, New York, 654pp.

Kuchment, L.S., Demidov, V.N. 2006. Modeling of influence of hydrological processes on the carbon cycle of a forest ecosystem. Environmental Modelling & Software. 21: 111-114.

Lavigne, M.B., Ryan, M.D., Anderson, D.E., Baldocchi, D.D., Crill, P.M., Fitzjarrald, D.R., Goulden, M.L., Gower, S.T., Massheder, J.M., McCaughey, J.H., Rayment, M., and Striegl, R.G., 1997. Comparing nocturnal eddy covariance measurements to estimates of ecosystem respiration made by scaling chamber measurements at six coniferous boreal sites. Journal of Geophysical Research, 102(D24): 28,977-28,985.

Law, B.E., Waring, R.H., Anthoni, P.M., and Aber, J.D. 2000. Measurements of gross and net ecosystem productivity and water vapour exchange of a Pinus ponderosa ecosystem, and an evaluation of two generalized models. Global Change Biology. 6(2), 155-168.

Lee, X., Massman, W., and Law, B., 2004. Handbook of micrometeorology: A guide for surface flux measurement and analysis, Boston, London, Kluwer Academic. Leuning, R., and Judd, M.J. 1996. The relative merits of open- and closed-path analysers for measurement of eddy fluxes. Global Change Biology. 2 (3), 241-254.

Liu, S., Mao, D., and Lu., L., 2006. Measurement and estimation of the aerodynamic resistance. Hydrology and Earth System Sciences Discussions, 3: 681-705.

Llorens, P. and Gallart, F., 2000. A simplified method for forest water storage capacity measurement. Journal of Hydrology, 240: 131-144.

Mielk, M.S., Oliva, M.A., de Barros, N.F., Penchel, R.M., Martinez, C.A., and de Almeida, A.C., 1999. Stomatal control on transpiration in the canopy of a clonal Eucalyptus grandis plantation. Trees, 13: 152-160.

Massman, W.J., 2000. A simple method for estimating frequency response corrections for eddy covariance systems. Agricultural and Forest Meteorology, 104: 185-198.

Massman, W.J. and Lee, X., 2002. Eddy covariance flux corrections and uncertainties in long-term studies of carbon and energy exchanges. Agricultural and Forest Meteorology, 113(1-4): 121-144.

McCaughey, J.H., Lafleur, P.M., Joiner, D.W., Bartlett, P.A., Costello, A.M., Jelinski, D.E., and Ryan, M.G., 1997. Magnitudes and seasonal patterns of energy, water, and carbon exchanges at a boreal young jack pine forest in the BOREAS northern study area. Journal of Geophysical Research, 102(D24): 28,997-29,007.

McNaughton, K.G., and Jarvis, P.G., 1983. Predicting effects of vegetation changes on transpiration and evaporation. In: T.T. Kozlowski (Editor), Water Deficits and Plant Growth. Academic Press Inc., New York, pp. 1-47.

Mkhabela, M.S., Amiro, B.D., Barr, A.G., Black, T.A., Hawthorne, I., Kidston, J., McCaughey, J.H., Nesic, Z., Orchansky, A.L., Shashkov, A., and Zha, T., 2008. Comparison of carbon dynamics following fire and harvesting in Canadian boreal forests. 28th Conference on Agricultural and Forest Meteorology.

Moncrieff, J.B., Malhi, Y., and Leuning, R. 1996. The propagation of errors in long-term measurements of land-atmosphere fluxes of carbon and water. Global Change Biology. 2(3), 231-240.

Monteith, J.L. and Unsworth, M.H., 1990. Principles of environmental physics, 2nd ed. Edward Arnold, London, 291pp.

Monteith, J.L., 1995. A reinterpretation of stomatal responses to humidity. Plant, Cell,

and Environment, 18(4): 357-364.

Oke, T.R. 1987. Boundary layer climates (2nd edition). New York, NY: Routledge.

Olson, R.J., Holladay, S.K., Cook, R.B., Flage, E., Baldocchi, D, and Gu, L. 2004. FLUXNET: Database of fluxes, site characteristics, and flux-community information. Oak Ridge, TN: Oak Ridge National Laboratory.

Priestly, C.H.B., and Taylor, R.J. 1972. On the assessment of surface heat flux and evaporation using large scale parameters. Monthly Weather Review. 100 (2), 81-92.

NRCan – Canadian Forest Service, 2005. The State of Canada's Forests: The Boreal Forest. Her Majesty the Queen in Right of Canada, Ottawa, ON.

NRCan – Canadian Forest Service, 2007. The State of Canada's Forests: Annual Report. Her Majesty the Queen in Right of Canada, Ottawa, ON.

Qualizza, C., Chapman, D., Barbour, S.L., and Purdy, B., 2004. Reclamation research at Syncrude Canada's mining operation in Alberta's Athabasca oil sands region. Proceedings, International Conference on Ecological Restoration SER2004, Victoria, B.C., Canada, August 24-26.

Restrepo, N.C., and Arain, M.A. 2005. Energy and water exchanges from a temperate pine plantation forest. Hydrological Processes. 19, 27-49.

Schuepp, P.H., Leclerc, M.Y., MacPherson, J.I., and Desjardins, R.L., 1990. Footprint prediction of scalar fluxes from analytical solutions of the diffusion equation. Boundary-Layer Meteorology, 50: 355-373.

Sellers, P., Hall, F., Margolis, H., Kelly, B., Baldocchi, D., den Hartog, G., Cihlar, J., Ryan, M.G., Goodison, B., Crill, P., Ranson., K.J., Lettenmaier, D., and Wickland, D.E., 1995. The Boreal Ecosystem-Atmosphere Study (BOREAS): An overview and early results from the 1994 field yield. Bulletin of the American Meteorological Society, 76(9): 1549-1577.

Shuttleworth, W.J. and Calder, I.R., 1979. Has the Priestly-Taylor equation any relevance to forest evaporation? Journal of Applied Meteorology, 18: 639-646.

Shuttleworth, W.J., Leuning, R., Black, T.A., Grace, J., Jarvis, P.G., Roberts, J., and Jones, H.G. 1989. Micrometeorology of temperate and tropical forests. Philosophical Transactions of the Royal Society of London. 324 (1223), 299-334.

Strong, W.L., and La Roi, G.H., 1985. Root density – soil relationships in selected boreal forests of central Alberta, Canada. Forest Ecology and Management, 12: 233-251.

Stull, R.B., 1988. An Introduction to Boundary Layer Meteorology. Kluwer Academic Publishers, Dordrecht, 666pp.

Tanner, C.B. and Thurtell, G.W., 1969. Anemoclinometer measurements of Reynolds stress and heat transport in the atmospheric surface layer. ECOM 66-G22-F, University of Wisconsin, Madison, Wisconsin.

The MathWorks, 2007. Using MATLAB, version 7.4. The MathWorks Inc., Natick, MA.

Twine, T.E., Kustas, W.P., Norman, J.M., Cook, D.R., Houser, P.R., Meyers, T.P., Prueger, J.H., Starks, P.J. and Wesely, M.L., 2000. Correcting eddy-covariance flux underestimates over a grassland. Agricultural and Forest Meteorology, 103: 279-300.

Vickers, D., Mahrt, L., 1997. Quality control and flux sampling problems for tower and aircraft data. Journal of Atmospheric and Oceanic Technology, 14(3), 512-526.

Ward, R.C., and Robinson, M., 2000. Principles of Hydrology, 4th ed. McGraw-Hill, London, 450pp.

Weaver, L.A., Flanagan, L.B., and Carlson, P.J., 2002. Seasonal and interannual variation in evapotranspiration, energy balance and surface conductance in a northern temperate grassland. Agricultural and Forest Meteorology, 112: 31-49.

Webb, E.K., Pearman, G.I., and Leuning, R., 1980. Correction of flux measurements for density effects due to heat and water vapour transfer. Quarterly Journal of the Royal Meteorological Society, 106: 85-100.

Wilczak, J.M., Oncley, S.P., and Stage, S.A., 2001. Sonic anemometer tilt correction algorithms. Boundary-Layer Meteorology, 99: 127-150.

Wilson, K.B. and Baldocchi, D.D., 2000. Seasonal and interannual variability of energy fluxes over a broadleaved temperate deciduous forest in North America. Agricultural and Forest Meteorology, 100: 1-18.

Wilson, K., Goldstein, A., Falge, E., Aubinet, M., Baldocchi, D., Berbigier, P., Bernhofer, C., Ceulemans, R., Dolman, H., Field, C., Grelle, A., Ibrom, A., Law, B.E., Kowalski, A., Meyers, T., Moncrieff, J., Monson, R., Oechel, W., Tenhunen, J., Valentini, R. and Verma, S., 2002. Energy balance closure at FLUXNET sites. Agricultural And Forest Meteorology, 113: 223-243.